Functions of SHIP1 for proliferation and migration of carcinoma cells

Dissertation

zur Erlangung des akademischen Grades eines

Doktors der Medizin (Dr. med.)

an der

Medizinischen Fakultät der Universität Hamburg

vorgelegt von

Luise Brakert

aus

Hamburg

2025

Betreuer:in / Gutachter:in der Dissertation: Prof. Dr. Manfred Jücker

Gutachter:in der Dissertation: PD Dr. Jasmin Wellbrock

Vorsitz der Prüfungskommission: PD Dr. Jasmin Wellbrock

Mitglied der Prüfungskommission: PD Dr. Stefan Werner

Mitglied der Prüfungskommission: Prof. Dr. Leticia Oliveira-Ferrer

Datum der mündlichen Prüfung: 25.02.2026

Table of Contents

1. Introduction

1.1. The cancer “pandemic”

Second only to cardiovascular diseases, cancer is a leading cause of death worldwide, but especially in high income countries. While mortality rates of the former have dropped significantly in the industrialized world, those of the latter have seen much slighter decreases (Araujo et al., 2014). With life expectancy rising as well as the adoption of a lifestyle characterized by physical inactivity, high calorie intake and smoking, cancer is also gaining importance in emerging and developing countries (Araujo et al., 2014) (Torre et al., 2016). Both sexes taken together, breast cancer is the most commonly diagnosed malignant tumor, followed by prostate and colorectal cancer. As cause of death, lung cancer leads before breast and colorectal cancer (Cancer today; GLOBOCAN 2018). Developing countries tend to have an above-average share of cancers associated with infectious agents (Torre et al., 2016).

1.2 An overview of colorectal carcinoma

Colorectal cancer is the third most frequently diagnosed cancer worldwide, as well as the third most common cause of death among all cancer types (Torre et al., 2016). In 41% of cases, the proximal colon is affected, leading before the rectum with 28% of cases and the distal colon with 22% (Cheng et al., 2011) (Thanikachalam and Khan, 2019). Over 70% of cases are considered sporadic, while 20% are associated with a family history of colorectal cancer and about 5% of are induced by specific genetic syndromes, mostly the Lynch Syndrome (HNPCC) and Familial adenomatous polyposis (FAP) (Cheng et al., 2011).

HNPCC stems from dysfunctional mismatch repair genes, leading to non-polypous cancer emergence in the colon and other organs. In FAP, on the other hand, a loss-of-function of the adenomatous polyposis coli (APC) tumor suppressor gene results in the development of numerous polyps beginning in childhood, which inevitably transform to cancer without treatment (Strate and Syngal, 2005). Sporadic colorectal cancers are associated with a number of environmental and internal risk factors, including inflammatory bowel disease, especially ulcerative colitis, physical inactivity, consumption of tobacco, alcohol, and processed and read meat, obesity, insulin resistance, age and male sex. Meanwhile, physical activity as well as a diversified diet featuring plenty of fruit and vegetable, dairy products, fish, fiber, micronutrients and vitamins, plus regular use of aspirin and nonsteroidal anti-inflammatory drugs (NSAIDs), were shown to have protective effects (Cheng et al., 2011).

In the course of time and in the presence of carcinogens, colon epithelial cells accumulate genetic mutations, which may eventually lead to malignant transformation. Two sequences of stepwise progression to cancer have been described, one of them involving tubular polyps becoming adenomas, the other sessile serrated polyps (Kuipers et al., 2015). On the molecular level, alterations in at least four to five genes are assumed to be necessary for malignant transformation. Oncogenes as well as tumor suppressor genes are involved, the greater importance being attributed to loss-of-function in tumor suppressor genes. Though traditionally considered recessive traits, heterozygous mutations in these genes can be relevant for a cell's phenotype as well. Mutations present in almost all cells of a tumor are suspected to be drivers of transformation, having given the cells that first possessed it an edge over less aggressive ones- especially if these mutations are found in a large number of tumors (Fearon and Vogelstein, 1990). The Wnt-ß-catenin, Epidermal Growth Factor Receptor (EGFR) –MAP-kinase (MAPK), PI3K-AKT and Transforming growth factor β (TGF-ß) pathways are the most commonly affected signaling cascades in colorectal cancer. In addition to genetic changes, epigenetic alterations also contribute to cancer advancement. Firstly, tumor suppressor genes can be silenced by hypermethylation in their promoter areas, and secondly, oncogenes can be activated or genetic instability increased due to hypomethylation in repetitive DNA- segments. The various DNA-level changes seem to correlate with tumor position in the colon, pointing at an association with the specific environment, such as the condition of surrounding tissues and the gut microbiome (Kuipers et al., 2015).

Colorectal cancer is a prevalent disease of the middle aged and elderly (Moreno et al., 2016). Patients typically present with symptoms like bloody stools, abdominal pain, unclear anemia, obstipation alternating with diarrhea, fatigue and weight loss (Kuipers et al., 2015) (Moreno et al., 2016). Due to the lack of symptoms in early stages and their low specificity even in later ones, patients often get diagnosed in advanced stages unless screened. Since treatment of localized colorectal cancer comes along with 90% 5-year survival compared to only 13% after metastatic spread, screening programs make a significant contribution to the reduction of mortality, as well as treatment costs (Moreno et al., 2016).

Among screening techniques, colonoscopy is considered the most comprehensive and precise, offering the possibility of taking tissue samples or resecting adenoma in the same session. It has been shown to reduce the risk for and mortality of colorectal cancer by about 80%. However, colonoscopy enjoys only moderate acceptance in the population, entails certain risks and relatively high costs. Other available screening measures include sigmoidoscopy, computer tomography (CT)-colonography, and the less sensitive but more widely accepted Fecal Immunochemical Test (FIT) and guaiac Fecal Occult Blood Test

(gFOBT) tests for occult blood in stool, which are frequently used for primary screening. In the future, multi-target faecal DNA-tests are likely to gain importance in primary screening (Kuipers et al. (2015).

Once diagnosed, colorectal cancer is surgically resected in most cases, either openly or laparoscopically. Patients with advanced stage rectal cancer may receive neoadjuvant chemo- or radiotherapy. Post-surgery adjuvant treatment for metastasis-free patients with stage T3 or T4 cancers is only considered in cases of high risk, e.g. low differentiation. Meanwhile, lymph node invasion is an indication for chemotherapy with 5-fluorouracil and oxaliplatin. In cases of distant metastasis, individual resectable liver or lung metastases may be treated surgically. Either way, double chemotherapies according to the FOLFOX or FOLFIRI protocols, or triples (FOLFOXIRI; folinic acid, 5-fluoruracil, oxaliplatin, irinotecan) are recommended for sufficiently fit patients. In addition to conventional chemotherapies, targeted therapies like monoclonal anti-EGFR (i.e. Cetuximab) and anti-vascular endothelial growth factor (VEGF)-A (i.e. bevacizumab) antibodies, as well as small molecule kinase inhibitors and fusion proteins against proangiogenic factors, are routinely employed. EGFR-antibodies, the most widely used biologicals, were shown to prolong survival in patients with EGFR-expressing tumors without KRAS and NRAS mutations. The mode of action of VEGF-A antibodies it not entirely clear yet, though VEGF-A is suspected to improve tumor blood supply by stimulating endothelium proliferation and enhancing capillary permeability.

Besides improvement of screening programs and surgical procedures, the development of new targeted therapies is likely to play a key role for further reduction of colorectal cancer mortality in the future. New targets for treatment continue to be discovered, some of them pertaining to the PI3K-AKT signaling pathway (Kuipers et al. (2015).

1.3 An overview of melanoma

Malignant melanoma is a widespread type of cancer especially in Caucasian populations, being the fourth most frequently diagnosed malignancy in Australia and New Zealand and the seventh in Europe and North America (Cancer today; GLOBOCAN 2018). Its incidence has increased steeply in the last decade, beginning to slow down only in the 1990s. It is a disease of the middle aged, affecting more men than women overall, but more women among under 40-year-olds. Since it is accessible to screening measures and often discovered while still in a localized stage, mortality rates of melanoma are comparatively low in relation to incidence (Rastrelli et al., 2014). As cause of death, it ranks tenth, sixth, and seventeenth, twice, in the above-mentioned countries (3). Once metastasized, however, melanomas are very aggressive and difficult to treat (Lo et al., 2009).

Melanomas stem from pigment-producing cells called melanocytes that reside in the skin, mucosal epithelium and eyes. Hormonal stimulation of melanocytes by α- melanocyte stimulating hormone (MSH) induces basal production of eumelanin, a dark pigment serving for protection against ultra violet (UV)-radiation. Exposed to UV-radiation, melanocytes further raise their eumelanin output. Malignant transformation can be triggered by intense intermittent exposure to UV-radiation, especially in the form of repeated sunburns during childhood, and also by artificial UVR in sunbeds. Immunosuppression, a fair skin type, high number of liver spots, family anamnesis of melanoma and specific genetic neoplasia syndromes like hereditary retinoblastoma, Lynch Type II and Li-Fraumeni Syndromes increase the melanoma risk (Rastrelli et al., 2014) (Lo et al., 2009).

On the molecular level, UVR-induced DNA damage, heightened levels of reactive oxygen species (ROS), distorted immune function and growth factor production in skin lacking eumelanin for UVR protection do their part. The presence of pheomelanin, the light, red counterpart of eumelanin, seems to contribute to melanomagenesis as well. Melanomas tend to carry broad arrays of mutations, making it difficult to differentiate between driver and passenger mutations. So far, mutations of BRAF and NRAS, leading to MAPK-pathway hyperactivation, as well as in Rac1, have been identified as common drivers. Loss of function in tumor suppressors like PTEN, TP53 and CDKN2A are frequently found in melanomas, but also amplification of AKT3, overexpression of growth factor receptors like EGFR, c-Kit, and MET, causing enhanced PI3K- and MAPK- signaling (Lo et al., 2009).

Malignant melanomas are divided into three subtypes: superficial spreading melanoma (SSM), nodular melanoma (NMM), and lentigo maligna melanoma (LMM). They are mostly found on the back, arms and legs of patients. Moles can be assessed for signs of malignancy by checking the ABCDE criteria, standing for asymmetry, border irregularity, color variegation, diameter >6mm and evolvement, which have been developed for self-screening and screening by non-dermatologist professionals. Dermatoscopy can give further hints by enabling in vivo microscopy of the tissue surface, making signs of malignancy like irregular pigmentation, globules, streaks and vascularization visible (Rastrelli et al., 2014). Patients with suspicious lesions mostly receive excisional biopsies for definite diagnosis by immunohistochemistry and determination of invasion depth. Depending on invasion depth, melanomas are resected with a safety margin of 0,5-2cm, and sentinel lymph node biopsies may be taken- followed by lymphadenectomy and potentially a search for distant metastases- in case of a positive result (Pavri et al., 2016).

Adjuvant treatment is advised for stages 3 (lymph node metastases) and 4 (distant metastases), occasionally also stage II (>1mm thickness). Options for adjuvant therapy are radiation, classical chemotherapy- mostly dacarbazine- immune stimulants like recombinant interleukin 2 (IL2) and interferon-α-2b (IFNα-2b), and various targeted

therapies, including Raf-kinase inhibitors, MEK1/2 inhibitors, and anti-CTL4-antibodies (21). IL2 stimulates cytotoxic T-cells, bearing a risk of strong toxicity, but also a chance on lasting remission in a few patients. Similarly, checkpoint inhibitors like anti-CTL4 and anti-PD1-antibodies reduce immune tolerance in cytotoxic T-lymphocytes, but yield long term survival in a higher percentage of patients and with fewer side effects. Further therapies focusing on T-cells are in development, including ex vivo sensitization and infusion of autologous T-lymphocytes as well as construction of transgenic T-cell-receptors. Other inhibitor therapies, although often initially potent, mostly fail to deliver long term remission due to various resistance mechanisms developed by melanoma cells. Resistance against BRAF-inhibitors can be conveyed by reactivation of MAPK-signaling as well as compensatory upregulation of PI3K-AKT-signalling by increased RTK-expression. While combination therapy with MEK-inhibitors improves survival, it doesn't prevent the occurrence of resistances (Lo et al., 2009).

To reduce melanoma mortality in the future, prevention by avoidance of UVR-exposure will play a crucial role, together with extensive screening and the development of new targeted therapies. Despite various new therapeutic options, metastasized melanomas remain difficult to treat and will continue to be a very relevant field of investigation (Lo et al., 2009) (Kozovska et al., 2016).

1.4 The PI3K-AKT-signaling pathway

The PI3K-signaling pathway, responsible for mediating survival, proliferation, migration, adhesion, and differentiation, is among the pathways most frequently altered in cancer. Its diverse effects on cell metabolism, cell cycle progression, viability and angiogenesis can give tumor cells with an overactivated PI3K-AKT-pathway a critical growth advantage and make it a promising target for future cancer therapies (Porta et al., 2014).

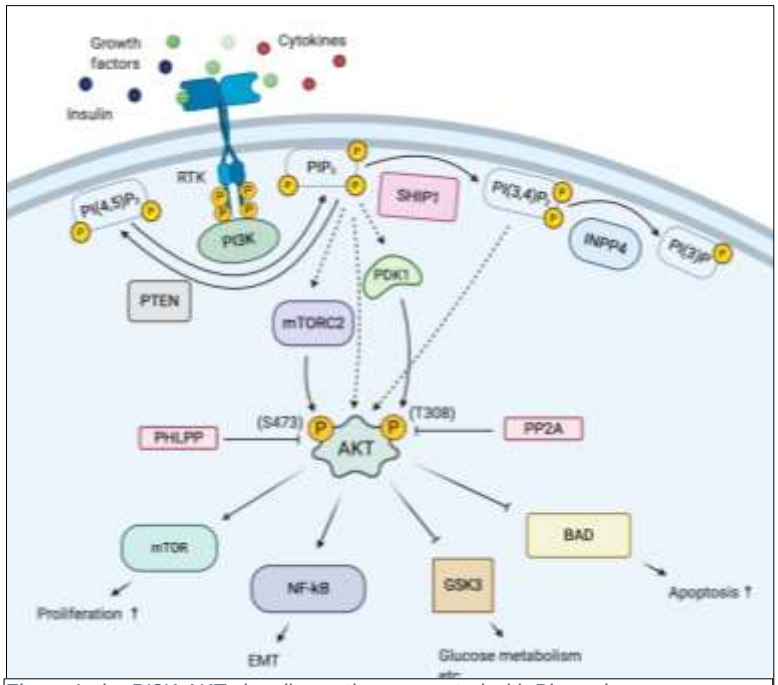

Figure 1: the PI3K-AKT signaling pathway, created with Biorender.com; Key: continuous arrows = conversion/ activation; dotted arrows = recruitment; blunted lines = inhibition/ deactivation

Physiologically, the pathway is activated via external stimulation by growth factors, insulin and cytokines, which bind to membrane-bound receptor tyrosine kinases (RTKs) or G-protein coupled receptors (GPCRs) (Hoxhaj and Manning, 2020). Growth factor binding to RTKs leads to dimerization and trans-autophosphorylation of intracellular tyrosine residues. The subsequent conformational change allows Src-homology-2 (SH2) domain and phosphotyrosine binding (PTB) domain possessing proteins to associate with the RTKs (Du and Lovly, 2018). Activated GPCRs link to intracellular G-proteins, which catalyze an exchange of GDP to GTP and then dissociate into two subunits (Latek et al., 2012). Class IA PI3-kinases are recruited to the phosphotyrosine residues of RTKs via the SH2 domains of their adapter subunits, leading to activation of their catalytic subunit, while class IB PI3Ks are activated by GPCRs (Porta et al., 2014). PI3Ks then convert $PI(4,5)P_2$ into the second messenger $PI(3,4,5)P_3$, which in turn recruits a variety of effectors with PH-domains like the protein kinase B (AKT) and PDK1. AKT is fully activated when phosphorylated at two sites, the tyrosine 308 residue- by PDK1- and the serine 473 residue -by mTORC2. Once activated, AKT in turn phosphorylates a multitude of substrates, suppressing apoptosis, facilitating cell cycle progression, and regulating glycogen metabolism and protein synthesis. Notably, it enhances degradation of the pro-apoptotic group of FoxO-transcription factors, Bad and Procaspase 9, and activates mTORC, which mediates proliferation. Also, it disinhibits targets of GSK3 by deactivating it, among them metabolic enzymes and transcription factors (Manning and Toker, 2017). By upregulating the transcription factors NFkB and, in turn, Snail, which enhance expression of the small G-protein Rac1, AKT can also support epithelial mesenchymal transition (Henderson et al., 2015).

AKT-signaling is terminated directly by the protein phosphatases PP2A and PHLPP, which dephosphorylate the residues crucial for activity. Indirectly, a range of lipid

phosphatases degrading PI(3,4,5)P_3 also stop AKT-activity. The best-known of them is PTEN, a much examined tumor suppressor that converts PI(3,4,5)P_3 back to its precursor substance PI(3,4)P_2. 5' phosphatases like SHIP1, SHIP2, synaptojanin etc., dephosphorylating PIP3 into PI(3,4)P_2, also play a role, though a more ambiguous one. Finally, 4' phosphatases like INPP4B, further degrading PI(3,4)P_2 to PI(3)P, are involved (Manning and Toker, 2017) (Martini et al., 2014).

Due to its effects on proliferation, apoptosis, protein synthesis and glucose metabolism, various components of the PI3K-AKT-pathway are frequently altered in cancer. Constitutive activation of Class IA and B PI3K and amplification or overactivation of AKT have been observed in carcinomas, as well as deactivation of PTEN and INPP4B. Also, loss-of-function mutations in SHIP1, a 5' phosphatase endemic to hematopoietic and bone cells, have been found in leukemias. On the other hand, overexpression of SHIP2, an ubiquitous 5' phosphatase, has been associated with breast cancer progression (Martini et al., 2014). Thus, the seemingly inconsistent impacts of 5'phosphatases require further elucidation.

1.5 Cell motility and Rac1

Cell motility is enabled by remodeling of the cytoskeleton, or more specifically, actin polymerization at the leading edge. Thus, cell protrusions called lamellipodia, which allow adhesion and dragging forward, can form. Cancer cells generate protrusions capable of degrading extracellular matrix and thereby invasion, called invadopodia. Actin polymerization is facilitated by the Arp2/3-complex of actin nucleators and maintained by the elongators ENA and VASP.

Arp2/3 is set into motion by the WAVE-complex, which can in turn be activated by the combination of PIP3 and GTP-bound Rac1. Some types of receptors, i.e. GPCRs, can also recruit WAVE to the plasma membrane directly. However, RTKs can't interact with WAVE and require signal conveyance by lamellipodin and phosphoinositides. Lamellipodin can bind to some RTKs, e.g. EGFR, but also associate with PI(3,4)P_2 via its PH-domain. Simultaneously, PI(3,4,5)P_3 and PI(3,4)P_2 enable activation of Rac-GEFs like PREX1, TIAM1, SOS and VAV2, which transpose Rac1 into its active, GTP-bound state.

Alternatively- or additionally- WAVE can also be activated via tyrosine phosphorylation by protein kinases like ABL and Src, themselves activated after RTK-stimulation. Not only tyrosine phosphorylation, but also serine and threonine phosphorylation by JNKs and ERKs, contribute to WAVE function (Krause and Gautreau, 2014).

1.6 5'phosphatases in PI3K-AKT-signalling

Ten different phosphoinositide 5' phosphatases have been described so far, among them the widely expressed SHIP2, hematopoietic system-specific SHIP1, and Synaptojanin 1 and 2. They generally dephosphorylate membrane-bound PI(3,4,5)P_3 and PI(4,5)P_2 as well as soluble In(1,2,3,4,5)P_5, In(1,3,4,5)P_4 and In(1,4,5,6)P_4 at the 5' position, with different specificities (31). In contrast to PI(4,5)P_2, the 5' phosphatase product PI(3,4)P_2 has been shown to have AKT-activating potential. The PH-domain of AKT even has a stronger affinity to PI(3,4)P_2 than PI(3,4,5)P_3. The two-PIP-hypothesis postulates that maximum AKT-activation is achieved in the presence of high PI(3,4,5)P_3 and PI(3,4)P_2 levels. Whether effects of the tumor suppressive reduction of PI(3,4,5)P_3 -levels, or the oncogenic production of PI(3,4)P_2 prevail, seems to depend on the specific signaling context (Kerr, 2011). However, it should also be considered that the function of different types of 5'phosphatases is not determined solely by their phosphatase activity, but also by their interaction with other proteins. Due to their diverse protein structures, their set of interaction partners can vary widely (Hakim et al., 2012).

1.7.1 Properties and regulation of SHIP1

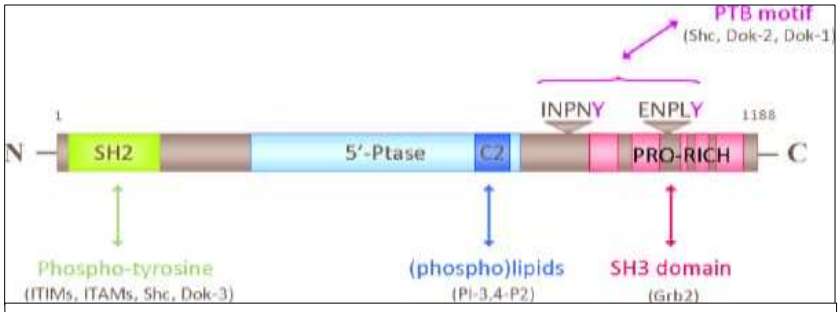

Figure 2: SHIP1, from Condé et al., 2011

SHIP1 is a 145kDa, 1188bp protein encoded by the INPP5D gene on chromosome 2. Under physiological conditions, it is expressed exclusively in hematopoietic cells, bone cells, and mesenchymal stem cells. It consists of an N-terminal SH2-domain, central catalytic 5'phosphatase domain, and in the C-terminal region a proline rich region and two phosphorylable tyrosine residues. Besides PI(3,4,5)P_3, the catalytic domain has also been shown to recognize Ins(1,3,4,5)P_4, as well as In(1,3,4,5)P_4, In(2,3,4,5)P_4 with high affinity and dephosphorylate them at the 5' position (Conde et al., 2011) (Viernes et al., 2014) (Nelson et al., 2020). Phosphorylation at the D6-position is unfavorable, leading to a weak catalytic activity of SHIP1 on In(1,4,5,6)P_4 and In(2,4,5,6)P_4, and none on In(1,2,3,5,6)P_5 (Nelson et al., 2020). The SH2-domain allows association with phosphorylated tyrosine residues of receptor tyrosine kinases and other proteins like Shc and Dok3. Meanwhile, the proline rich motif can bind to proteins with SH3-domains such as Grb2, and the phosphorylable tyrosines connect with PTB-domains i.e. of Shc, Dok1 and 2, when phosphorylated (Conde et al., 2011).

Phosphorylation of tyrosine residues in the C-terminal region is likely performed by Src-family kinases, among others, subsequent to receptor stimulation. While tyrosine phosphorylation doesn't seem to influence catalysis, it was shown to regulate SHIP1 activity by enabling interaction with other proteins as well as inducing polyubiquitination and subsequently degradation (Ruschmann et al., 2010). That being said, SHIP1 is supposed to have a phosphorylable serine residue in its catalytic domain, which might alter catalytic activity directly (Edimo et al., 2012). SHIP1 being an allosteric enzyme, catalytic activity can also be enhanced by association of its product t $PI(3,4)P_2$ o a C2-domain within its phosphatase domain (Conde et al., 2011). Another mode of modulation is upregulation of SHIP1 mRNA and protein levels in response to cytokines, i.e. TGF-ß (Sly et al., 2003). Post-transcriptional downregulation can occur as a result of mRNA destabilization or translation inhibition. Specifically, SHIP1 expression was shown to be curbed by increased levels of miR155 in the context of malignant and autoimmune diseases (Mraz and Kipps, 2013).

1.7.2 SHIP1 in the hematopoietic system

Present in leucocytes, SHIP1 is an important modulator of hematopoiesis and immune function. Soon after SHIP's discovery, experiments were conducted with SHIP1-knockout mice to elucidate its specific functions in blood cells. Both the myeloid and lymphoid compartment of these mice were strongly affected, leading to a myeloproliferative disorder- like phenotype, splenomegaly, lymphadenopathy, and mucosal inflammation of lungs and small intestine. Pronounced myeloid lung infiltration caused premature death (Conde et al., 2011) (Park et al., 2014).

In the myeloid compartment, SHIP1 was shown to negatively regulate M-CSF-induced monocyte and macrophage proliferation, differentiation and survival. In the absence of SHIP1, monocytes become hypersensitive to M-CSF, giving rise to myeloproliferation (Baran et al., 2003) (Conde et al., 2011). In addition to counteracting proliferation and survival, it is also involved in macrophage skewing. Upon stimulation with IL4, SHIP1 is tyrosine phosphorylated, polyubiquitinated and degraded. The subsequently increased levels of $PI(3,4,5)P_3$ promote skewing towards the anti-inflammatory M2 type instead of the pro-inflammatory M1 (Conde et al., 2011). Moreover, SHIP1 is essential for the induction of endotoxin tolerance by inhibiting the production of pro-inflammatory cytokines upon LPS-induced TLR4-activation. Endotoxin tolerance is essential to avoid sepsis caused by immune overactivation in case of maintained systemic inflammation. SHIP1-ko mice turned out to be overresponsive to LPS and unable to induce endotoxin tolerance. Besides macrophages, also mast cells and natural killer cells depend on SHIP1-activity for normal function. In mast cells, SHIP1 was shown to inhibit IgE-stimulated degranulation and production of inflammatory cytokines. In NK-cells, SHIP1 reduces

cytotoxicity and production of IFN-y, both mediated by activation of CD16-receptors, by decreasing PI(3,4,5)P_3 levels (Conde et al., 2011).

Functions of the lymphoid compartment are significantly modulated by SHIP1-activity, too. In B-cells, SHIP1 participates in negative regulation of B-cell-receptor signaling in several ways, by means of its catalytic activity but also as an adapter for other proteins. Activation of BCRs by antigens and signaling via adjacent cascades is crucial for B-cell expansion and antibody production (Conde et al., 2011). Accordingly, B-cells of SHIP1-ko mice were more responsive to antigen. Numbers of mature B-cells were increased in the periphery, but progenitors reduced in the bone marrow. Compromised B-cell development, however, is assumed to be caused by SHIP1-deficiency in the bone marrow environment (Conde et al., 2011) (Kerr, 2011). Similarly, SHIP1 is also involved in negative T-cell-receptor signaling in T-cells. Yet, specific functional aberrations in SHIP1-deficient T-cells have not been reported. In germline, but not T-cell specific SHIP1-ko mice, T-cells were reduced in numbers, more frequently T-reg differentiated and CD4+ cells less responsive. The latter merely exhibited reduced Th2-response, indicating that the other effects were caused by a SHIP1-deficient and inflammatory environment (Conde et al., 2011) (Kerr, 2011).

Mucosal inflammation and myeloid infiltration of the lungs limited the lifespan of germline SHIP1-deficient mice. Their distal ileums were affected in a similar way, reminding of Crohn's disease. However, myeloid-restricted SHIP1-knockout was not sufficient to generate this phenotype. Rather, the lack of CD4+ and CD8+ at mucosal sites seemed to drive myeloid infiltration and inflammation (Maxwell et al., 2014).

1.7.3 SHIP1 function in bone formation

The fact that SHIP1-ko mice also developed severe osteoporosis indicated that apart from hematopoiesis, SHIP1 also participates in bone formation and homeostasis. This was first explained with increased M-CSF-induced proliferation of, and bone resorption by, osteoclasts, a specific type of macrophages (Iyer et al., 2013). Yet, myeloid-restricted SHIP1-deletion did not result in hyper-resorptive macrophages, leading to the assumption that defective differentiation of mesenchymal stem cells into osteoblasts and chondrocytes may be the major cause (So et al., 2020).

In the course of bone formation, mesenchymal stem cells differentiate into chondrocytes, which over time hypertrophy and initiate angiogenesis, allowing the influx of osteoblast progenitors. In this process, hypoxia is an important driver for chondrocyte proliferation and differentiation by regulating the expression of specific genes. Generating PI(3,4)P_2, SHIP1 was shown to raise AKT-phosphorylation in hypoxic mesenchymal stem cells. Accordingly, SHIP1-deficiency lead to reduced proliferation in a hypoxic environment.

In SHIP1-ko mice, chondrocyte hypertrophy and vessel invasion occurred earlier than in wild type mice, resulting in smaller skeletons and a disordered bone structure (So et al., 2020).

It should be considered that besides skeleton formation, the bone environment is also involved in supporting the hematopoietic niche. Disturbances in mesenchymal stem cell proliferation and differentiation is assumedly co-responsible for some of the above-described effects of germline SHIP1-deficiency on the hematopoietic system (Iyer et al., 2013) (So et al., 2020).

1.7.4 SHIP1 in cancer…

As part of the PI3K-AKT pathway, often hyperactivated in malignancies, SHIP1 seems to be a likely candidate for participation in carcinogenesis. But considering that both its substrate $PI(3,4,5)P_3$ as well as its product $PI(3,4)P_2$ were shown to promote AKT-activation, it is not obvious whether SHIP1 exerts tumor suppressive or oncogenic influence, if altered in function.

1.7.4.1 …Of the hematopoietic system

Early research on SHIP1 in malignancies has focused on the hematopoietic system, where SHIP1 is physiologically expressed. Indeed, downregulation of expression and loss of function have been described in various types of leukemia and lymphoma. In CML, mostly associated with expression of the BCR-ABL oncogene, SHIP1 levels are frequently lowered. SHIP1 is exceedingly tyrosine phosphorylated either by BCR-ABL directly or by a BCR-ABL activated Src-family kinase, which leads to increased polyubiquitination and eventually degradation (Conde et al., 2011) (etc.). Downmodulation of SHIP1 expression as a consequence of increased miRNA155 levels was described in CLL, especially in aggressive types. What is more, targeting miRNA-155 by anti-sense oligonucleotides inhibited proliferation of B-CLL cells. (Mraz and Kipps, 2013). In MPN (myeloproliferative neoplasia), which include CML, ET (essential thrombocytemia), PV (polycythemia vera) and PMF (primary myelofibrosis), a mutation of JAK2 has been shown to downregulate SHIP1 protein expression, thereby raising PI3K-AKT signaling (Glück et al, 2022).

Not only chronic, but also acute leukemia are associated with SHIP1 loss or defects. In 50-70% of AML cases, the PI3K-AKT pathway is hyperactivated and SHIP1-expression was shown to be reduced in some patients, apparently as a result of targeting by miRNA-155 as well (Xue et al., 2014). Possibly, increased tyrosine phosphorylation by protein kinases like Flt3 and c-Kit is also involved in depleting SHIP1 (Metzner et al., 2009). Occasionally, its enzymatic activity is compromised by punctual missense mutations in the catalytic domain (Brauer et al., 2012). Overexpression of SHIP1 in patient-derived AML

cells inhibited growth factor-induced proliferation (Metzner et al., 2009). Also, SHIP1-overexpression in an AML cell line improved survival in a mouse experiment compared to an enzymatically inactive SHIP1-mutation and the negative control (Tager et al., 2017). In a study on primary T-ALL, SHIP1 was shortened or conspicuous by its absence in some samples. Probably, deletions, insertions and alternative splicing had produced truncated, inactive SHIP1 versions (Lo et al., 2009). In a more recent study, SHIP1 was not lost but downregulated on mRNA level in 6/8 T-ALL samples, which was associated with increased PI3K-AKT signaling. Reconstitution of SHIP1 in the Jurkat leukemia cell line, which is deficient in PTEN, led to a reduction in PI(3,4,5)P_3-dependent signaling, MAPK signaling, calcium signaling and expression of certain RTK subfamilies. Their proliferation was reduced in vitro as well as in vivo, and after several weeks in cell culture, SHIP1 expression was significantly downregulated (Ehm et al, 2023). Based on these findings, a number of inhibitors of PI3K-AKT signaling have been tested on ALL cells. A combination therapy of an AKT-inhibitor, mTOR inhibitor and tyrosine kinase inhibitor seems promising in vitro, preventing the mechanisms of cellular resistance that quickly arise under monotherapies (Ehm et al, 2022). Another possible therapeutic approach is the inhibition of the tyrosine kinases BCR-ABL and Flt3 as well as Src kinases, all of which are frequently involved in the depletion of SHIP1 in ALL (Ehm et al, 2023). Leukemias induced by infections also presented with alterations in SHIP1 expression, i.e. adult T-cell leukemia (ATLL), which is triggered by HTLV1-infection. Infected T-cells express the viral protein Tax, which suppresses SHIP1-expression via the transcription factor NFkB (Conde et al., 2011) (etc).

Taken together, these findings established SHIP1 as a tumor suppressor in the hematopoietic system, which is in line with the myeloproliferative phenotype of SHIP1-ko mice. They also make SHIP1 induction, or reconstitution of SHIP1-expression, a promising new approach for leukemia treatment. Knocking down miRNA-155 with siRNA in AML cells was demonstrated to raise SHIP1-levels and reduced AKT-phosphorylation. Another study has identified miRNA-155 as a potential therapeutic target in pediatric Hepatitis C virus (HCV4-) associated ALL (Hassan et al., 2020). Also, the SHIP1 activator AQX-453 has recently been tested on primary CLL and diffuse large B-cell lymphoma (DLBCL) cells in vitro, leading to enhanced apoptosis in the former and inhibited proliferation in the latter (Lemm et al., 2020). Interestingly, both SHIP1-activation with the agonist AQX-MN100 (Kennah et al., 2009) and SHIP1-inhibition with the selective inhibitor 3AC have led to cell cycle arrest and apoptosis in multiple myeloma cells (Fuhler et al., 2012). This indicates that activation of SHIP1, as well as inhibition- when regularly expressed- has adverse effects on malign hematopoietic cells. Probably, the respective signaling context and subsequently the balance of PI(3,4,5)P3 and PI(3,4)P2 are decisive, since according to the

two-PIP-hypothesis, both phosphoinositides are necessary for maximum AKT-activation (Fernandes et al., 2013).

1.7.4.2 … Outside of the hematopoietic system

Considering that SHIP1 is not physiologically expressed outside of the hematopoietic system and mesenchymal stem cells, and can have both inhibiting and enhancing effects on AKT-activation, its role in solid tumors is still ambiguous. Other phosphoinositide 5'phosphatases have already been discussed in this context. The SHIP1-homologue SHIP2, physiologically involved in insulin signaling, was associated with EGFR-stabilization, EGF-mediated AKT-activation, migration and adhesion in breast cancer cells. SHIP2-silencing decreased EGF-induced and unstimulated pAKT levels, as well as overall AKT-expression. Both surface adhesion and migration turned out to be decelerated. The authors traced these effects back to maintained EGFR-signaling and suggested interactions of SHIP2 with other proteins to be implicated in AKT stabilization (Prasad, 2009). (Prasad, 2009)

Oncogenic potential has also been attributed to Synaptojanin 2, which participates in the development of clathrin-coated pits and possibly also the ensuing stages of endocytosis. Synaptojanin 2 interacts with the small GTPase Rac1- known to promote invasion and metastasis- suggesting Synaptojanin 2 to be involved in metastasis, too. Actually, Synaptojanin 2-knockdown curbed Matrigel invasion to a similar extent as Rac1-knockdown in glioblastoma as well as lung and breast cancer cells. Also, lamellipodia and invadopodia were inhibited in glioblastoma cells, though to a lesser degree than with Rac1-knockdown (Chuang et al., 2004). The phosphoinositide 5'phosphatase PIB5PA, on the other hand, was observed to be downregulated in melanoma. Overexpressed, it reduced viability and proliferation in melanoma cells (Ye et al., 2013). Similarly, PIPP- also called INPP5J- has been ascribed tumor suppressive qualities in melanoma. It was demonstrated to reduce AKT-phosphorylation and cell viability of melanoma cells in vitro, as well as proliferation both in vitro and in vivo, when overexpressed (Myers et al., 1998).

SHIP1 itself is ectopically expressed in some solid tumor entities, i.e. in about 60% of examined colorectal carcinoma samples (Schaks et al., 2020). In metastases of colorectal cancers, expression levels were observed to be higher than in the primary tumors (Ehm et al, 2023). The frequency of ectopic expression raises the question whether SHIP1 confers an advantage to the cancer cells, or merely constitutes a "passenger mutation", a byproduct of genomic instability. SHIP1-expression in the investigated colorectal carcinoma samples had no impact on patient survival and was negatively correlated with tumor grading, lymph node metastasis and vascular invasion (Schaks et al., 2020). Trials with colorectal cancer cells showed a slightly decreased proliferation, but also significantly

accelerated migration upon SHIP1-overexpression in one of two cell lines compared to the control (Allgöwer-Martin, 2015). In CRC-derived cells with intrinsic SHIP1-expression, on the other hand, SHIP1-inhibition enhanced cell death by accumulation of reactive oxygen species as a result of PI3K-AKT hyperactivation. These findings spawned the hypothesis that, contrary to the assumption that more PI3K-AKT signaling is always better, CRC cells benefit from SHIP1 expression, because it allows them to fine-tune PI3K-AKT signaling and avoid cell death by overactivation (Ehm et al, 2023).

Besides colorectal carcinoma, SHIP1-expression has also been studied in non-small cell lung cancer (NSCLC). In NSCLC samples, SHIP1-expression was reduced by contrast with normal lung tissue and a bronchial epithelial cell line. Low SHIP1 levels were associated with poor survival, more advanced stages and higher T and N classifications. High SHIP1 levels decreased expression of cell cycle and EMT-related proteins and hampered cell migration in NSCLC cell lines (Fu et al., 2019).

In view of the findings on PIB5PA and PIPP, SHIP1 has been speculated to have tumor suppressive properties in melanomas, too. SHIP1-expression has been observed in 14% of all analyzed melanoma samples (Drechsel, 2019), and mutations in the INPP5D-gene are found in 5,9% of entries in the COSMIC database (Drechsel, 2019) . Both wild type SHIP1 and leukemia-derived SHIP1-mutants with impaired catalytic activity have been overexpressed in melanoma cell lines to investigate their localization in the cells as well as consequences for proliferation, migration and chemotaxis. SHIP1 turned out to inhibit proliferation in two of three cell lines, while the SHIP1 mutant Y643H- with enzymatic activity reduced by over 80%- enhanced it in all three cell lines. Expression of the catalytically inactive mutant R673Q yielded significantly slower proliferation than Y643H. The mutants accelerated migration in all cell lines, while wild type SHIP1 had diverging effects. Both mutants showed a higher ratio of membrane association than wild type SHIP1 in two out of three cell lines (Drechsel, 2019).

1.7.4.3 Substrate Trapping

The presence of catalytically less or in-active SHIP1-mutants in AML samples posed the question how they affect PI3K-AKT-signaling. Findings on catalytically impaired PTEN-, and later on also SHIP1-mutants have suggested that reduced enzymatic activity can lead to delayed dissociation of the enzyme-substrate/product-complex. Consequently, these SHIP1-mutants may form more stable associations with $PI(3,4,5)P_3$ and thereby protect it from degradation by other phosphoinositide phosphatases like PTEN or SHIP2. Heightened $PI(3,4,5)P_3$ -levels may then lead to increased activation of AKT and its downstream effectors (Myers et al., 1998) (Luo et al., 2003). Accordingly, this model- called “substrate trapping”- ascribes oncogenic potential to catalytically less active mutants. To trap their

substrate, SHIP1-mutants would be expected to be localized at the cell membrane at a higher ratio than wild type SHIP1 (Drechsel, 2019).

1.8 Project outline

This thesis aims at further elucidating the role of wild type SHIP1 and SHIP1-mutants with impaired catalytic activity in the development and progression of solid tumors. Wild type SHIP1 and the mutant R673Q have been overexpressed in a colorectal carcinoma cell line (HCT116) without endogenous SHIP1. In addition, two melanoma cell lines (WM164 and WM793), which had previously been stably transduced with wild type SHIP1 as well as R673Q and Y643H, were examined. AKT-phosphorylation was quantified by Western Blot and cellular localization of SHIP1 and mutants analyzed with membrane fractionation and confocal microscopy.

The impact of SHIP1 and mutants on proliferation, migration and invasion has been examined with IncuCyte live cell imaging. Moreover, the cell lines have been treated with the Rac1-inhibitor NSC23766, to further analyze signal transduction downstream of AKT. To validate the findings of Rac1-inhibition, a transient Rac1-knockdown has been conducted in one cell line, and migration measured.

2 Materials and Methods

2.1 Materials

2.1.1 Devices

Autoclave:	Evo 120, MediTech (Wedemark, Germany)
Cell counter:	Countess II FL Automated Cell Counter, Fisher Scientific (Waltham, MA, USA)
Cell counting chamber:	Neubauer, Braun (Melsungen, Germany)
Centrifuges:	5415 C, 5415 D, 5415 R, Eppendorf (Hamburg, Germany); Varifuge 3.0R, Heraeus (Hanau, Germany); L60-Ultracentrifuge Beckman Coulter (Unterschleißheim, Germany)
Centrifuge cups:	80Ti centrifuge tubes, Beckman Coulter (Unterschleißheim, Germany)
Fluorescence microscope:	HBO50/AC, Zeiss (Oberkochen, Germany)
Gel electrophoresis chamber:	SE 600 Cooled Vertical Electrophoresis Unit, 18x16cm , Hoefer (Boston, MA, USA)
Glassware:	Schott (Mainz, Germany)
Heating block:	Eppendorf Thermomixer 5426, Eppendorf (Hamburg, Germany)
Heating panel/ magnetic stirrer:	Ikamag RH, IKA laboratory equipment (Staufen, Germany); MR 1, Heidolph (Gleichen, Germany)
Horizontal shaker:	Rocky N, Fröbel laboratory equipment (Lindau, Germany)
Incubator (cell culture):	Heraeus (Hanau, Germany)
Incubator (IncuCyte):	Panasonic
Incubator shaker:	Model G25 Incubator Shaker, New Brunswick Scientific Co.Inc (Edison, New Jersey, USA)
Live cell imager:	Incucyte Zoom S3 live-cell analysis system, Sartorius, Essen BioScience (Ann Arbor, Michigan, USA)
Light microscope:	Labovert, Leitz (Stuttgart, Germany)
Luminescent Image Analyzer:	LAS-3000, Fujifilm (Düsseldorf, Germany) LAS-4000, Fujifilm (Düsseldorf, Germany)
Microtitre plate reader:	Infinite M200, Tecan (Männedorf, Germany)
Nanodrop 2000c:	Thermo Fisher Scientific (Waltham, MA, USA)

Pipets:	0,5-10, 2-20, 10-100, 20-200, 100-1000 µl, Eppendorf Research, (Hamburg, Germany)
Pipetting aid:	Accu-jet pro, Brand (Wertheim, Germany)
pH meter:	CG 820, Schott-Devices (Ludwigshafen, Germany)
pH electrode:	SenTix 21 (WTW, Weilheim, Germany)
Powering devices:	PowerPac universal, PowerPac 200, Biorad (Munich, Germany)
Precision scale:	UniBloc, Shimadzu (Duisburg, Germany)
Rotors:	80Ti, Beckman Coulter (Unterschleißheim, Germany)
Safety workbench class II:	HERA safe Type HS 12, Heraeus (Hanau, Germany)
Scale:	Type PM 2000, Mettler (Gießen, Germany)
Sonifier:	BRANSON Sonifier 450, Branson Ultrasonics (Danbury, USA)
Transfer cell:	Trans-Blot Electrophoretic Transfer Cell, Bio-Rad (Munich, Germany)
Ultra centrifuge tubes:	80Ti Centrifuge Tubes, Beckman (Unterschleißheim, Germany)
Ultrapure water system:	Synergy UV, Millipore (Schwallbach, Germany)
Vortexer:	MS2 Minishaker IKA-Werk (Staufen, Germany)
Water bath:	Type 1002; Typ 1012 GFL (Burgwedel, Germany)
Wound maker:	IncuCyte Zoom S3 live-cell analysis system, Sartorius, Essen BioScience (Ann Arbor, Michigan, USA)

2.1.2 Consumables

Cell culture flasks:	T 25 (25 cm^2) flasks, Greiner bio-one; Sarstedt (Nümbrecht, Germany)
	T75 (75 cm^2) flasks, Greiner bio-one; Sarstedt (Nümbrecht, Germany)
	T175 (175 cm^2) flasks, Greiner bio-one; Sarstedt (Nümbrecht, Germany)
Cell culture plates:	6-Well, Greiner bio-one; Sarstedt (Nümbrecht, Germany)
	12-Well, Greiner bio-one; Sarstedt (Nümbrecht, Germany)
	96-Well, Greiner bio-one; Sarstedt (Nümbrecht, Germany)

	96-well Incucyte Imagelock plates, Sartorius, Essen BioScience (Ann Arbor, Michigan, USA) TC-dish, 100 mm, Standard; Sarstedt (Nümbrecht, Germany) µ-Slide 4-well, standard bottom; ibidi (Munich, Germany)
Coverslips:	Laboratory Glassware, Superior-Marienfeld (Lauda-Königshofen, Germany)
Cryotubes:	Cryotube vials 1ml, Thermo Fisher Scientific (Waltham, MA, USA)
Disposable pipets:	5, 10, 25 and 50ml serological pipettes, Sarsted (Nümbrecht, Germany)
Filters:	Acrodisc 25mm syringe filter w/0.45µm HT Tuffryn membrane, Pall Corporation (New York, USA)
Nitrocellulose membrane:	Amersham Protran 0.45µm NC; 0.45µm 300mm x 4m; Amersham / GE Healthcare; (Amersham, England)
Pipet tips:	10, 200, 1000µl Eppendorf (Hamburg, Germany)
Syringes:	Injekt 10ml, Braun (Melsungen, Germany)
Test tubes:	1,5 und 2,0ml, Eppendorf (Hamburg, Germany) 15 und 50ml tubes, Sarstedt (Nümbrecht, Germany)
Whatman paper:	Whatman 460 x 570mm; GE Healthcare; (Amersham, England)

2.1.3 Chemicals

Unless otherwise specified, chemicals were sourced from Merck (Darmstadt, Germany), Invitrogen/ Thermo Fisher Scientific (Karlsruhe, Germany), Roth (Karlsruhe, Germany), Serva (Heidelberg, Germany) and Sigma-Aldrich (Taufenkirchen, Germany).

2.1.4 Buffers and solutions

Blocking solution:	25g skimmed milk powder, 0,5% Tween-TBS ad 0,5L
LB-broth agar plates:	250ml LB-Broth medium; 3,75g agar
LB-broth medium:	6,25g LB-Broth; 250ml H2O
3x Loading buffer:	18ml Tris-HCl pH 6,8; 23,8ml 25%-SDS; 28ml 87%-Glycerol; 5ml 10%-bromphenol blue add DTT before use 3:7
NP40 lysis buffer (10ml):	0,82ml ddH2O; 2,5ml 0,2m Hepes 7,5; 0,3ml 5m NaCl; 0,5ml 20% NP40; 0,2ml aprotinin; 80µl 250mm EDTA;

	1ml 500mm NaF; 1ml 100mm NaPP1; 2,5ml 40% glycerin; 1ml 10mm vanadate; 0,1ml 100mm pefabloc
1x PBS pH 7,4:	8g NaCl; 0,2g KCl; 1,78g Na2HPO4 x 2H2O; 0,24g KH2PO4 x 2H2O; filled up to 1L with ddH2O; pH adjusted to 7,35-7,45 with NaOH if necessary
10x Running buffer:	144g glycine; 30g Trizma Base; ad 1L ddH2O
Running buffer SDS-Page:	300ml 10x running buffer; 30ml 10% SDS; 2670ml ddH2O
Running gel 10% (2x):	4,25ml ddH2O; 5,635ml 1M Tris pH 8,8; 5ml 30% acrylamide; 150µl 10% SDS; 20µl TEMED, 100µl 10% APS
Stacking gel (2x):	6,9ml ddH2O; 1,9ml 2M Tris pH6,8; 1,34ml 30% acrylamide; 100ml 10% SDS; 5µl TEMED, 150µl 10% APS
10xTBS (1L):	84,15g NaCl; 100ml 1M Tris-HCl pH 8,0; filled up to 1L with ddH2O
TBS-Tween:	5ml Tween 20; 995ml TBS
Transfer buffer:	300ml 10x running buffer; 600ml methanol; 30ml 10% SDS; 2070ml ddH2O
Washing solution:	12,5g skimmed milk powder, 0,5% Tween-TBS ad 0,5L

2.1.5 Kits, markers and reagents

DC protein assay:	Bio-Rad (Munich, Germany)
LB-Broth medium:	Difco LB-Broth, Miller (Luria-Bertani), Becton, Dickinson and Company (Le Pont de Caix, France)
Matrigel:	Corning Matrigel Matrix, Corning (Corning, NY, USA)
NucleoBond Xtra:	Macherey-Nagel (Düren, Germany)
Prestained protein marker:	SpektraTM Multicolor Broad Range Protein Ladder, (SM1841) Fermantas (Burlington, Canada)
Protease inhibitor:	cOmplete, mini protease inhibitor cocktail, Roche (Mannheim, Germany)
Super Signal West Dura chemiluminescence substrate kit:	SuperSignal West Pico Chemiluminescent Substrate and SuperSignal West Dura Extended Duration

	Substrate, Thermo Fisher Scientific (Waltham, MA, USA)
Transfection reagents:	Lipofectamine 2000-/ 3000- reagent, gibco, Thermo Fisher Scientific (Waltham, MA, USA)
	P2000/ P3000 reagent, gibco, Thermo Fisher Scientific (Waltham, MA, USA)
Trypan blue solution:	Sigma-Aldrich (Taufkirchen, Germany)
Trypsin/EDTA in PBS:	0,05% trypsin-EDTA, gibco, Thermo Fisher Scientific (Waltham, MA, USA)

2.1.6 Antibodies

Primary antibodies:	SHIP1 (P1C1), [sc-8425], Santa Cruz Biotechnology (Heidelberg, Germany)
	Rac1 purified mouse monoclonal antibody, BD Biosciences (Waltham, MA, USA)
	Rac1b purified rabbit polyclonal antibody, Merck Millipore (Billerica, MA, USA)
	HSC70 (B-6), [sc-7298], Santa Cruz Biotechnology (Heidelberg, Germany)
	GAPDH (6C5), [sc-32233], Santa Cruz Biotechnology (Heidelberg, Germany)
	Phospho-Akt (S473/D9E) #4060S, rabbit monoclonal antibody, Cell Signaling Technology (Beverly, MA, USA)
	CD-109 (C-9), [sc-271085], mouse monoclonal antibody, Santa Cruz Biotechnology (Heidelberg, Germany)
	EGFR, #2232, Cell Signaling Technology (Beverly, MA, USA)
	Anti-HA High Affinity (Ref: 11867423001), Roche, (Mannheim, Germany)
Secondary antibodies:	anti-mouse IgG, HRP-linked antibody, #7076, Cell Signaling Technology (Beverly, MA, USA)
	anti-rabbit-IgG HRP-linked antibody, #7074, Cell Signaling Technology (Beverly, MA, USA)

2.1.7 Cell culture media and additives

Medium for parental cells:	Dulbecco′s Modified Eagle′s Medium (DMEM) 10% fetal calf serum (FCS) 1% penicillin/ streptomycin G
Medium for transduced cells:	Dulbecco′s Modified Eagle′s Medium (DMEM) 10 % fetal calf serum (FCS) 1 % Penicillin/ Streptomycin G 1,5 µg/ml Puromycin
Medium for HEK293-cells:	Dulbecco′s Modified Eagle′s Medium (DMEM) 10 % fetal calf serum (FCS) 1 % Penicillin/ Streptomycin G 1% NaPy; 2% L-Glutamin; 2% Hepes
Freezing medium:	90% FCS; 10% DMSO
DMEM:	GIBCO, Thermo Fisher Scientifc (Waltham, MA, USA)
FCS:	GIBCO, Thermo Fisher Scientific (Waltham, MA, USA)
Penicillin/ streptomycin:	GIBCO, Thermo Fisher Scientific (Waltham, MA, USA)
Puromycin:	Sigma-Aldrich (Taufenkirchen, Germany)

2.1.8 Inhibitors

Rac1-Inhibitor:	NSC23766; Calbiochem/ Merck-Millipore (Darmstadt, Germany)

2.1.9 Vectors

SHIP1-WT:	pLeGO-iG2 Puro(+)-HA-hSHIP1wt
SHIP1-R673Q:	pLeGO-iG2 Puro(+)-HA-hSHIP1-R673Q
Lego/ control:	control vector LeGo-iG2 Puro

2.1.10 siRNA

anti-Rac1:	Hs_RAC1_6; Flexitube Gene Solution GS5879 for Rac1; Qiagen (Venlo, Netherlands)
Scr/ control:	AllStars negative control siRNA; Qiagen (Venlo, Netherlands)
anti-Rac1b:	Stealth siRNA from set of three validated siRNAs targeting TGFBR1; Life Technologies (Thermo Fisher Scientific, Waltham, MA, USA); supplied by Prof. Dr. Hendrik Ungefroren, UKSH Lübeck

Scr/ control:	Stealth siRNA negative control; Life Technologies (Thermo Fisher Scientific, Waltham, MA, USA); supplied by Prof. Dr. Hendrik Ungefroren, UKSH Lübeck

2.1.11 Cell lines

HCT116:	Human colorectal carcinoma cell line, male (Brattain et al., 1981) with constitutively activated PI3K- and RAS/RAF/ERK- signaling pathways, SHIP1-deficient
HCT116 lego:	Parental HCT116 cells transduced with control vector Lego-IG2; selected by puromycin resistance
HCT116 SHIP1-wt:	Parental HCT116 cells transduced with pLeGO-iG2 Puro(+)-HA-hSHIP1wt; selected by puromycin resistance, SHIP1-expression verified by western blotting
HCT116 SHIP1-R673Q:	Parental HCT116 cells transduced with pLeGO-iG2 Puro(+)-HA-hSHIP1-R673Q, selected by puromycin resistance, SHIP1-expression verified by western blotting
WM793:	Human melanoma cell line, male, with BRAF-mutation, (Herlyn et al., 1985) (Smalley et al., 2006), SHIP1-deficient
WM793 lego:	Parental WM793 cells transduced with control vector lego-IG2 and selected by puromycin resistance (obtained from Oliver Drechsel)
WM793 SHIP1-wt:	Parental WM793 cells transduced with pLeGO-iG2 Puro(+)-HA-hSHIP1wt and selected by puromycin resistance (obtained from Oliver Drechsel)
WM793 SHIP1-R673Q:	Parental WM793 cells transduced with pLeGO-iG2 Puro(+)-HA-hSHIP1-R673Q and selected by puromycin resistance (obtained from Oliver Drechsel)
WM793 SHIP1-Y643H:	Parental WM793 cells transduced with pLeGO-iG2 Puro(+)-HA-hSHIP1-Y643H and selected by puromycin resistance (obtained from Oliver Drechsel)

WM164:	Human Lymph node melanoma metastasis cell line, male, with BRAF-mutation, (Herlyn et al., 1985) (Smalley et al., 2006), SHIP1-deficient
WM164 lego:	Parental WM793 cells transduced with control vector lego-IG2 and selected by puromycin resistance (obtained from Oliver Drechsel)
WM164 SHIP1-wt:	Parental WM164 cells transduced with pLeGO-iG2 Puro(+)-HA-hSHIP1wt and selected by puromycin resistance (obtained from Oliver Drechsel)
WM164 SHIP1-R673Q:	Parental WM164 cells transduced with pLeGO-iG2 Puro(+)-HA-hSHIP1-R673Q and selected by puromycin resistance (obtained from Oliver Drechsel)
WM164 SHIP1-Y643H:	Parental WM164 cells transduced with pLeGO-iG2 Puro(+)-HA-hSHIP1-Y643H and selected by puromycin resistance (obtained from Oliver Drechsel)
HEK293T:	Human embryonic kidney cell line; transformed by sheared fragments of adenovirus type 5 DNA (Graham et al., 1977)
Xl1 Blue (E. coli bacteria):	Pierce Thermo Fisher Scientific (Waltham, MA, USA)

2.1.12 Software

AIDA Image Analyzer:	Version 3.44
Endnote	Version X9
FIJI (Imagej)	downloaded 12/2020
Graphpad Prism:	Version 8.2
Microsoft Office Home and Student 2018	
Biorender	

2.2 Methods

2.2.1 Cell defrosting, cultivation and freezing

All cell culture procedures posing a risk of contaminating the cells were performed under a stage 2 safety bench. Disposables such as pipet tips were autoclaved and the working surface of the safety bench as well as all devices needed for cell culture tasks were cleaned with 70% ethanol prior to usage.

Cell lines intended for experiments were taken from the nitrogen tank and placed on ice. The appropriate medium (DMEM +10% FCS +1% P/S; +1,5µg/ml puromycin for previously transduced cells) was warmed up to at least room temperature before 5ml were pipetted into 15ml falcons. Cryotubes were held into a 37°C water bath until the cell suspension was almost entirely thawed. Cells were then transferred into the 15ml falcons to be centrifuged at 1400rpm for 5min. The medium was taken off, the pellet resuspended in 5ml medium and transferred into culture flasks, where another 5ml of medium were added.

Cells were routinely cultivated in T75 culture flasks with 10ml medium and split upon reaching a confluence of 80-90%. Then, the medium was taken off, cells were washed with 10ml PBS and treated with 2ml trypsin to detach them from the flask base. After incubating for 2-4 minutes, trypsin was deactivated with 4ml medium and the cell suspension thoroughly mixed by pipetting up and down. The share of cell suspension remaining in the culture flask was filled up to 10ml with medium and returned to the incubator while the other share was either used for experiments or discarded. HCT116 cells were split at a ratio of 1:10-12, WM164 at 1:8-10 and WM793 at 1:4-6 to maintain splitting intervals of 3 days.

When no longer needed for experiments, cells were frozen to be stored in the nitrogen tank again. For this purpose, the cell suspension was transferred to a 15ml falcon and centrifuged at 1400rpm for 5 minutes. The medium was taken off and the cell pellet resuspended in 0,5-1ml freezing medium (90% FCS +10% DMSO) and pipetted into a labeled 1ml cryotube. Cryotubes were placed in a freezing aid and left in a -80°C freezer for at least 24 hours before transfer to the nitrogen tank to ensure gradual freezing of the cells.

2.2.2 Stable transduction

2.2.2.1 High copy plasmid purification (Midi Prep with NucleoBond Xtra kit)

To start with, 25g LB broth base were dissolved in 1l ddH2O and the pH adjusted to 7 if necessary. One Erlenmeyer flask with 150ml LB broth was prepared for each plasmid to be transduced. Similarly, 12,5g LB broth base were dissolved in 500ml ddH2O in a Schott flask and pH adjusted, before agar granulate was added. Both the broth and agar flasks

were autoclaved. Meanwhile, 100mg/ml ampicillin solution was mixed by dissolving 1g of ampicillin in 10ml ddH2O. 500µl of this were added to the 500ml autoclaved LB agar while still warm. LB broth was stored in the fridge after autoclaving. Uncoated 10cm dishes were filled with 10ml LB agar, one for each plasmid, and given time to dry. In the meantime, 100µl competent XL1 blue cells were treated with 1µl plasmid, each (SHIP1-WT, SHIP1-R673Q, lego control, VSV-G, gag/pol), mixed by snipping, incubated on ice for 30 minutes and warmed to 42°C for 90 seconds. Then, 900µl warm LB broth were added to each tube and incubated at 37°C for 1 hour. 150µl of each plasmid/ cell mix were pipetted on LB agar plates, spread out with one-way eyelets and placed upside down in a 37°C incubator overnight. The next day, 150µl 100mg/ml ampicillin were added to each 150ml LB broth flask. A single colony was picked from each agar plate with a pipet tip, and the tips were ejected into LB broth flasks. They incubated in a shaking incubator at 37°C and 250rpm overnight. Broth opacity served as a growth control the following day. LB broth with bacteria was transferred into centrifuge cups without the pipet tips and centrifuged at 4°C and 5000rpm for 10 minutes. The supernatants were discarded while the pellets were resuspended in 8ml resuspension buffer RES + RNase A and transferred into 50ml falcon tubes. 8ml lysis buffer LYS were added to each tube, mixed by inverting and incubated for 5 minutes. Meanwhile, column filters were equilibrated with 12ml equilibration buffer EQU each. 8ml neutralization buffer NEU were added to each tube and inverted to mix, before the suspensions were pipetted on the column filters. After the suspensions had run through the column filters, they were rinsed with 5ml EQU. The filters were removed and columns washed again, this time with wash buffer WASH. Then, they were placed on new 50ml falcon tubes for DNA extraction with 5ml elution buffer ELU. Of each DNA suspension, 830µl were pipetted into six 1,5ml reaction tubes. 580µl isopropanol were added to each tube and inverted, before tubes were centrifuged at 4°C and 13200rpm for 30 minutes. The supernatants were discarded and pellets resuspended in 200µl ethanol by vortexing. Tubes were centrifuged at room temperature and 13200 rpm for 5 minutes, supernatants, again, discarded and pellets dried at room temperature with lids open. Afterwards, DNA pellets were resuspended in 20µl sterile ddH2O, soaked for 5 minutes and whirled. All tubes pertaining to one plasmid were joined, filled up with 80µl sterile ddH2O, and whirled again. DNA quantity and purity were measured with the NanoDrop 2000c at the settings “nuclein acid”, “DNA”. After a blank value was determined with water, 2µl of each DNA sample were pipetted on the black dot, the lid closed and properties measured. Quantity and purity were listed for all plasmids, and tubes were frozen at -20°C.

2.2.2.2 HEK293 transfection

1,5x10^6 HEK293T cells were seeded in 10cm dishes and incubated at 37°C overnight. The following day, a sterile 1,5ml reaction tube with 250µl DMEM was prepared for each plasmid. 2,5µg shRNA, 8µg psPAX2 (lenti gag/pol), 1µg pMD2.G (VSV-G) and 5µl P3000 were added to each tube and carefully mixed. A master mix of 7,5µl Lipofectamine and 250µl DMEM for each vector was prepared in a 15ml tube, 250µl of which were then added to each shRNA tube and incubated at room temperature for 15 minutes. Meanwhile, the medium was taken off the HEK293T-cells and replaced with 5ml DMEM+10%FCS+1% P/S. 500µl Lipofectamin/shRNA mix were added to each dish of HEK cells and given 3 hours incubation time, before the cells received another 5ml DMEM+10%FCS+1% P/S to incubate overnight. The next day, the medium (24h virus supernatant) was taken off with syringes, filtered with 0,2µm filters and filled into 15ml tubes, either for immediate treatment of target cells or storage in a -80°C freezer. Each dish of HEK cells was fed with 10ml fresh medium and returned to the incubator. The same procedure was repeated the next day.

2.2.2.3 Transduction and selection of target cells

For stable transduction, target cells were seeded in 6-well plates at a density of 2-4x10^5 cells/ well and given time to adhere overnight, so they would be semi-confluent. On the following day, virus supernatant was either taken freshly from transfected HEK293 cells (24 hours post-transfection) or, if previously bottled and stored in the -80°C freezer, defrosted on ice. The medium was taken off the target cells and replaced with 2ml virus supernatant plus 1ml regular medium. Cells in a control well received 3ml medium only. After incubating for 24 hours at 37°C, the virus supernatant/ medium was removed individually and replaced with 2ml new virus supernatant (48 hours post-transfection; either fresh or defrosted) and 1ml medium, while the control cells had new regular medium for incubating another 24 hours. The next day, virus supernatant/ medium was discarded again and the cells fed with medium containing 1,5µg/ml puromycin. Dose-dependent puromycin sensitivity had previously been determined for all utilized cell lines, so control cells could be expected to die after 3 days of treatment at the latest. From then on, all wells were examined under a microscope daily, and medium was exchanged every other day. Once sufficiently confluent, transduced cells were trypsinated and transferred to T25 or T75 culture flasks. Upon consecutive splitting, at least 5 cryotubes of transduced cells were frozen and stored in the nitrogen tank.

2.2.3 Transient transfection

For a transient transfection with siRNA, cells were seeded in a 6-well plate, so they would be 60-80% confluent the following day, and incubated overnight. The next day, after

checking confluence and cell viability, 2,5µl siRNA and 100µl Optimem (without additives) for each well were mixed, as well as 5µl lipofectamine 2000 and 100µl Optimem/ well in a second reaction tube. The two solutions were then brought together and incubated at room temperature for 20 minutes. After washing the cells with Optimem, the transfection mix plus 800µl additional Optimem were pipetted into each well and incubated for 4 hours at 37°C. Then, the transfection medium was taken off and 2ml normal medium (DMEM+ 10% FCS+ 1% P/S) added to each well. The same procedure was repeated the next day. On the third day of trial, lysates were made for expression control by western blotting, and cells were plated for live cell imaging.

2.2.4 NP40 lysates

Cells as well as tissue samples were lysed with NP40 buffer to determine protein expression by western blotting. For this purpose, cells were washed and trypsinated as usual and 5x10^6 cells seeded into 10cm dishes. The appropriate medium was added to obtain a volume of 10ml. After incubating at 37°C overnight, the cells were placed on ice while NP40 buffer was prepared- also on ice- by adding aprotinin, vanadate and pefabloc to the stock solution. The medium was then taken off the cells and a wash with cooled PBS done, before 600-1000µl of NP40, depending on confluence, were pipetted on each dish of cells. After incubating briefly, the cells were scratched off the dish base with a cell scraper and transferred into a 1,5ml reaction tube. The suspension was centrifuged at 4°C and 13000 rpm for 10 minutes. Then, the supernatant was pipetted into another reaction tube and frozen at -80°C, while the pellet was discarded.

2.2.5 Western Blotting

2.2.5.1 Protein determination

Protein determination for Western Blotting was performed with the DC protein assay of Biorad. First, a BSA calibration series with 8 concentrations (0,125mg/ml, 0,25mg/ml, 0,5mg/ml, 0,75mg/ml,1mg/ml, 1,25mg/ml and 1,5mg/ml) was dissolved in the buffer which had been used for samples. 1000µl of reagent A and 20µl of reagent S were mixed to obtain the working solution A´. Then, triplicates of the calibration series and lysates were pipetted into the wells of a microtiter plate, 5µl each, followed by 25µl of solution A´ and 200µl solution B. They were mixed thoroughly and rid of bubbles before incubating at room temperature for 15 minutes. Finally, extinction at 595nm was measured by the Tecan reader. After establishing a standard curve, the samples' protein content could be calculated.

2.2.5.2 SDS-Page

In preparation for the SDS-Page, 1x running buffer had to be mixed (300ml 10x running buffer, 30ml 10% SDS, 2670ml ddH2O) and stored at 4°C overnight. The Hoefer chamber glass plates were assembled, fixed in the brackets and checked for watertightness, before the separating gels were prepared (8,5ml ddH2O, 11,25ml Tris pH 8,8 buffer, 10ml acrylamide, 300µl 10% SDS, 200µl 10% APS, 40µl TEMED for 2 10% separating gels). 13ml gel fluid were filled into each space, covered with isopropanol and given 1,5-2 hours to polymerize. Thereafter, the isopropanol was taken off, combs put in place, the collecting gel mixed (6,9ml ddH2O; 1,9ml Tris pH 6,8; 1,34ml 30% acrylamide; 100µl 10% SDS; 150µl 10% APS and 5µl TEMED) and inserted. While the collecting gel hardened, lysates were defrosted on ice and diluted with the appropriate buffer according to their determined protein content. 300µl DTT solution were freshly added to 700µl 3x loading buffer, which was then mixed with the lysates at a ratio of 1:3. These samples were heated to 100°C for 5 minutes and briefly centrifuged. The combs were taken out and gel pockets filled with 1x running buffer, before the samples were carefully pipetted into the pockets in triplicates. The gels were transferred into the chamber, which was then filled with 1x running buffer up to the mark. If possible, bubbles at the glass plates were removed. Electrophoresis was started at a voltage of 80V, which was turned up to 120V once the migration front reached the middle of the collecting gel, and 170V at arrival in the separating gel. Finally, power was switched off shortly before the migrating front reached the end of the separating gel.

2.2.5.3 Western Blot

In preparation for western blotting, transfer buffer had to be mixed of 300ml 10x running buffer, 600ml methanol, 30ml 10% SDS and 2070ml ddH2O and stored at 4°C overnight. For each gel, one piece of nitrocellulose membrane was cut to the size 8x14cm and two pieces of whatman paper to 9x15cm. Sponges and whatman paper were soaked in transfer buffer, while nitrocellulose membranes calibrated in ddH2O. A tray was placed in a bowl filled with transfer buffer dark side down, before a black sponge, whatman paper and nitrocellulose membrane were layered on it. The gels were taken out of the chamber, rinsed with ddH2O and laid on the nitrocellulose membrane “right side up”. Another whatman paper was placed on the gel and all bubbles remaining between membrane and gel rolled out, before a white sponge was stacked on top. The closed tray was suspended, in the correct orientation, in a blotting chamber filled with transfer buffer and an agitator. The chamber was then placed on a stirring panel in the cool room, where the transfer proceeded for 2 hours at 60V. Meanwhile, 0,5% Tween TBS was mixed (11,1g Tween; 200ml 10x TBS; 1,8l ddH2O), as well as 5% blocking solution (25g skimmed milk powder;

0,5% Tween TBS ad 500ml) and 2,5% washing solution (12,5g skimmed milk powder; 0,5% Tween TBS ad 500ml). After transfer was completed, the membranes were labeled and washed with ddH2O twice to prepare for Ponceau staining. The Ponceau solution was left on the membrane until protein bands became visible. Surplus stain was washed off with ddH2O before an incident light photo was taken at the imager (LAS4000 or LAS3000). Afterwards, Ponceau stain was removed from the membrane by washing with 0,5% Tween-TBS or washing solution several times. The membrane was blocked in 5% blocking solution at room temperature for 1 hour. If desired, it could be cut into two or more pieces with a scalpel for simultaneous antibody staining. It was then incubated with primary antibody, diluted 1:1000 in washing solution, at 4°C overnight. The next day, the antibody solution was filled into a 15ml or 50ml reaction tube and stored at 4°C for reutilization. While the membrane was washed thrice for ten minutes in washing solution, the secondary antibody solution was prepared by diluting the appropriate antibody 1:5000 in washing solution. The secondary antibody incubated on the membrane for 1 hour at room temperature. Subsequently, the antibody solution was discarded, and the membrane was washed with 0,5% Tween TBS five times for 15 minutes and with 1x TBS twice for ten minutes. At the end of the washing procedure, ECL solution was prepared by mixing 500µl Pico peroxide and Pico enhancer each, with 50µl Dura peroxide and enhancer each. The membrane was laid on a foil and incubated with ECL solution for 5 minutes, before excess solution and bubbles were rolled out. Chemiluminescence was measured with the LAS4000 or LAS300 at sensitivity “super” and exposure type “precision” or “increment” for a few seconds up to several minutes, depending on the primary antibody. Images with clear, non-overexposed protein bands were saved, and later on quantified with AIDA Image Analyzer. Either HSC70 or Ponceau bands were used as loading controls.

2.2.6 Differential centrifugation

For differential centrifugation, at least one fully confluent T75 flask was needed of each cell line. Cells were washed with PBS and trypsinated as usual before being centrifuged at 4°C and 1200 rpm for five minutes. Meanwhile, the sonifyer was switched on and cooled, and digestion buffer was freshly mixed by dissolving two cOmplete protease inhibitor cocktail pills in 20 ml cooled PBS. For each cell line, about 8ml digestion buffer was needed in the course of the experiment. Cell pellets were resuspended in 2ml digestion buffer each, distributed to four reaction tubes and always kept on ice from then on. They were sonified at the highest level for ten seconds thrice, with ten second breaks in between, and given 1one minute to cool. This procedure was repeated twice, before the cell suspension was checked for complete lysis under the microscope with. If whole cells persisted, it was repeated again.

When fully lysed, the cell suspension was centrifuged in a pre-cooled Eppendorf centrifuge at 16000g for ten minutes and the supernatant transferred to ultracentrifuge tubes. Each pellet was resuspended in 0,5ml digestion buffer, centrifuged again at the same settings, and the supernatant added to the ultracentrifuge tubes. The pellets were then discarded while supernatants were centrifuged at 4°C and 200000g in a 80Ti rotor in the L60 ultracentrifuge for 45 minutes. The supernatants (S200) were decanted into 15ml reaction tubes, and pellets immediately resuspended in 2-3ml digestion buffer to be ultracentrifuged again. Afterwards, the supernatants were discarded and pellets (P200) suspended in 150µl 1x loading buffer, sonified at highest level for 30 seconds twice, with a one minute break and frozen at -80°C. Supernatants of the first ultracentrifuge run were distributed into 1,5ml reaction tubes, 1ml each, and treated with 100µl TCA/ 1ml. After incubating on ice for 30 minutes, they were centrifuged at 4°C and 16000g for 5 minutes, and supernatants were discarded. Pellets were suspended in 100µl 1x loading buffer, had 10µl Tris pH 8,8 added to each tube and were sonified and frozen like the P200 fraction.

2.2.7 Immunohistochemical staining & confocal microscopy

Cells were seeded into 6-well chamber slides the day before staining at a density of 5-10x10^4/ well and incubated at 37°C overnight. The next day, medium was taken off and the cells were washed with 200µl PBS thrice. Then, they were fixed with 150µl 3% paraformaldehyde/ well, which incubated at 37°C for ten minutes and was followed by another three washes with PBS. In the next step, they were permeabilized with 150µl 0,3% triton X-100 in PBS, which took three minutes to incubate at 37°C and was washed off with PBS thrice. Non-specific binding sites were blocked with 5%BSA in PBS for 30 minutes at room temperature, before 250µl/ well of the primary antibody, diluted 1:100 in 0,7% BSA/PBS, incubated another 60 minutes at room temperature. After washing with PBS thrice, 250µl/ well of a fluorescent secondary antibody (Alexa Fluor 546), diluted 1:1000 in 0,7% BSA/PBS were added and left in the wells for an hour. Another three washes with PBS followed, and the cells were covered with 200µl PBS to prevent drying. They were then examined under the confocal microscope, which was kindly operated by Dr. Antonio Virgilio Failla.

2.2.8 IncuCyte live cell imaging

For all IncuCyte live cell imaging trials, cells were trypsinated, resuspended in 2-6ml medium- depending on confluence and desired concentration- and transferred into 15ml falcons. 0,5ml were pipetted into 1ml Eppendorf reaction tubes for counting. 15µl cell suspension were then thoroughly mixed with 15µl trypan blue and cells counted either manually in Neubauer cell counting chambers or automatically by the *Countess II FL.* The cell concentration was calculated and the cell suspension diluted, so that 100µl suspension

would contain the cell number intended for each well. The outer rows and columns were generally omitted and instead filled with PBS or medium to prevent distorted results due to evaporation. After plating, the 96-well plates were gently shaken to encourage even cell spreading and adhesion to the well base.

2.2.8.1 Proliferation assays

For proliferation assays, cells were plated into standard 96-well Greiner plates. Cell numbers were chosen so confluence would ideally be between 10-20% at the start of measurements the next day. All wells were examined under the microscope to check for pipetting errors. After incubating for a day, another 100µl of either pure medium, 0,5% DMSO or a dilution series of Rac1-inhibitor in medium were added to each well. Plates were then placed in the IncuCyte and scans scheduled via the IncuCyte's operating system. First, the vessel was added to the scanning schedule, the 96-well Greiner plate chosen, scan type set to standard and a scan pattern with four pictures of each used well entered. Also, a plate map representing the cells, compounds and growth conditions in each well was established. Once all settings were applied, the new plate was included in the next scanning session. After scanning was completed, at least eight images of different wells at varying confluences were picked for an image collection. Based on this collection, the IncuCyte software developed a processing definition suited for the cells, which could then be further adjusted manually. When sufficiently precise, the mask was applied to all images, allowing quantitative evaluation of confluence progression. Data could be exported for each well individually or grouped by replicates with standard deviation.

2.2.8.2 Scratch assays

Migration assays required the use of 96-well Imagelock plates to ensure correct focusing on the scratches. The cell suspension was diluted so cells would be 90-100% confluent for scratching either on the following day or eight hours later. (HCT116 cells had to be scratched on the day of plating, otherwise they formed strong intercellular adhesions causing grossly uneven scratches). The wells were checked for pipetting errors/ appropriate confluence after plating out and before scratching. If not already done, all unused wells were filled with PBS to avoid damage to the wound maker, as well as medium evaporation in the other wells. The Imagelock plate was locked in the bottom part of the wound maker and the upper part was cleaned with ddH2O and ethanol before being placed on top. Then, the wells were scratched and the plate taken out of the wound maker. If scratches looked sufficiently even under the microscope, the medium was taken off and wells washed with 100µl PBS before 200µl of either pure medium, 0,5% PBS or a dilution series of Rac1-inhibitor in medium were added to each well. Meanwhile, the wound maker was washed

with *Alconox, Virkon,* ddH2O and ethanol according to the washing protocol. If scratches were too inconsistent, the plate was rotated by 180° and scratched again before washing with PBS and adding medium, and the wound maker washing protocol repeated. Finally, the plate was placed in the IncuCyte and scans scheduled, Imagelock chosen as vessel, scan type set to scratch wound and a plate map entered. As for proliferation assays, an image collection and processing definition were created after scanning was completed, so wound overgrowth could be quantified and data exported for evaluation.

2.2.8.3 Invasion assays

In preparation for invasion assays, matrigel was defrosted in an ice box in a fridge at 4°C and disposable pipets as well as pipet tips were stored at -20°C the day before plating. To avoid premature matrigel polymerization, matrigel, plates, disposable pipets and pipet tips were always kept on ice when outside of the freezer or fridge. On the first day of trial, 50µl of 100µg/ml matrigel (diluted in medium) were plated into each well of an Imagelock plate. The plate was incubated at 37°C overnight for the matrigel to polymerize. The next day, excess fluid matrigel was taken out of the wells. Cells were trypsinated, resuspended and diluted so they would be 90-100% confluent once adherent. 100µl cell suspension/ well were plated and given 4 hours to adhere to the well base before they were scratched with the wound maker and washed with PBS as in migration assays. Meanwhile, matrigel was mixed with medium to obtain an 8mg/ml solution, 50µl of which were pipetted into each well. After letting the matrigel harden for 30 minutes in the incubator, 100µl of medium were added to each well and the plate placed in the IncuCyte. Scans were scheduled, settings made and scratch overgrowth analyzed as for migration assays.

3 Results

3.1. SHIP1-expression control

After transducing HCT116 cells with wild type SHIP1, R673Q and a control vector, expression was controlled by Western Blotting of NP40 lysates. Control cells didn't express detectable amounts of SHIP1 while SHIP1-wt transduced cells had high SHIP1 levels. R673Q was detected at much lower amounts, around 5% of wild type-SHIP1 levels. This can be explained with faster polyubiquitination and subsequent proteasomal degradation of the SHIP1-mutant due to intramolecular instability, reducing the half-life of R673Q to 1,5 hours compared to 24-32 hours of wild type SHIP1 as described previously (Nelson, 2017) (Ehm et al, 2023).

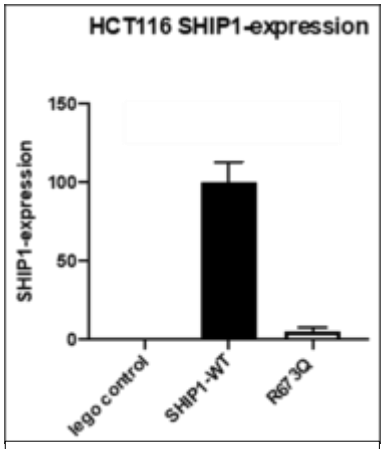

Figure 3.2: SHIP1-expression, SHIP1-wildtype normalized to 100%

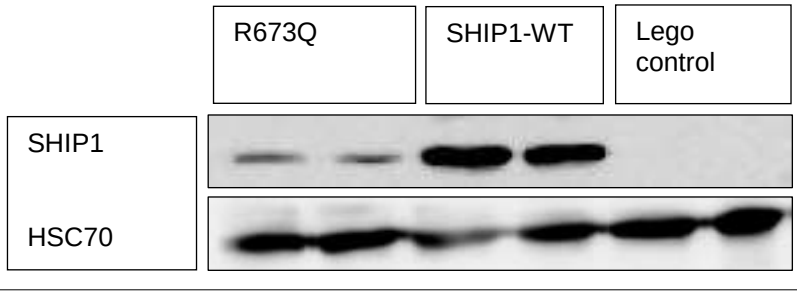

Figure 3.1: Western Blot of SHIP1-expression

3.2 AKT phosphorylation

SHIP1's substrate $PI(3,4,5)P_3$ and product $PI(3,4)P_2$ have both been observed to recruit AKT to the cell membrane and promote its phosphorylation. Accordingly, changes in pAKT levels are expectable as a result of SHIP1-overexpression and consequent shifts in the $PI(3,4,5)P_3$ / $PI(3,4)P_2$ balance. To examine the effects of SHIP1 on AKT-phosphorylation in the three cell lines, they were Western blotted with the pAKT S473 antibody.

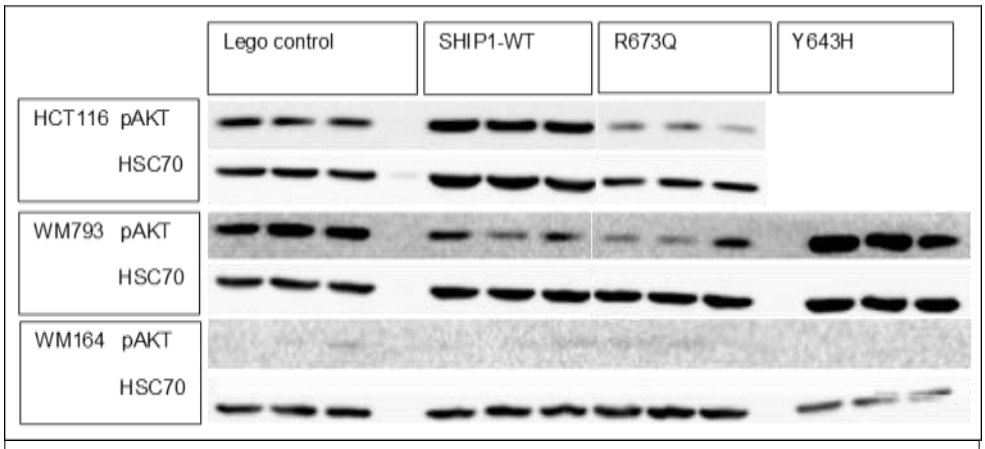

Figure 4.1: Western Blot of AKT, phosphorylated at S473

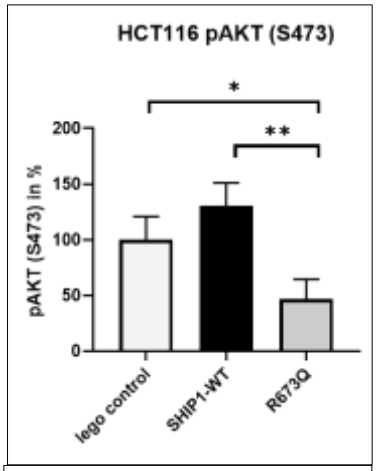

Figure 4.2: pAKT (S473) in HCT116, lego control normalized to 100%

In HCT116 cells, SHIP1-overexpression led to an increase of pAKT (S473) levels by 30,5%, which was not significant, though. R673Q overexpression led to a significant decrease by 53,4%. In WM793 cells, both wild type SHIP1 and R673Q caused declines compared to the control by 82,3% and 88,2%, respectively, which were not significant by ANOVA but had a p< 0,01 (**) with t-tests. Y643H yielded an insignificant increase by 22,1%. Since in WM164 cells pAKT bands were hardly recognizable at all, they were not quantified and compared.

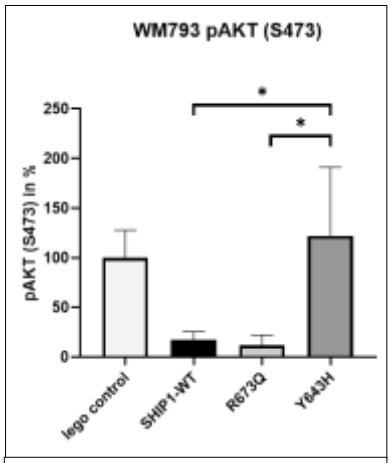

Figure 4.3: pAKT (S473) in WM793, lego control normalized to 100%

3.3 SHIP1 location

3.3.1 …by differential centrifugation

The SHIP1-mutants R673Q and Y643H have been suspected to “trap” their substrate PI(3,4,5)P_3 as a consequence of reduced catalytic activity. Their compromised ability to convert PI(3,4,5)P_3 to PI(3,4)P_2 may stabilize the enzyme-substrate complex and thus prevent degradation of PIP3 by other phosphoinositide phosphatases (Myers et al., 1998, Luo et al., 2003). To examine the association of wild type SHIP1 and the SHIP1-mutant R673Q with their membrane-bound substrate PI(3,4,5)P_3, differential centrifugation was performed with the three cell lines to separate the membrane fraction from the cytosolic fraction. In the next step, SHIP1 wild type and R673Q levels in the two fractions could be determined by Western Blotting. The cytosolic protein GAPDH was blotted to verify the

separation of membrane and cytosolic fraction. Ponceau staining was used to quantify the amount of protein in each lane and adjust for variations.

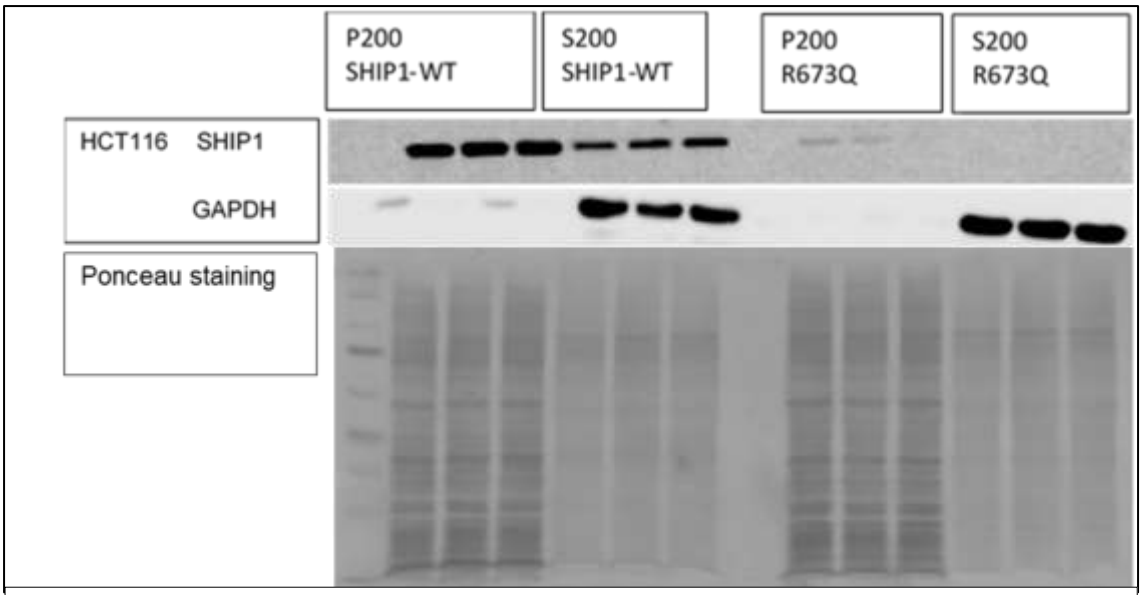

Figure 5.1: Western Blot of SHIP1 and Ponceau-staining of lysates from HCT116

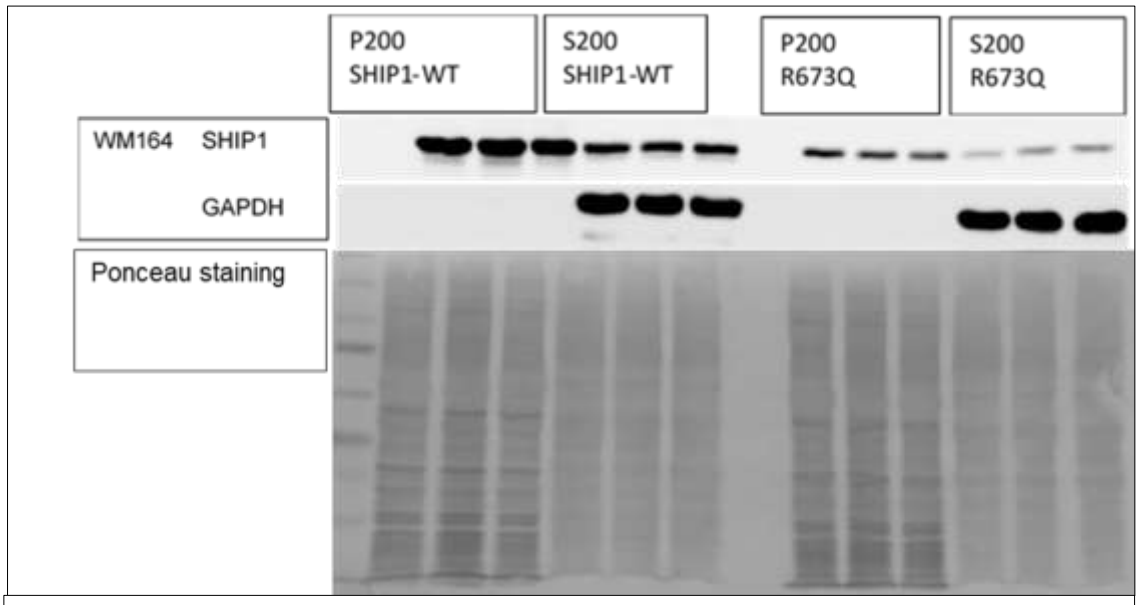

Figure 5.2: Western Blot of SHIP1 and Ponceau-staining of lysates from WM164

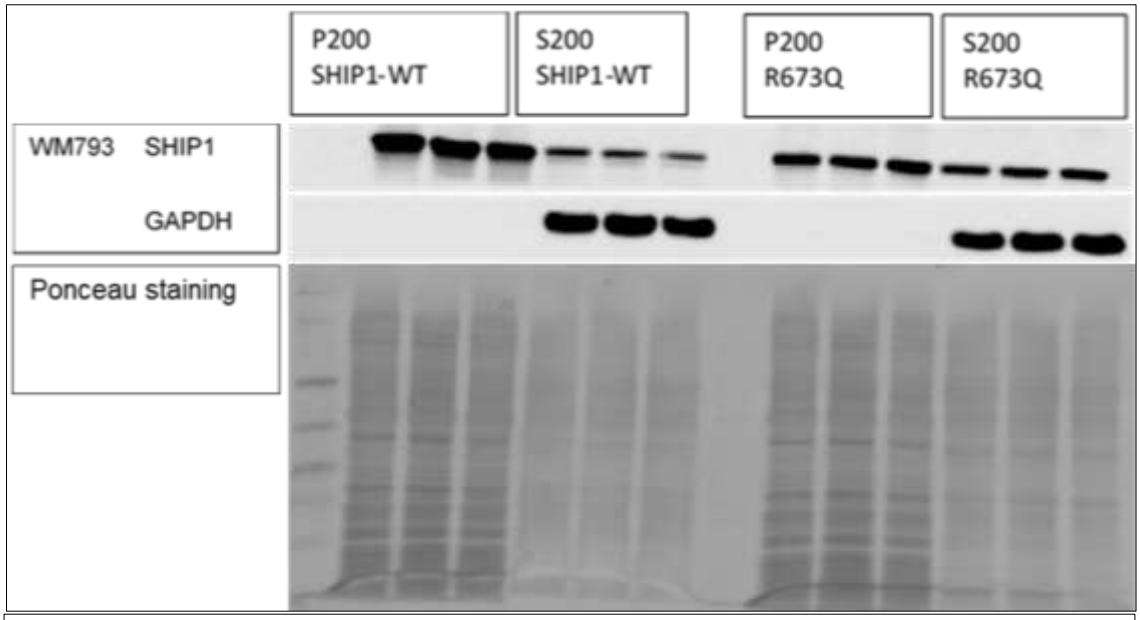

Figure 5.3: Western Blot of SHIP1 and Ponceau-staining of lysates from WM793

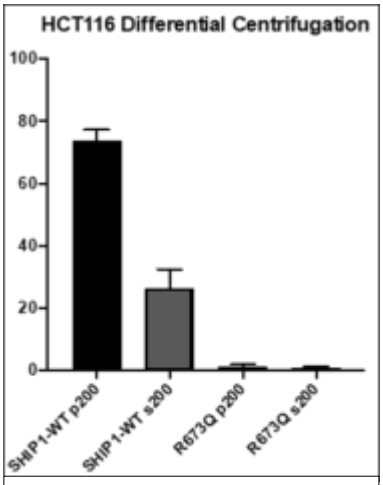

Figure 5.4: SHIP1 in membrane and cytosol fractions of HCT 116, sum of wildtype SHIP1 in both fractions normalized to 100%

The Western Blot showed that membrane fractions were largely free from GAPDH, indicating they contained no cytosolic cell components. SHIP1 was apparent in all lysates except the cytosolic fraction of R673Q-transduced HCT116 cells. The mutant R673Q was previously reported to be instable in this cell line in our group. This may result from increased poly-ubiquitination and subsequent degradation compared to wild type SHIP1 (Nelson, 2017). SHIP1-levels were quantified and graphed with the amount of wild type SHIP1 in both fractions taken together as 100%. Since quantification of the bands confirmed that SHIP1-R673Q levels were close to zero in both fractions of HCT116 cells, its distribution has not been further evaluated statistically. In the melanoma cell lines, R673Q levels were also lower than wild type SHIP1, but in a reasonably quantifiable range- so the p200/ s200 ratios were calculated and compared in these cells.

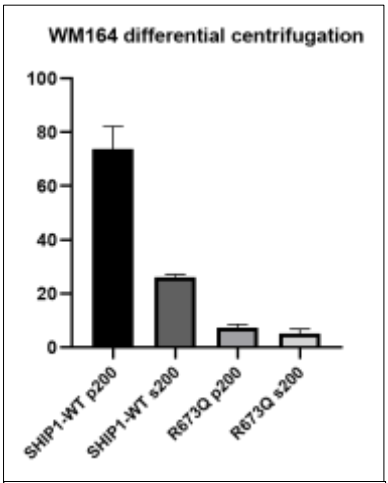

Figure 5.5: SHIP1 in membrane and cytosol fractions of WM164, sum of wildtype SHIP1 in both fractions normalized to 100%

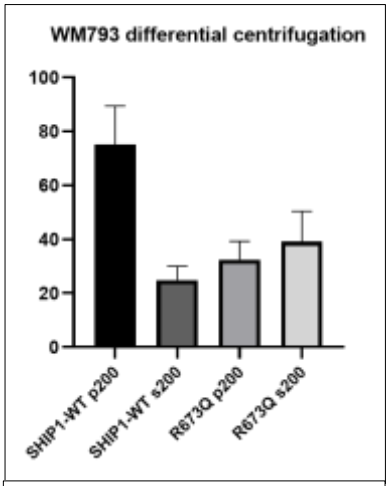

Figure 5.6: SHIP1 in membrane and cytosol fractions of WM793, sum of wildtype SHIP1 in both fractions normalized to 100

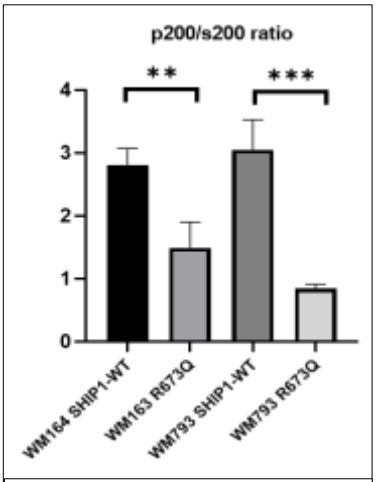

Figure 5.7: ratio of SHIP1 in membrane to cytosol fractions of WM164 and WM793 in comparison

The distribution of wild type SHIP1 varied only slightly between the three cell lines. Around 73-75% of SHIP1 was detected in the membrane fraction. For SHIP1-R673Q however, there were bigger differences. In WM164 cells, about 58,5% of R673Q was detected in the membrane, corresponding to a p200/s200 ratio of 1,49. In WM793 cells, on the other hand, only 45,4% was determined in the membrane fraction, equaling a p200/s200 ratio of 0,84. These results indicate that wild type SHIP1 has a higher affinity to the membrane than SHIP1-R673Q, contradicting earlier findings with WM164 and WM793 cells of our group (Drechsel, 2019) (Cremer, 2018). However, it should be considered that for differential centrifugation, cells are shredded by sonification and lysates cooled after that, so the SHIP1-distribution determined here doesn't necessarily reflect the situation in living cells.

3.3.2 SHIP1-location: by confocal microscopy

Confocal microscopy was used to validate the results of differential centrifugation. Cells were seeded in chamber slides, fixated, and incubated with the primary SHIP1-antibody P1C1. After dying with anti-mouse Alexa Flour 546, they were examined by confocal microscopy. High rates of membrane association would lead to bright cell outlines, while predominant cytosolic presence would generate evenly stained cell bodies. Color intensity was measured and graphed with Image J. Though this trial is not suited for statistical evaluation, and only individual cells were examined, it can give a rough impression of SHIP1-distribution in "undamaged" cells.

3.3.2.1 HCT116

1) Lego control

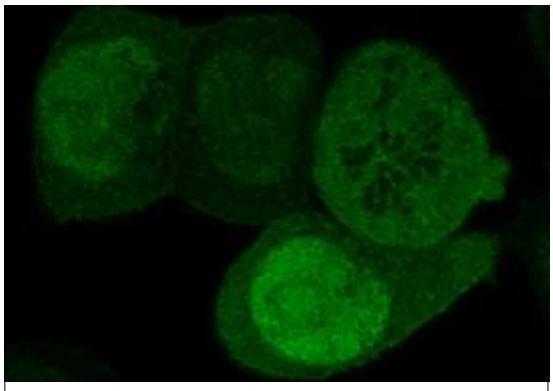

Figure 6.1: EGFP in HCT116, lego control

Figure 6.2: SHIP1 in HCT116-cells, lego control

As expected, control cells expressed EGFP- located in the nucleus and cytosol- but no SHIP1.

2) SHIP1-WT

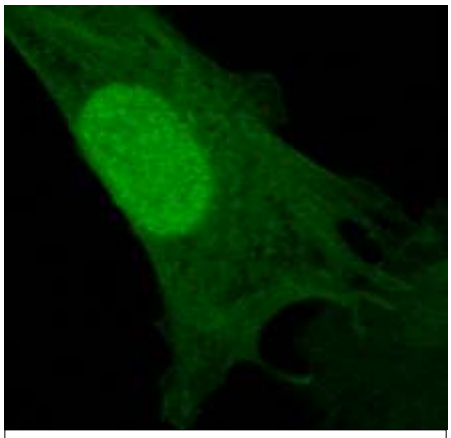

Figure 6.3: EGFP in HCT116, SHIP1-wt (1)

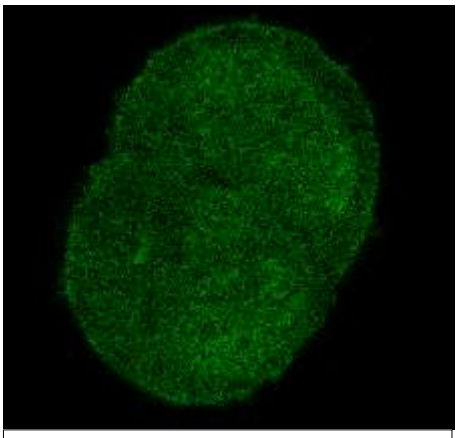

Figure 6.4: EGFP in HCT116, SHIP1-wt (2)

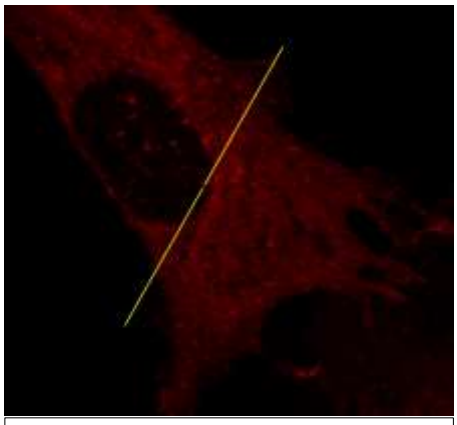

Figure 6.5: SHIP1-wt in HCT116, SHIP1-wt (1)

Figure 6.6: SHIP1-wt in HCT116, SHIP1-wt (2)

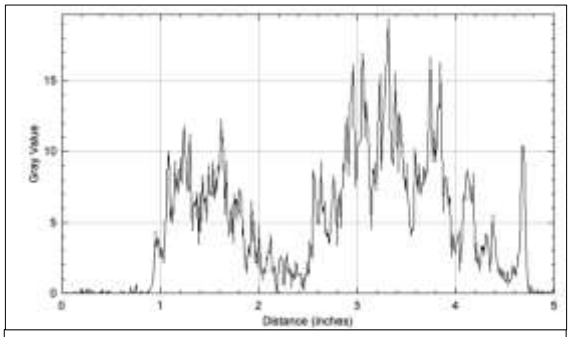

Figure 6.7: SHIP1 in HCT116, SHIP1-wt, fluorescence intensity (1)

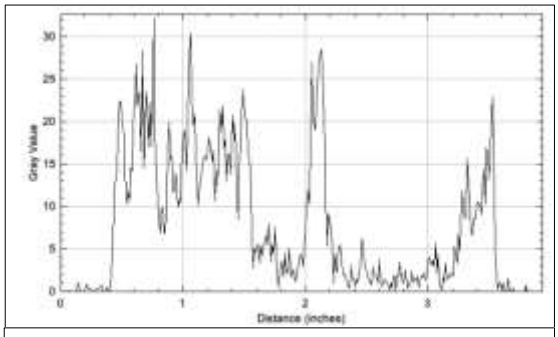

Figure 6.8: SHIP1 in HCT116, SHIP1-wt, fluorescence intensity (2)

SHIP1-transduced HCT116-cells show strong expression of EGFP and SHIP1. The first cell, apparently caught in the act of migrating, has a spike of fluorescence at the right side, indicating increased levels of membrane-associated SHIP1 at this spot, possibly a filopodium. The second one, about to divide, seems to have peaks at both sides. Otherwise, they also show high levels of fluorescence throughout the cytosol.

3) R673Q

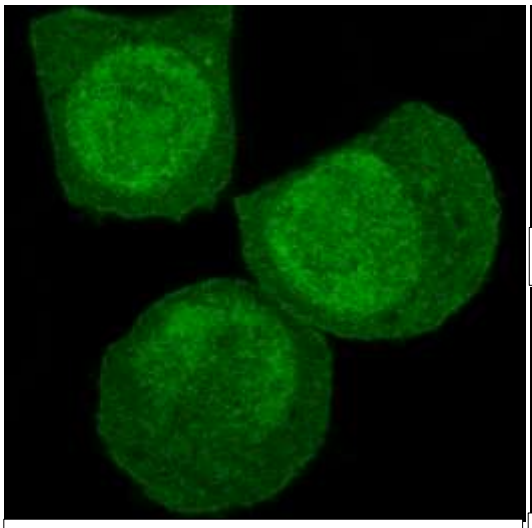

Figure 6.9: EGFP in HCT116, SHIP1-R673Q

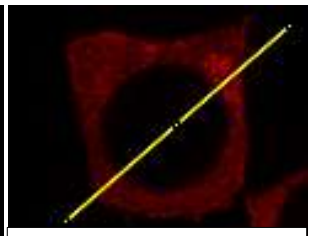

Figure 6.10: SHIP1 in HCT116, SHIP1-R673Q (1)

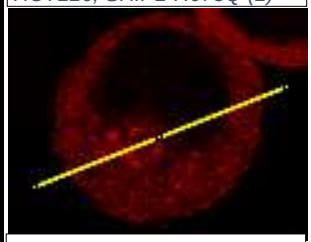

Figure 6.11: SHIP1 in HCT116, SHIP1-R673Q (2)

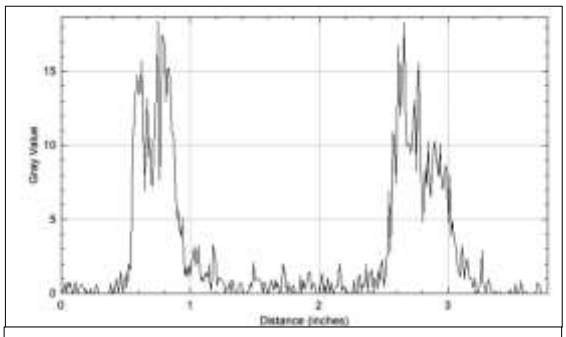

Figure 6.12: SHIP1 in HCT116, SHIP1-R673Q, fluorescence intensity (1)

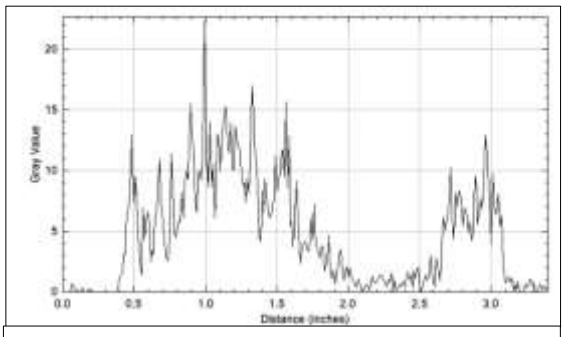

Figure 6.13: SHIP1 in HCT116, SHIP1-R673Q, fluorescence intensity (2)

In the two chosen R673Q-transduced cells, fluorescence is only slightly lower than in SHIP1-widtype cells, unlike in the Western Blot. Both have spikes of color intensity at the left, the second one more noticeably, which may indicate higher levels of membrane-associated SHIP1. Apart from that, SHIP1 seems to be evenly spread in the cytosol.

3.3.2.2 WM793

1) Lego control

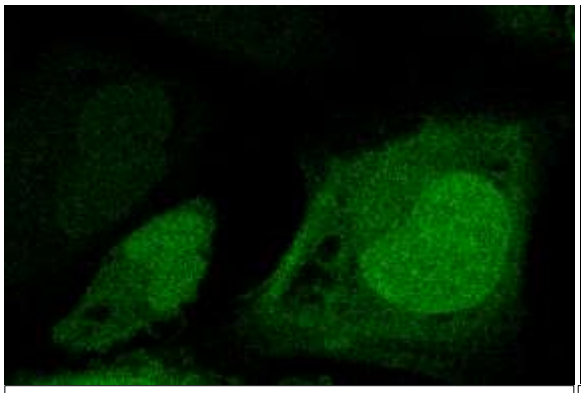

Figure 7.1: EGFP in WM793, lego control

Figure 7.2: SHIP1 in WM793, lego control

2) SHIP1-WT

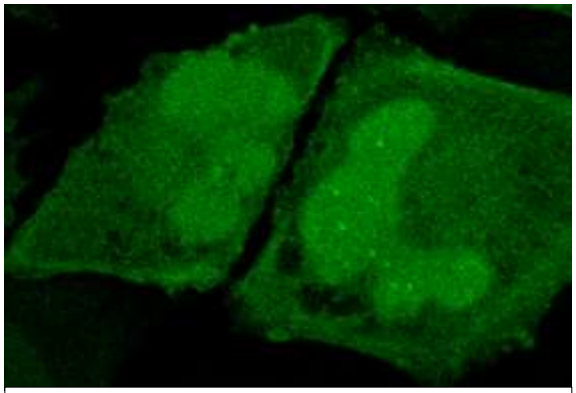

Figure 7.3: EGFP in WM793, SHIP1-wt

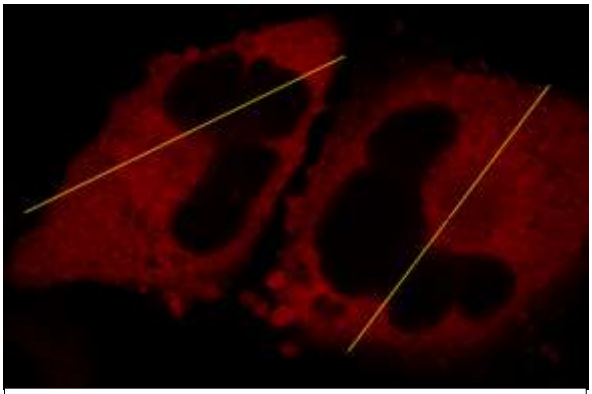

Figure 7.4: SHIP1 in WM793, SHIP1-wt

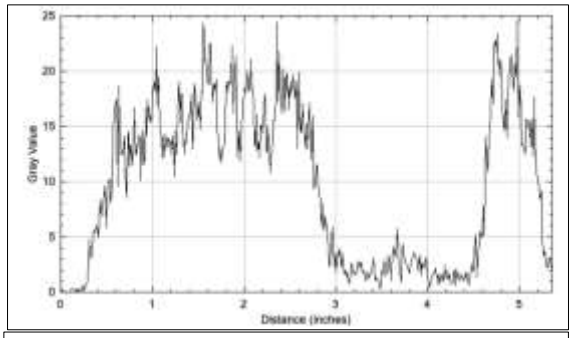

Figure 7.5: SHIP1 in WM793, SHIP1-wt, fluorescence intensity (1)

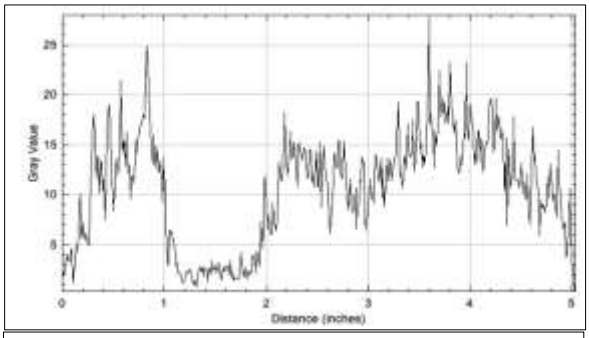

Figure 7.6: SHIP1 in WM793, SHIP1-wt, fluorescence intensity (2)

Wild type SHIP1-transduced cells looked evenly red, with the nucleus left out, and possessed no obvious outlines. Color intensity plots confirm even staining and show no intensity peaks at cell borders, indicating that most SHIP1 is located in the cytoplasm. Their

outlines appear less clear than those of wild type-SHIP1-transduced HCT116 cells. These findings may hint at a lower proportion of membrane associated wild type SHIP1 in this cell line in contrast to HCT116 cells.

3) R673Q

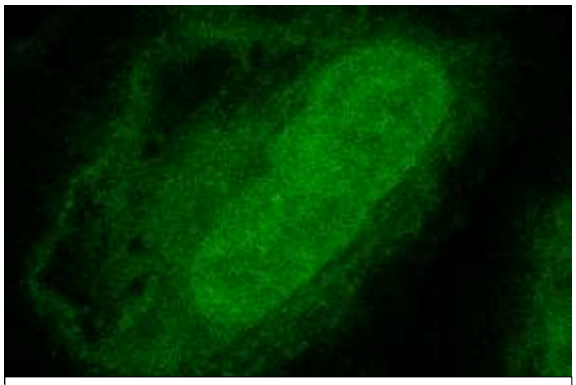

Figure 7.7: EGFP in WM793, SHIP1-R673Q (1)

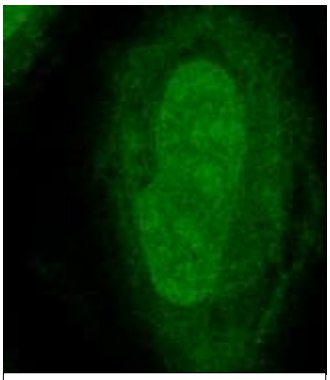

Figure 7.8: EGFP in WM793, SHIP1-R673Q (2)

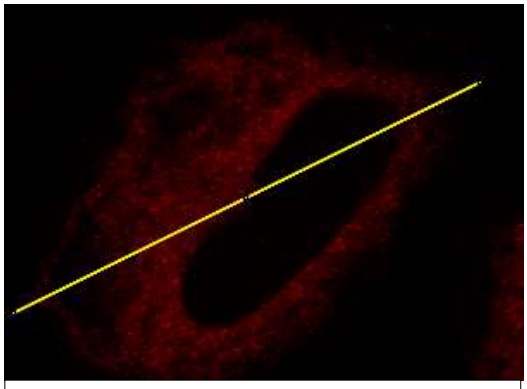

Figure 7.9: SHIP1 in WM793, SHIP1-R673Q (1)

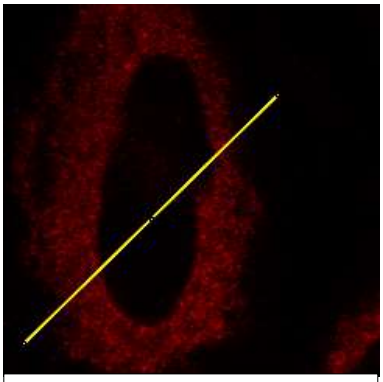

Figure 7.10: SHIP1 in WM793, SHIP1-R673Q (2)

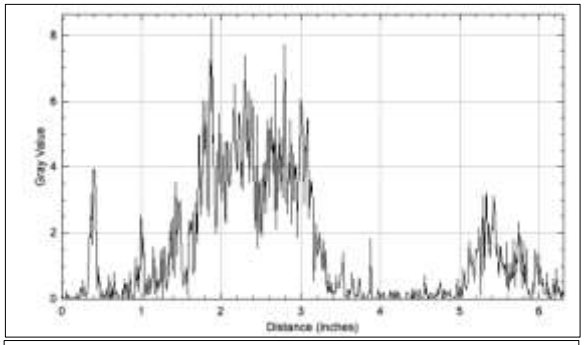

Figure 7.11: SHIP1 in WM793, SHIP1-R673Q, fluorescence intensity (1)

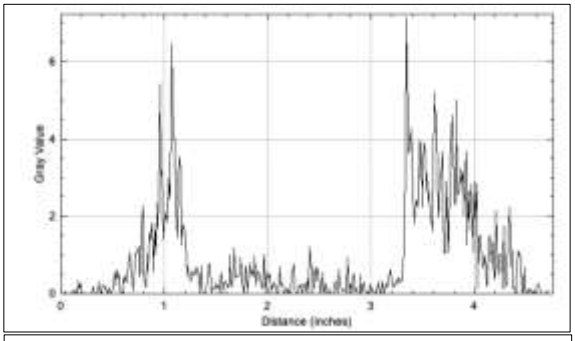

Figure 7.12: SHIP1 in WM793, SHIP1-R673Q, fluorescence intensity (2)

SHIP1-R673Q levels were much lower than those of SHIP1-wt. To make it visible at all, brightness of the images was subsequently increased. One cell showed a small peak of color intensity at the left, possibly a sign of increased membrane association there. In the other cell, there appeared to be peaks around the nucleus and lower levels in the periphery. Like wild type SHIP1, R673Q seems to be located mostly in the cytosol.

3.3.2.3 WM164

1) Lego control

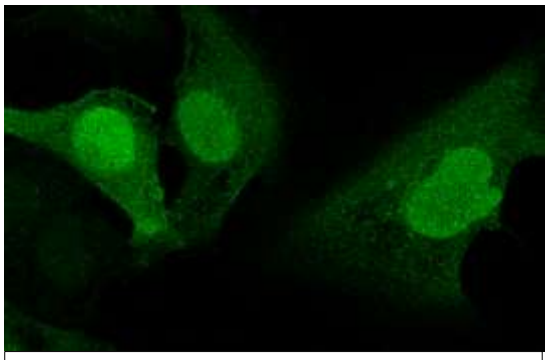

Figure 8.1: EGFP in WM164, lego control

Figure 8.2: SHIP1 in WM164, lego control

2) SHIP1-WT

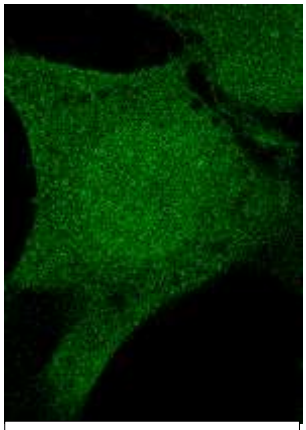

Figure 8.3: EGFP in WM164, SHIP1-wt (1)

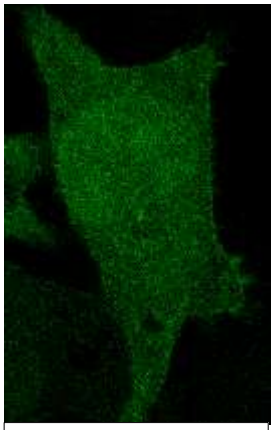

Figure 8.4: EGFP in WM164, SHIP1-wt (2)

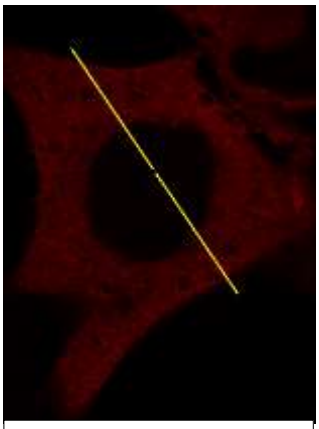

Figure 8.5: SHIP1 in WM164, SHIP1-wt (1)

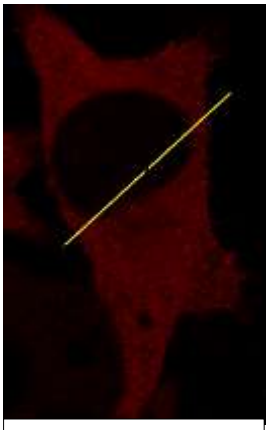

Figure 8.6: SHIP1 in WM164, SHIP1-wt (2)

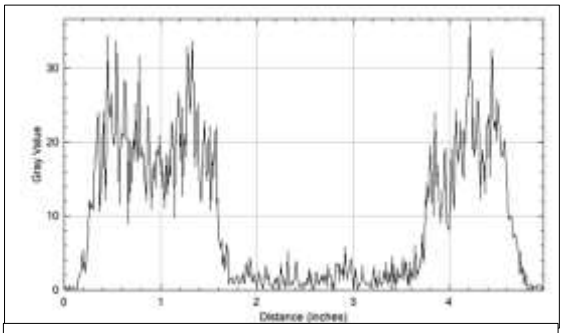

Figure 8.7: SHIP1 in WM164, SHIP1-wt, fluorescence intensity (1)

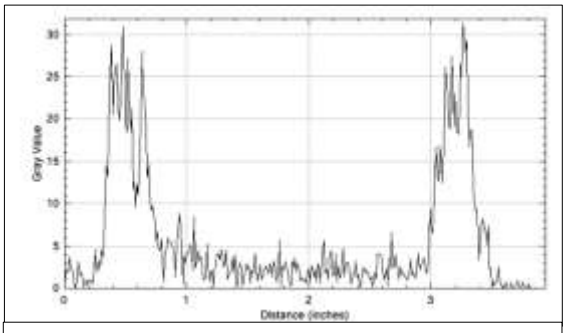

Figure 8.8: SHIP1 in WM164, SHIP1-wt, fluorescence intensity (2)

The first examined SHIP1-wild type overexpressing WM164 cell didn't show conspicuous spikes of color intensity at the membrane, the second one possibly at the left side. Otherwise, SHIP1 appears to be evenly distributed in the cytosol.

3) R673Q

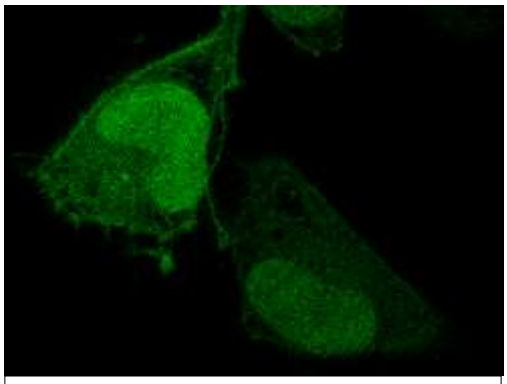

Figure 8.9: EGFP in WM164, SHIP1-R673Q

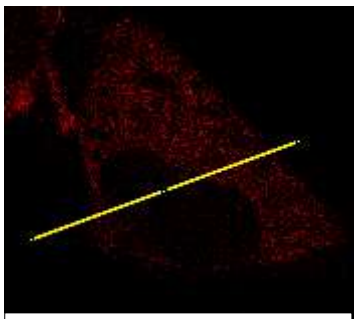

Figure 8.10: SHIP1 in WM164, SHIP1-R673Q (1)

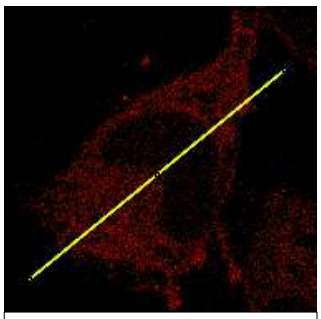

Figure 8.11: SHIP1 in WM164, SHIP1R673Q (2)

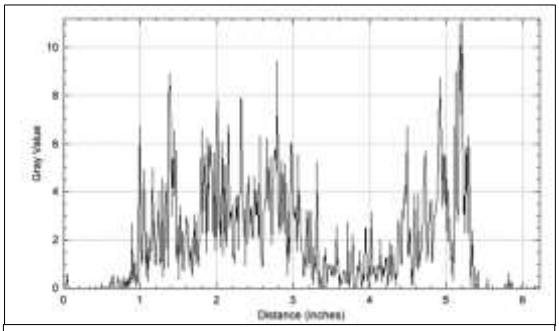

Figure 8.12: SHIP1 in WM164, SHIP1-R673Q, fluorescence intensity (1)

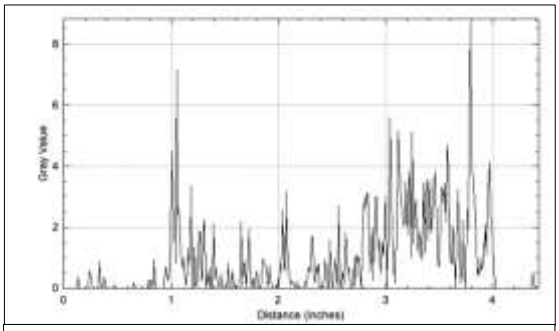

Figure 8.13: SHIP1 in WM164, SHIP1-R673Q, fluorescence intensity (1)

In the depicted cells, SHIP1-R673Q is expressed at much lower levels than SHIP1-wt, which is in line with Western Blotting results, and resembles expression patterns in WM793 cells. The second cell appears to have SHIP1-level peaks at the membrane- however, the generally low level of fluorescence makes it more difficult to discern.

Overall, confocal microscopy results suggest that both wild type SHIP1 and R673Q are located in the cytosol rather than the membrane, especially in the melanoma cell lines. They challenge the findings of membrane fractionation, where most wild type SHIP1 was associated with the membrane. However, this trial only depicts a few samples and doesn't allow quantification and comparison between the three cell lines and two SHIP1-variants.

3.4 IncuCyte Live Cell Imaging

3.4.1 HCT116

3.4.1.1 Proliferation

HCT116 cells are small, adherent and very rapidly proliferating. Seeded at a starting confluence of 10-15%, they grew fully confluent within three to three and a half days. Since growth pace depends on confluence, small differences in starting confluence between the cell lines can make significant differences in absolute confluence at a later time, even if cells grow at identical rates. Proliferation turned out to be fastest- and almost completely linear- in a medium confluence range.

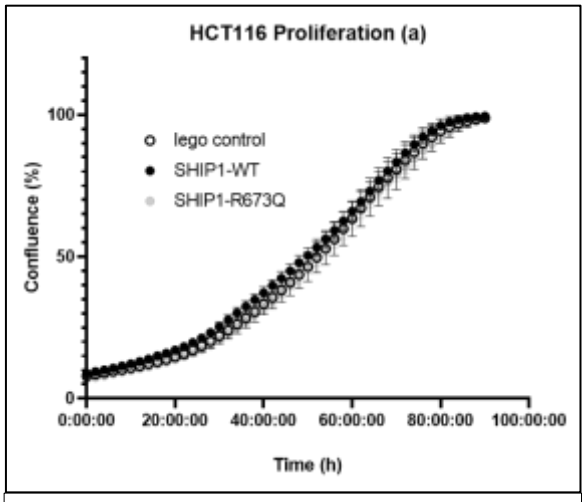

Figure 9.1: HCT116 proliferation (1)

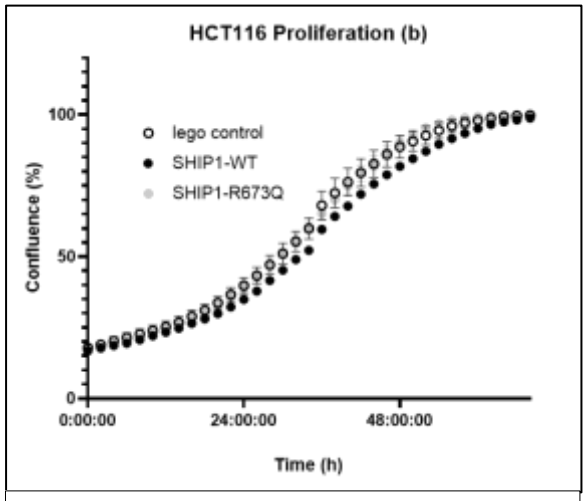

Figure 9.2: HCT116 proliferation (2)

Accordingly, maximum proliferation speed instead of absolute confluence was compared. The increase in confluence in percent/ hour in the range of 35% -65% confluence was calculated for every well and the standard deviation for each cell line determined from the gradients. Growth rates were normalized to the control cell line.

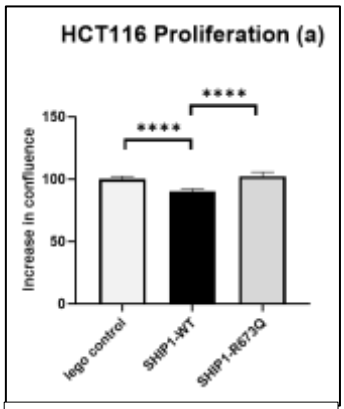

Figure 9.3: HCT116 proliferation speed, lego control normalized to 100% (1)

HCT116 cells exhibited a uniform growth behavior and were precisely captured by the IncuCyte processing definition due to their strong contrast to the background. Though proliferation rates of transduced HCT116 cells only differed slightly, the disparity between wild type SHIP1 and control- about 10%- as well as R673Q- about 11,9%- was highly significant in the first trial. The difference between wild type SHIP1 and R673Q (2,3%) was not significant.

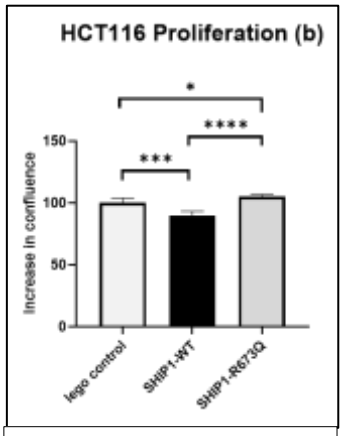

Figure 9.4: HCT116 proliferation speed, lego control normalized to 100% (2)

In the second experiment, the proliferation rate of wild type SHIP1-transduced cells was again highly significantly lower than that of control cells (by 10,3%) and R673Q-transduced cells (by 14,6%). This time, there was also a small but significant increase in the proliferation rate of R673Q-transduced cells compared to the control by 5,1%. Considering both trials, there seems to be a clear, reproducible inhibition of proliferation by wild type SHIP1 in HCT116 cells. There may also be slight growth enhancement by SHIP1-R673Q, which has only been observed in one of two trials, though.

Influence of Rac1-Inhibition on Proliferation

As an effector of the PI3K-AKT signaling cascade as well as other pathways, the small GTPase Rac1 is involved in mediating a wide range of cellular functions like viability, proliferation and cell motility (Kotelevets and Chastre, 2020). To examine in how far proliferative signals are conveyed by Rac1 in the three HCT116 cell lines, and differentiate the inhibitor's effects on proliferation vs. migration, they were treated with the Rac1-inhibitor NSC23766. The data sheet indicates an IC50 value of 50µM for this inhibitor. Accordingly, the cells have been treated with inhibitor concentrations between 0,4µM and 50µM in provisional tests, to find a concentration range that slows down proliferation but doesn't bring it to a standstill or kill the cells. The "therapeutic range" of NSC23766 turned out to be very narrow in HCT116 cells and standard deviations higher than in inhibitor-free experiments. Since the IC50 value of 50µM was lethal in some, though not all, pre-trials, lower concentrations were chosen, and the cells were treated with a 1:2 dilution series from 2,5µM to 40µM NSC23766 in medium.

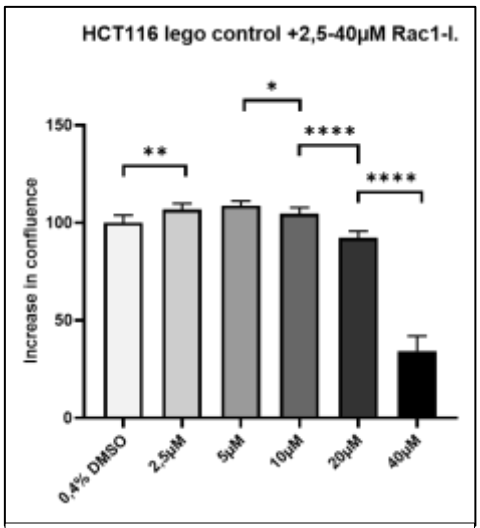

Figure 9.5: HCT116 lego control proliferation speed with Rac1-inhibitor, DMSO control normalized to 100%

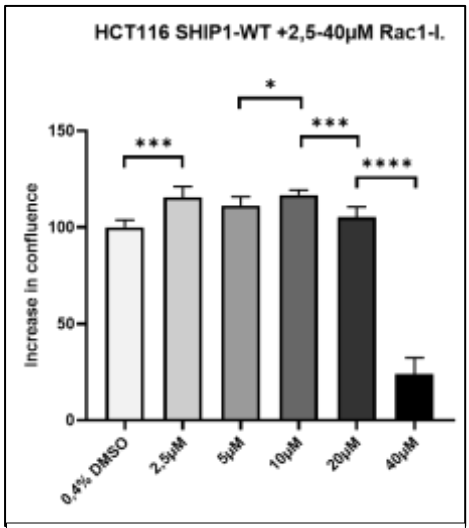

Figure 9.6: HCT116 SHIP1-wt proliferation speed with Rac1-inhibitor, DMSO control normalized to 100%

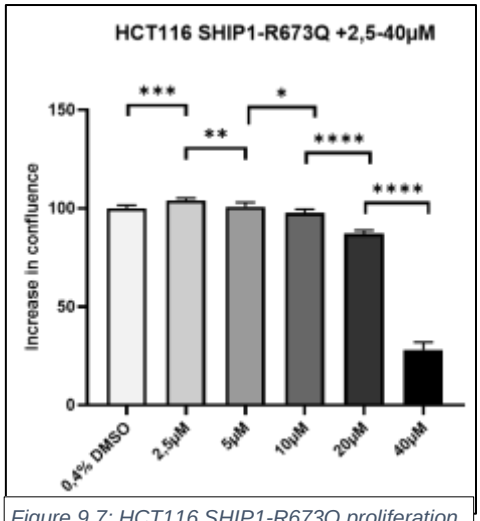

Figure 9.7: HCT116 SHIP1-R673Q proliferation speed with Rac1-inhibitor, DMSO control normalized to 100%

HCT116 cells began to show signs of proliferation inhibition at a concentration of 10µM-20µM NSC23677, and were strongly curbed at 40µM- by 65,6%, 76% and 71,9% compared to the DMSO control. Like in the inhibitor-free trials, wild type SHIP1-transduced cells were slower proliferating at this inhibitor dilution factor by 37,3% compared to control and 27% to R673Q-transduced cells, but standard deviations were much higher. However, the narrow therapeutic range, in combination with medium evaporation during live cell imaging, should be considered when comparing the three lines at a specific inhibitor concentration.

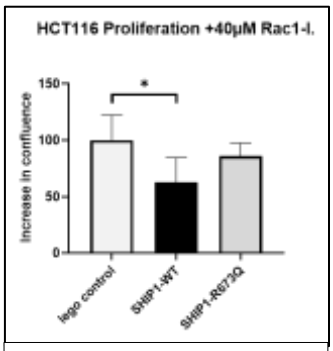

Figure 9.8: HCT116 proliferation speed with 40µM Rac1-inhibitor, DMSO control normalized to

3.4.1.2 HCT116 Migration

Migration assays were conducted with the Wound Maker of Essen BioScience, simultaneously scratching the cell layers in all wells of a 96-well plate. When plated 90-100% confluent, HCT116 cells formed strong intercellular adhesions by the next day, which led to wide, irregular scratches. To attain more even wounds, they were scratched on the day of plating. Prior to evaluation, scratches were checked for consistency. Those obviously wider, narrower or uneven were not included. As cells had less time to adhere to the well base, a few always swam into the wounds after scratching. To reflect this, wound confluence instead of relative wound density was used for analysis.

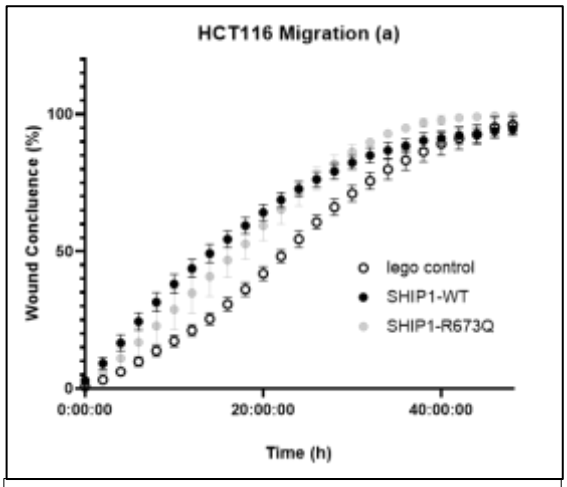

Figure 10.1: HCT116 migration (1)

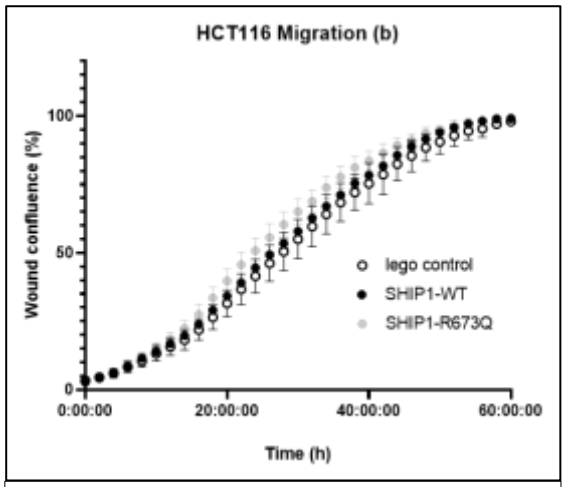

Figure 10.2: HCT116 migration (2)

HCT116 cells overgrew the wounds within two and a half days. Migration picked up a few hours after scratching and slowed down at around 70-80% wound confluence. Again, migration rate instead of absolute wound confluence at a certain time was calculated to avoid distortions due to differences in starting wound confluence or delays in “migration spurts”. For standardization, the increase in wound confluence from 20-60% was calculated for each well and standard deviations determined from the gradients.

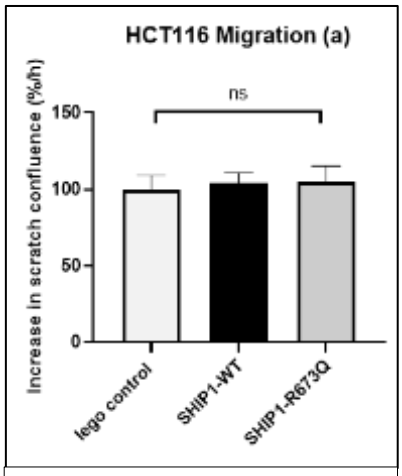

Figure 10.3: HCT116 migration speed, lego control normalized to 100% (1)

In the first trial, there were no significant differences in migration rate between wild type SHIP1-, R673Q-overexpressing and control cells. In the second experiment, SHIP1-R673Q-transduced HCT116 cells were slightly faster at closing the scratch than the other two cell lines, by 16,2% (control) and 15,4% (SHIP1-WT). This type of migration assay didn’t show any differences between wild type SHIP1 and the control.

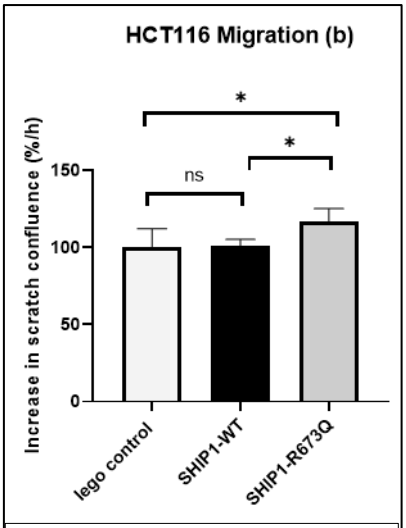

Figure 10.4: HCT116 migration speed, lego control normalized to 100% (2)

Influence of Rac1-Inhibition on Migration

An important factor in the modulation of cell polarity, actin remodeling, migration and adhesion, Rac1 can drive cancer progression by promoting EMT, invasion and metastasis (Kotelevets and Chastre, 2020). Therefore, the question arose in how far migration is

mediated by Rac1 in HCT116 cells, and if there are any discrepancies between wild type SHIP1-overexpressing, R673Q- and control cells. As in proliferation assays, they were treated with different concentrations of the Rac1-inhibitor NSC23766. Preliminary experiments indicated that HCT116 cells were a little less sensitive to the inhibitor when 90-100% instead of 10-15% confluent. Accordingly, they were treated with higher inhibitor concentrations in migration assays.

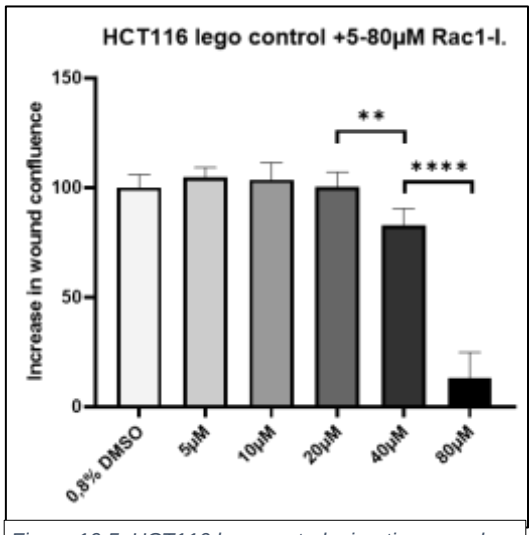

Figure 10.5: HCT116 lego control migration speed with Rac1-inhibitor, DMSO control normalized to

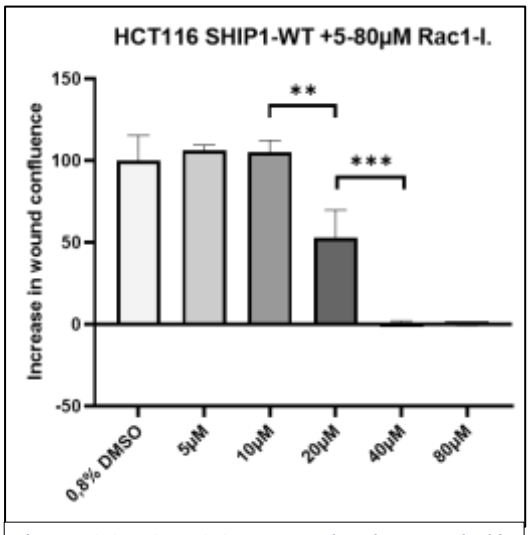

Figure 10.6: HCT116 SHIP1-wt migration speed with Rac1-inhibitor, DMSO control normalized to 100%

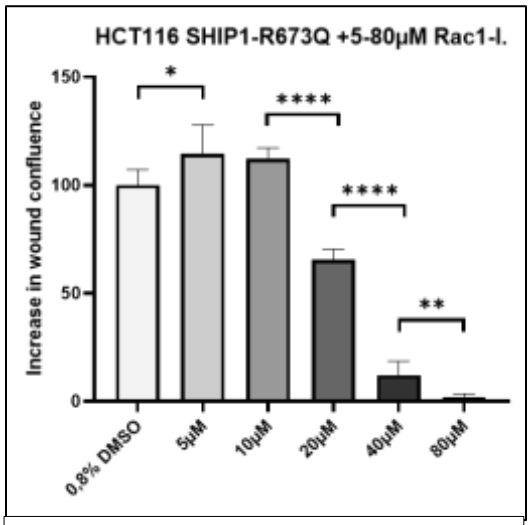

Figure 10.7: HCT116 R673Q migration speed with Rac1-inhibitor, DMSO control normalized to 100%

However, they were slightly more susceptible in subsequent trials and a considerable share appeared to go into apoptosis at 80µM. Similar to proliferation, significant inhibition of migration was observed with 40µM in all HCT116 cell lines- by 17,3%, 99,2% and 87,2% compared to the respective DMSO control. Again, the therapeutic range proves to be very small, which may explain the deviations in vulnerability to the inhibitor compared to the pre-trials- especially in combination with medium evaporation from the wells during live cell imaging.

Compared at 40µM Rac1-inhibitor concentration, both wild type SHIP1- and R673Q-overexpressing HCT116 cells were highly significantly slower at migrating than control cells, by 99% and 85,7%, respectively. There was also a significant difference between R673Q and wild type SHIP1. The latter cells barely migrated at all and looked mostly senescent or apoptotic. This trial indicates that especially wild type SHIP1, but also R673Q, might make HCT116 cells more vulnerable to migration inhibition by NSC23766.

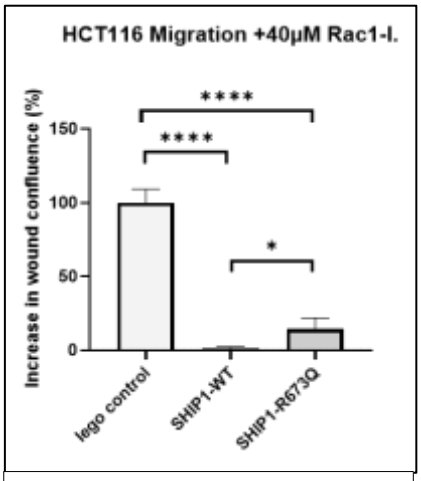

Figure 10.8: HCT116 migration speed with 40µM Rac1-inhibitor, lego control normalized to 100%

3.4.1.3 HCT116 Invasion

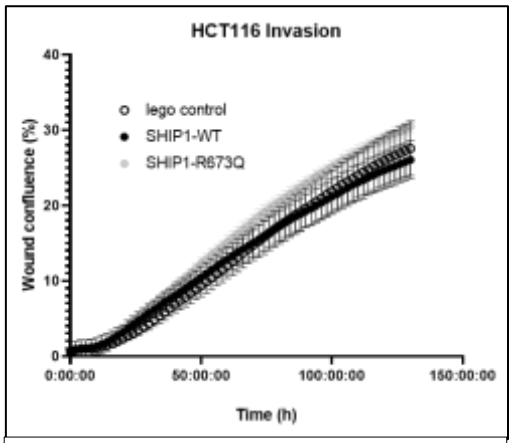

Figure 11.1: HCT116 invasion in Matrigel

For invasion assays, cells were seeded at the same density as for migration assays, and were likewise scratched with the EssenBioscience Wound maker. After scratching, the cell layers were covered with Corning Matrigel, simulating extracellular matrix. HCT116 cells presented themselves a lot slower at "invading" the Matrigel than migrating on the well base. After more than five days, the wounds had become only about 25% confluent and invasion started to slow down. This was probably caused by increasing medium consumption by the cells plus evaporation. Thus, invasion speed was calculated in a wound confluence range of 10-15% instead of 20-60%. SHIP1-R673Q transduced cells were significantly faster at invading than wild type SHIP1 cells (23,1%). Control cells didn't differ significantly to either of the other cell lines.

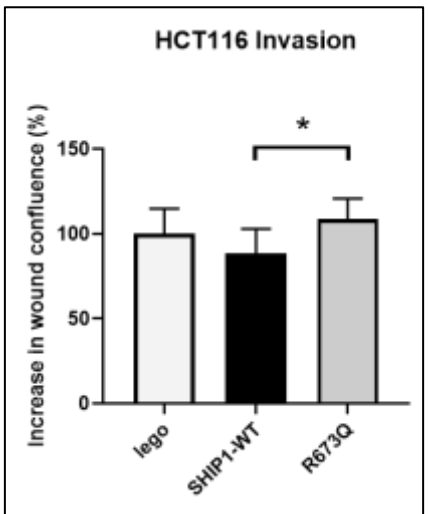

Figure 11.2: HCT116 invasion speed in Matrigel, lego control normalized to 100%

3.4.2 WM793

3.4.2.1 Proliferation

WM793 cells are big, almost transparent and relatively slow-growing compared to HCT116 and WM164 cells. Seeded at a starting confluence of 10-15% they can take a week or more to grow fully confluent. That can be problematic due to high levels of medium consumption and evaporation in this period of time. Taking plates out of the IncuCyte to feed the cells, on the other hand, poses the risk of a shift in focus position. Thus, a higher starting confluence was favorable. To compensate variance in initial confluence, proliferation rate was calculated and compared instead of absolute confluence at a certain time, as for HCT116 cells. Another difficulty was the lack of contrast between cells and background, complicating precise capturing of confluence by the IncuCyte's processing definition.

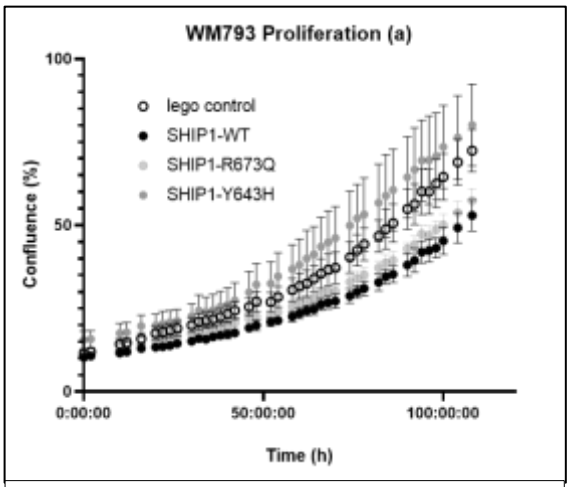

Figure 12.1: WM793 proliferation (1)

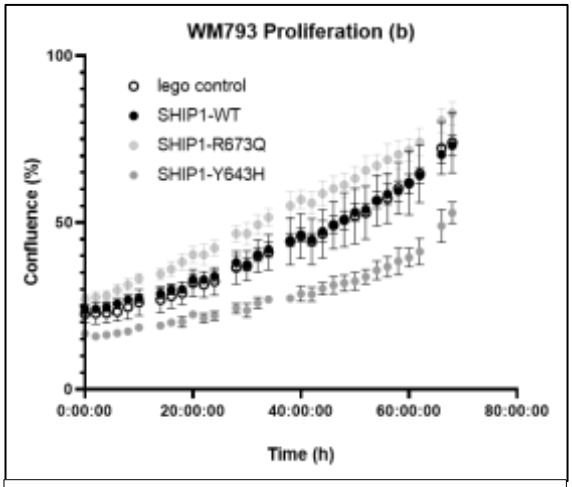

Figure 12.2: WM793 proliferation (2)

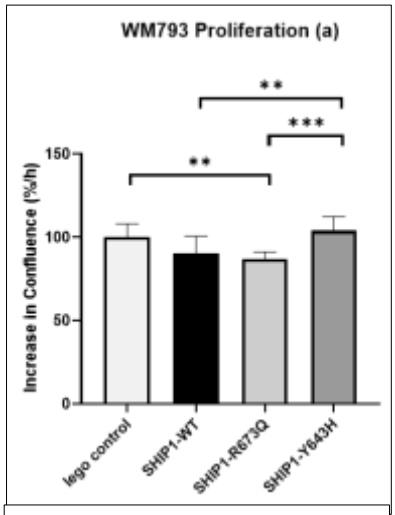

Figure 12.3: WM793 proliferation speed, lego control normalized to 100% (1)

In one trial, SHIP1-R673Q expressing WM793 cells were significantly slower proliferating (-12,8%) and SHIP1-wt insignificantly (-9,6%), compared to the control. Y643H-transduced cells were significantly faster than wild type SHIP1 and R673Q cells, but not the control (+4%). In another experiment, however, wild type SHIP1

overexpressing cells were the slowest-growing (-7,7% compared to the control), significantly lagging behind SHIP1-R673Q (+6,6%/ control) and Y643H cells (+38,5%/ control). Again, there was a clear difference between R673Q and Y643H. Both trials consistently show enhanced proliferation with SHIP1-Y643H compared to the other two SHIP1 versions, and an insignificant reduction with wild type SHIP1 by contrast with the control. The effect of SHIP1- R673Q -in contrast to wild type SHIP1 and the control- is not clear, though. Small deviations in starting confluence as well as the cells' relatively slow growth rate and lack of contrast to the background may have complicated precise measuring.

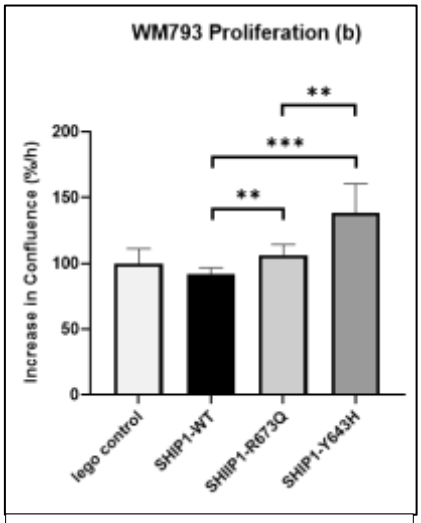

Figure 12.4: WM793 proliferation speed, lego control normalized to 100% (2)

Influence of Rac1-Inhibition on Proliferation

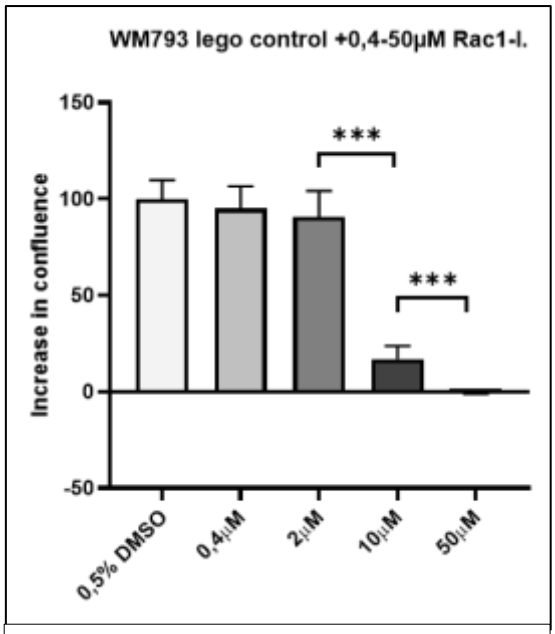

Figure 12.5: WM793 lego control proliferation speed with Rac1-inhibor, DMSO control normalized to 100%

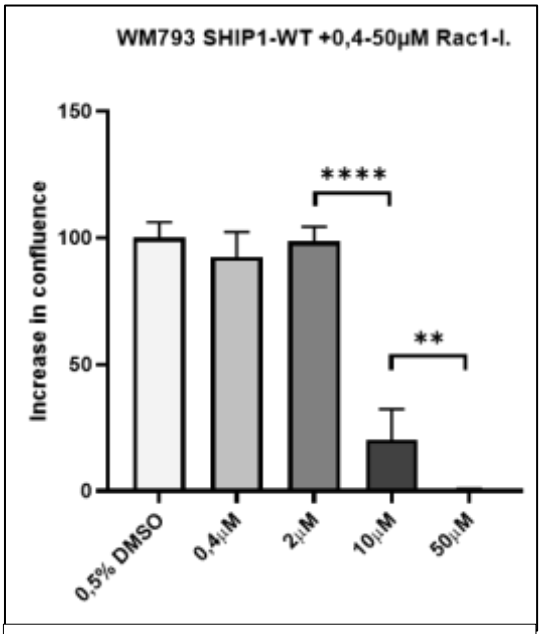

Figure 12.6: WM793 SHIP1-wt proliferation speed with Rac1-inhibitor, DMSO control normalized to 100%

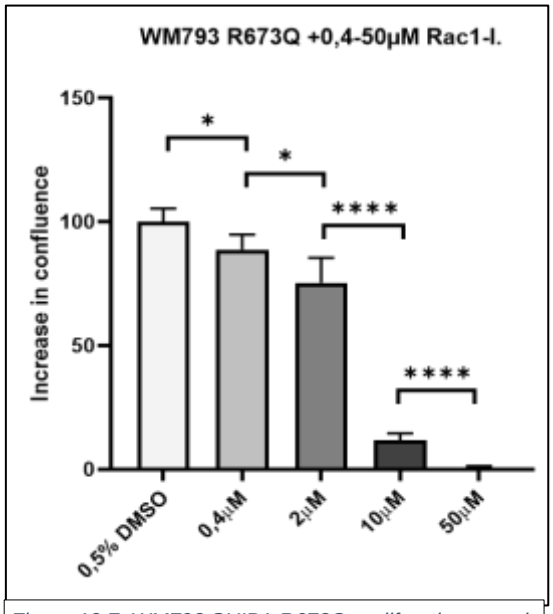

Figure 12.7: WM793 SHIP1-R673Q proliferation speed with Rac1-inhibor, DMSO control normalized to 100%

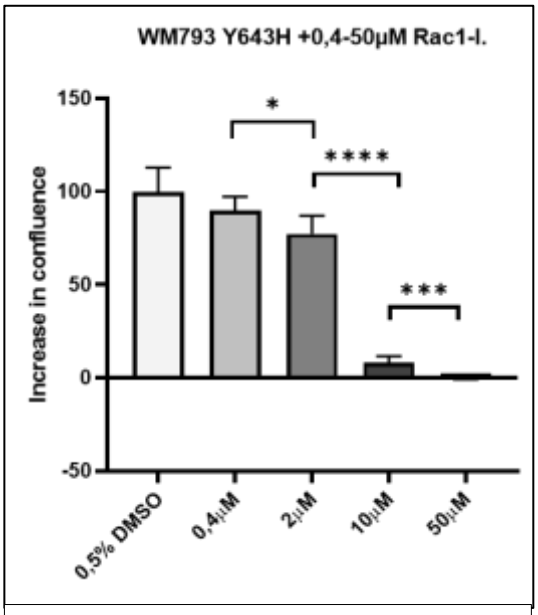

Figure 12.8: WM793 SHIP1-Y643H proliferation speed with Rac1-inhibor, DMSO control normalized to 100%

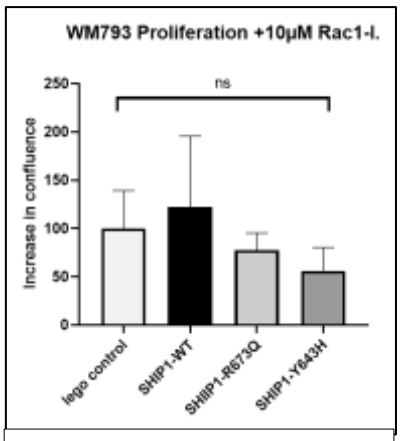

Figure 12.9: WM793 proliferation speed with 10µM Rac1-inhibor, lego control normalized to 100%

Like HCT116, WM793 cells were treated with the Rac1-inhibitor NSC23677 and proliferation was compared. Proliferation of all four WM793 cell lines was strongly decelerated at 10µM and nonexistent at 50µM. R673Q- and Y643H- expressing cells already showed significant signs of growth inhibition at 0,4µM and 2µM, respectively. They might be slightly more sensitive to low inhibitor concentrations. However, there were no significant differences observable at 10µM. In comparison with control cells, SHIP1-wild type led to an increase of 22,4%, R673Q a decrease of 22,5% and Y643H 43,8%.

2.4.2.2 WM793 Migration

Though slowly proliferating, WM793 cells are very fast at migrating. Control cells overgrew the scratches within two days. Unlike HCT116 cells, they could be scratched cleanly on the day after plating. Obviously uneven, narrower or wider scratches were not evaluated. Migration speed between 20% and 60% wound confluence was calculated and compared.

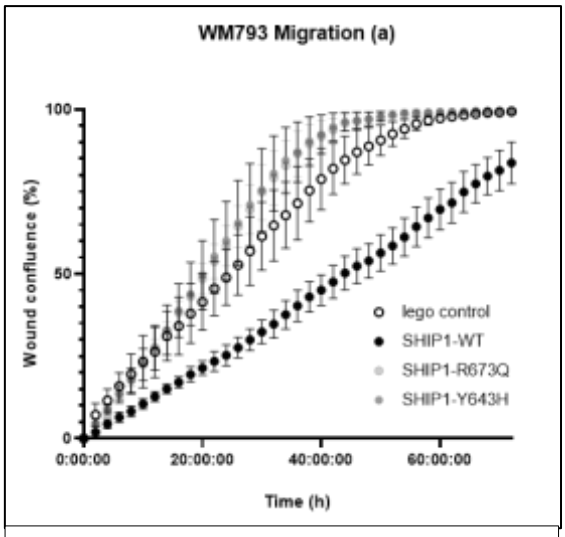

Figure 13.1: WM793 migration (1)

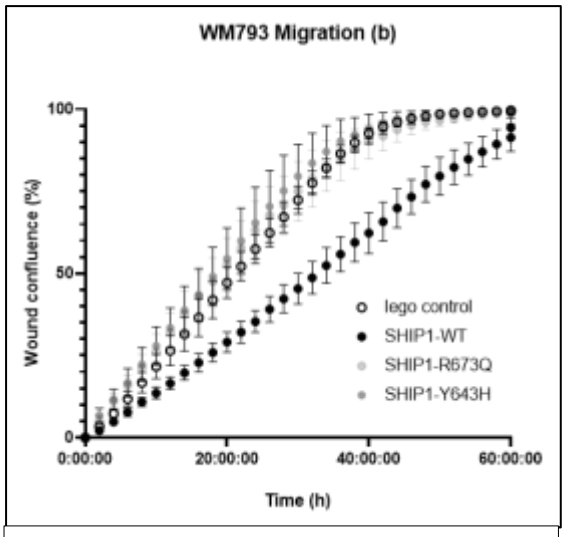

Figure 13.2: WM793 migration (2)

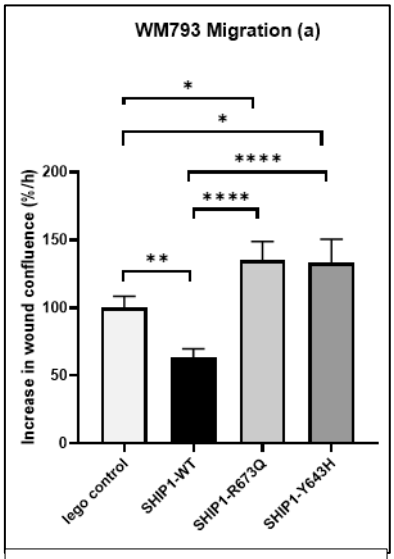

Figure 13.3: WM793 migration speed, lego control normalized to 100%(1)

In the first experiment, the SHIP1-mutants R673Q and Y643H led to slightly significant increases in migration rate by 35% and 33% respectively, in contrast to the control. However, these differences could not be reproduced in the second trial. Both trials demonstrated a strong, significant inhibition of migration by wild type SHIP1 compared to both SHIP1-mutants as well as the control, by 36,2% in the first and 37,8% in the second trial. As this effect of wild type SHIP1 has not been observed in proliferation assays, it appears to be specific for migration in WM793 cells.

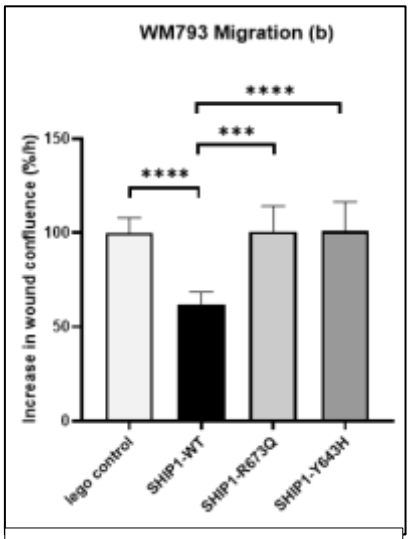

Figure 13.4: WM793 migration speed, lego control normalized to 100%(2)

Influence of Rac1-Inhibition on Migration

In the next step, all WM793 cell lines were treated with NSC23766 and migration inhibition was quantified. As they were slightly more sensitive to the inhibitor than HCT116 cells, the initial concentration range of 0,4-50µM was retained. Migration of WM793 cells was considerably inhibited from 10µM upwards. At 50µM, migration was almost completely halted and some cells looked apoptotic.

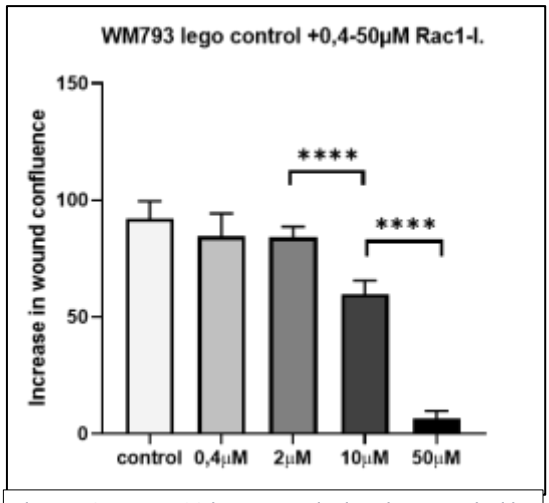

Figure 13.5: WM793 lego control migration speed with Rac1-inhibitor, DMSO control normalized to 100%

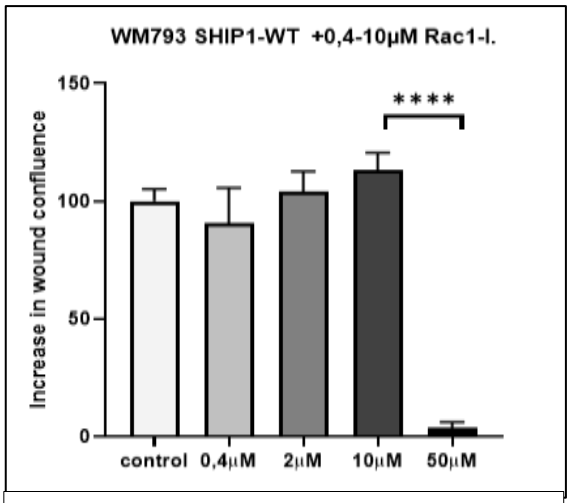

Figure 13.6: WM793 SHIP1-wt migration speed with Rac1-inhibitor, DMSO control normalized to 100%

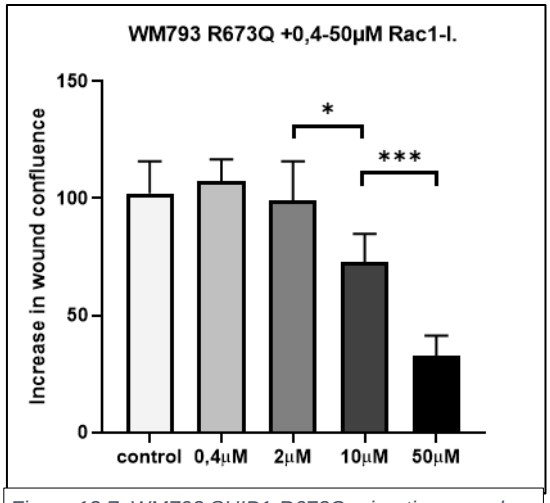

Figure 13.7: WM793 SHIP1-R673Q migration speed with Rac1-inhibitor, DMSO control normalized to 100%

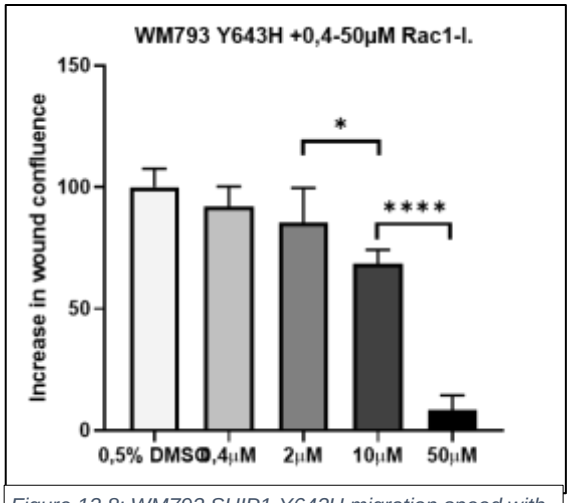

Figure 13.8: WM793 SHIP1-Y643H migration speed with Rac1-inhibitor, DMSO control normalized to 100%

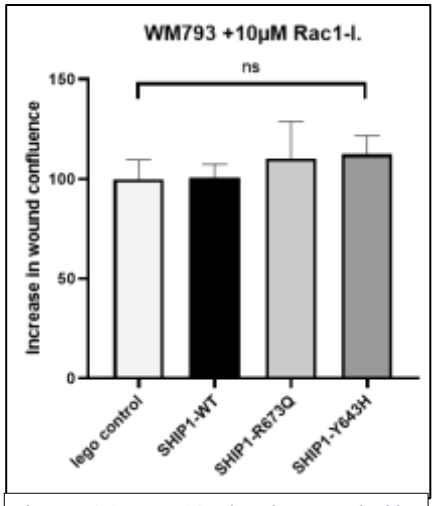

Figure 13.9: WM793 migration speed with 40µM Rac1-inhibitor, lego control normalized to 100%

Similar to HCT116 cells, the degree of inhibition was not fully congruent with preliminary trials, especially with higher inhibitor concentrations. While control cells as well as R673Q- and Y643H-transduced cells showed dose-dependent inhibition between 2µM and 50µM, those with SHIP1-WT were affected only at the highest inhibitor concentration. Accordingly, there was no significant variance between migration rates of the four cell lines compared at 10µM NSC23766.

3.4.2.3 WM793 Invasion

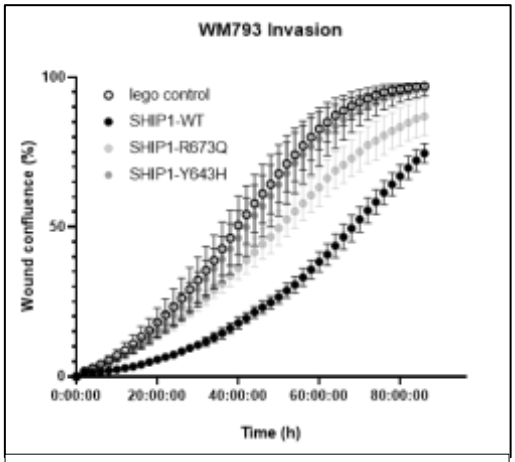

Figure 14.1: WM793 invasion in Matrigel

For the invasion assay, cell layers were coated with Corning Matrigel after scratching, and medium was added. Since cells were seeded at the same density as for migration assays, but scratched the same day, they were not fully confluent at the start of scanning. Considerably more invasive than HCT116 cells, WM793 cells overgrew the Matrigel-filled wounds within less than four days. Therefore, invasion rate was calculated in a wound confluence range of 20-60%- were it was fastest and almost linear.

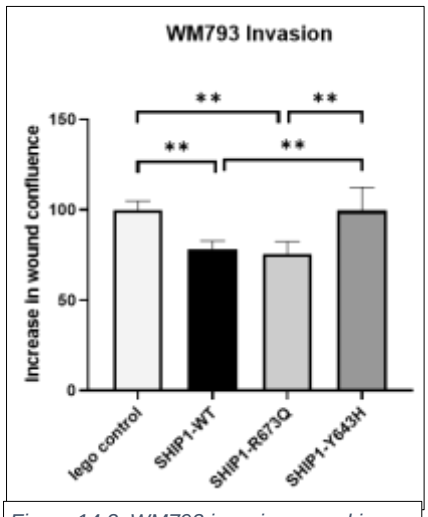

Figure 14.2: WM793 invasion speed in Matrigel, lego control normalized to 100%

In this confluence range, both control and SHIP1-Y643H transduced WM793 cells were significantly faster invading than wild type SHIP1 (-22,1%/ control) and SHIP1-R673Q
(-24,2%/ control). For wild type SHIP1, decelerated invasion is in line with a clear inhibition of migration, though less pronounced. For SHIP1-R673Q, it is at variance with unchanged or slightly increased migration. In one proliferation assay, however, R673Q also had inhibitory effects.

3.4.3 WM164

3.4.3.1 Proliferation

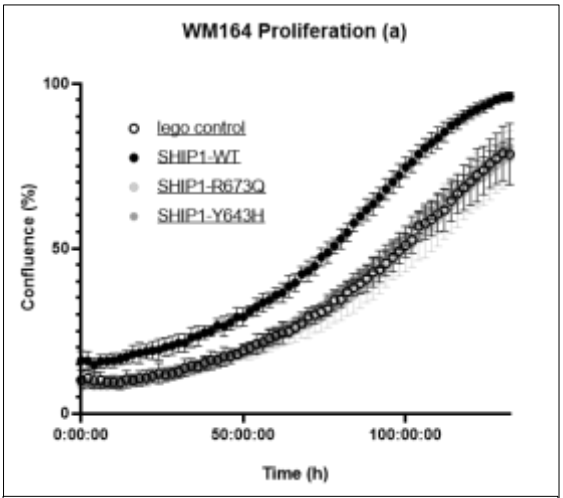

Figure 15.1: WM164 proliferation (1)

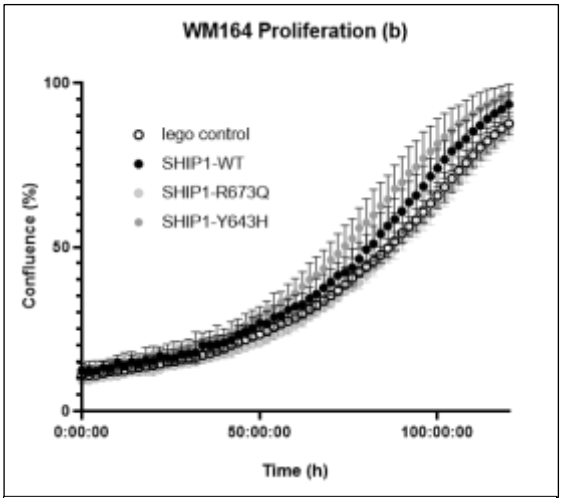

Figure 15.2: WM164 proliferation (2)

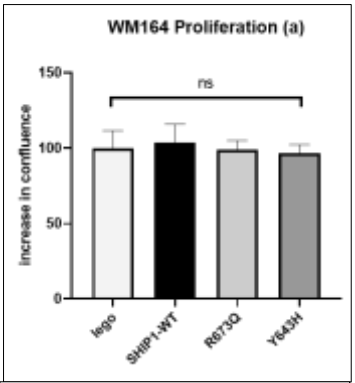

Figure 15.3: WM164 proliferation speed, lego control normalized to 100% (1)

WM164 are slightly smaller than WM793 cells and faster proliferating. Starting at 10-15% confluence, they overgrow the well bases within about five days. Again, proliferation rate was compared between 35% and 65% confluence. In the first trial, the three SHIP1-transduced cell lines deviated from the control by less than 4%. In the second, their proliferation rates were slightly increased by 3,9% (R673Q), 8,5% (SHIP1-wt) and 11,7% (Y643H). Neither experiment demonstrated any significant differences in growth rates.

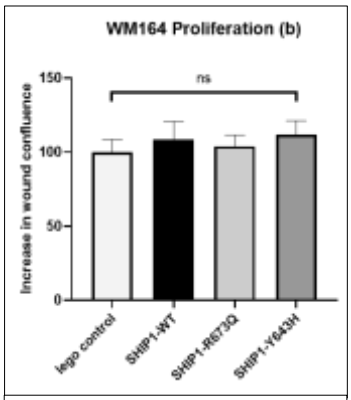

Figure 15.4: WM164 proliferation speed, lego control normalized to 100% (2)

Influence of Rac1-Inhibition on Proliferation

Proliferation of WM164 cells was curbed by NSC23766 concentrations higher than 4µM, with the SHIP1-mutant transduced cells showing clearer gradients at low inhibitor dosages. Minimal or no proliferation took place with 32µM, and a considerable share of cells went into apoptosis. At 16µM, all SHIP1-transduced cell lines grew significantly slower than the control. Proliferation rates were reduced by 51,8%, 62,7% and 76% respectively, compared to control cells.

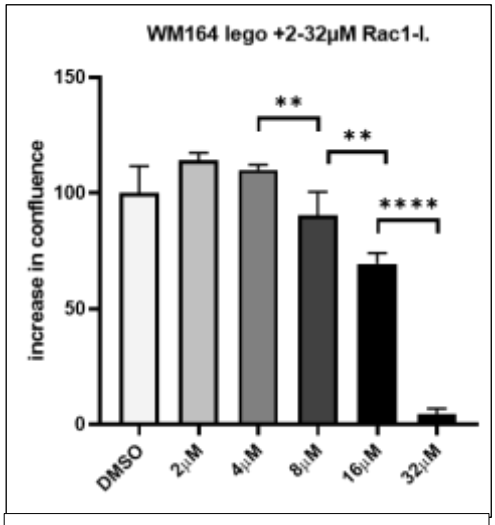

Figure 15.5: WM164 lego control proliferation speed with Rac1-inhibor, DMSO control normalized to 100%

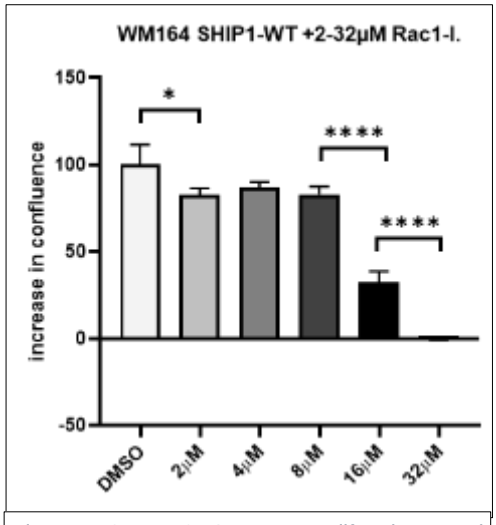

Figure 15.6: WM164 SHIP1-wt proliferation speed with Rac1-inhibitor, DMSO control normalized to 100%

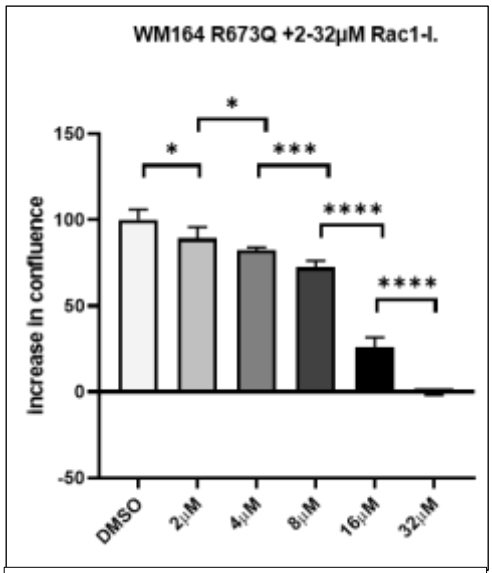

Figure 15.7: WM164 SHIP1-R673Q proliferation speed with Rac1-inhibitor, DMSO control normalized to 100%

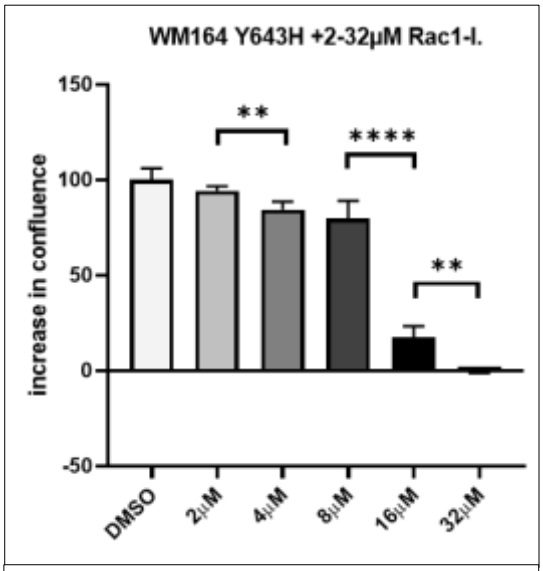

Figure 15.8: WM164 SHIP1-Y643H proliferation speed with Rac1-inhibitor, DMSO control normalized to 100%

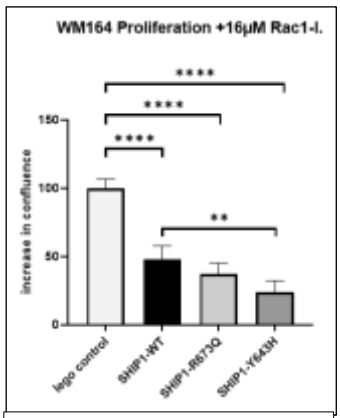

Figure 15.9: WM164 proliferation speed with Rac1-inhibitor, lego control normalized to 100%

3.4.3.2 WM164 Migration

WM164 cells are even faster migrating than HCT116 and WM793 cells, closing the scratch wounds within in one to two days. They were scratched the day after plating. Scratches diverging in width were taken out, and migration rates between 20% and 60% calculated.

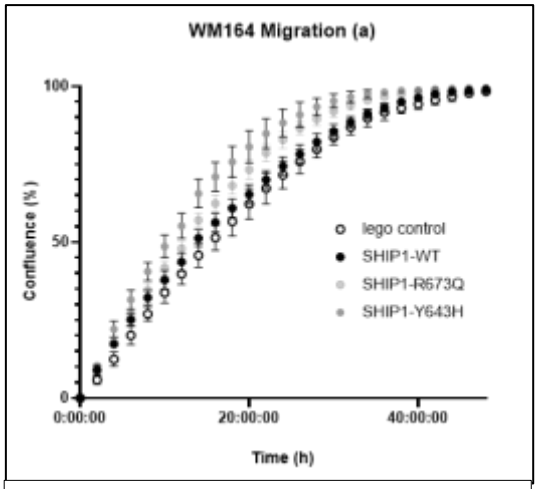

Figure 16.1: WM164 migration (1)

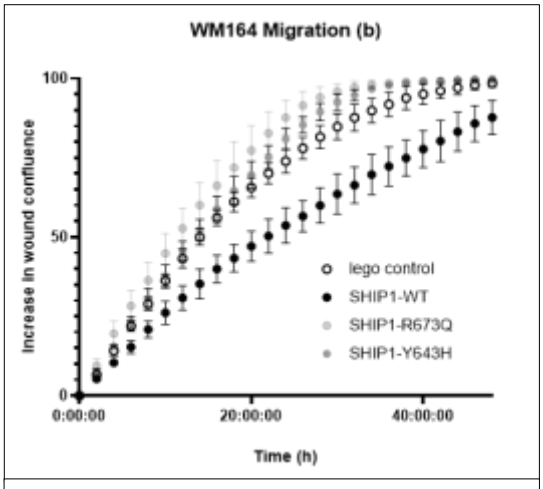

Figure 16.2: WM164 migration (2)

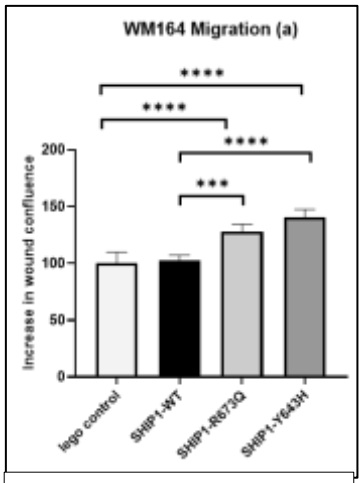

Figure 16.3: WM164 migration speed, lego control normalized to 100% (1)

In the first experiment, both SHIP1-R673Q and Y643H-transduced cells were significantly faster migrating than the other two cell lines, with migration rates increased by 27,8% and 40,4% compared to the control. With SHIP1-wt, there was an increase by 2,9%. In the second, wild type SHIP1 led to a highly significant inhibition of migration by 42,8% compared to the control. With R673Q and Y643H, there were nonsignificant increases by 17,4% and 4,9%, respectively.

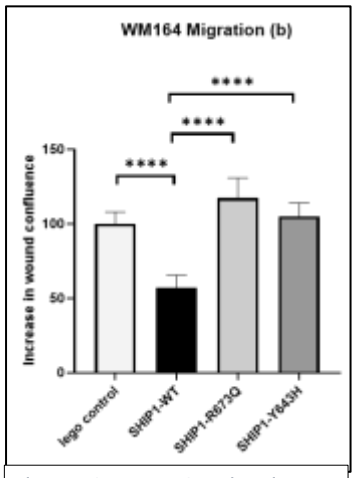

Figure 16.4: WM164 migration speed, lego control normalized to 100% (2)

Both trials consistently show the difference between wild type SHIP1 and SHIP1 mutants. However, it is not clear in how far this is effect is caused by an inhibitory impact of wild type SHIP1, migration promoting effects of the SHIP1-mutants, or a combination of both. There is some resemblance to the migration behavior of WM793 cells, with the limitation that inhibition by wild type SHIP1 is more pronounced in the other melanoma cell line.

Influence of Rac1-inhibition on migration

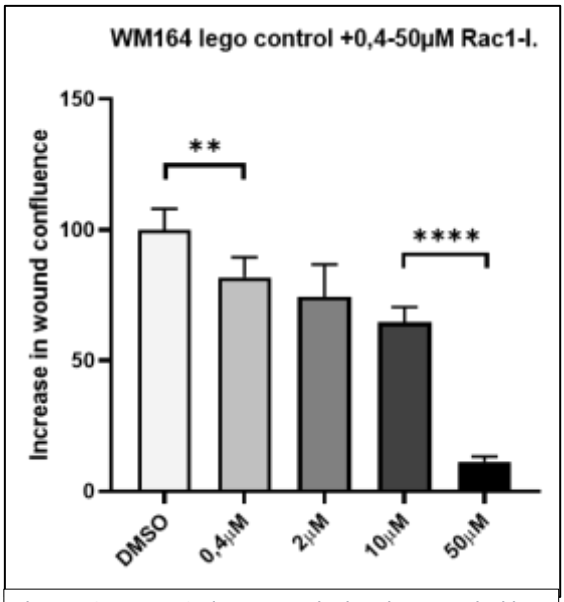

Figure 16.5: WM164 lego control migration speed with Rac1-inhibor, DMSO control normalized to 100%

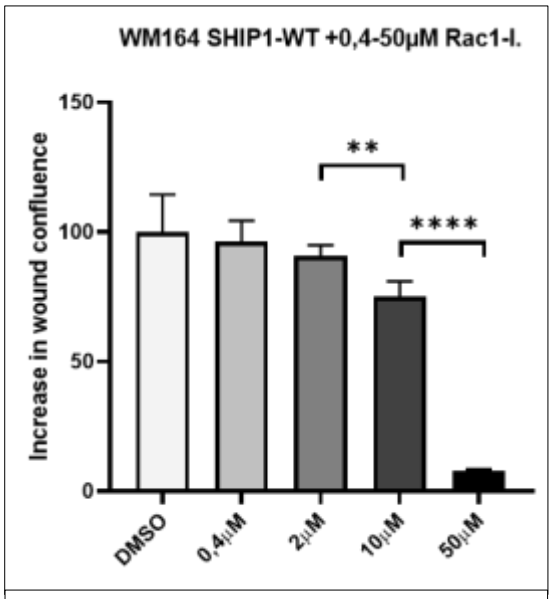

Figure 16.6: WM164 SHIP1-wt migration speed with Rac1-inhibor, DMSO control normalized to 100%

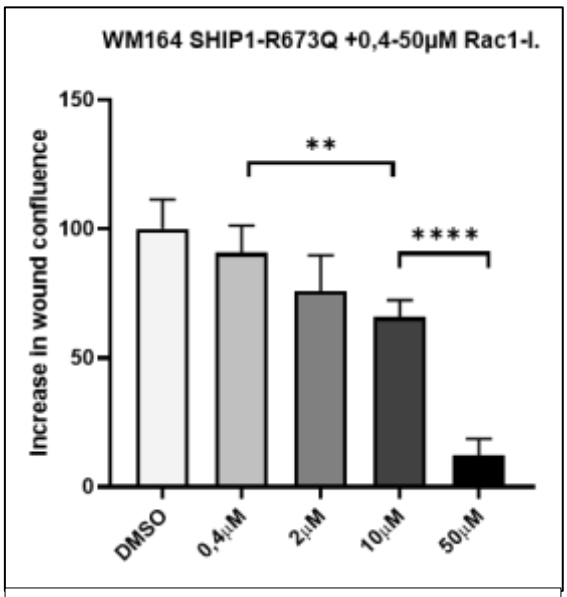

Figure 16.7: WM164 SHIP1-R673Q migration speed with Rac1-inhibor, DMSO control normalized to 100%

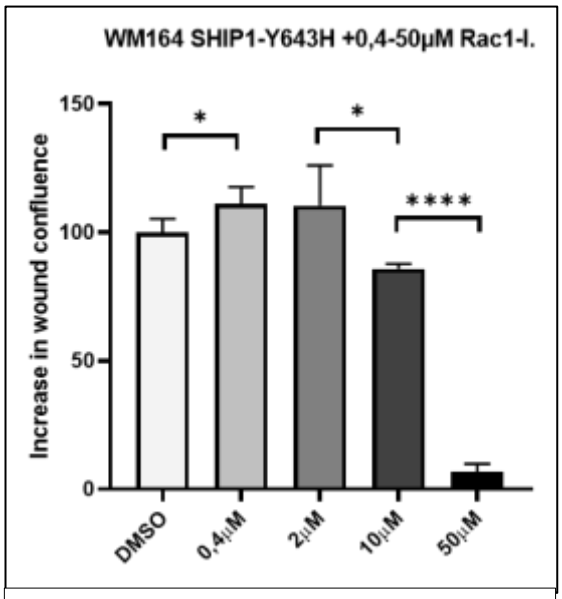

Figure 16.8: WM164 SHIP1-Y643H migration speed with Rac1-inhibor, DMSO control normalized to 100%

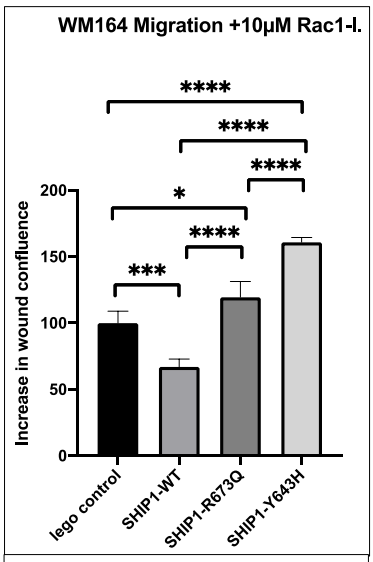

Figure 16.9: WM164 migration speed with 10µM Rac1-inhibor, DMSO control normalized to 100%

Next, migration of WM164 cells was measured under treatment with NSC23766. As in WM793 cells, an inhibition gradient was observed within the initial concentration range of 0,4-50µM. Migration was moderately inhibited at 10µM and strongly curbed at 50µM. Seeded at a higher confluence, they appeared to be slightly more tolerant to high inhibitor concentrations than in proliferation assays. Comparison at 10µM demonstrated a similar tendency as the inhibitor free trials. Wild type SHIP1-overexpressing cells overgrew the scratch wounds slowest (-33,1%), while the SHIP1 mutants R673Q (+19,4%) and Y643H (+60,9%) accelerated migration.

3.4.3.3 WM164 Invasion

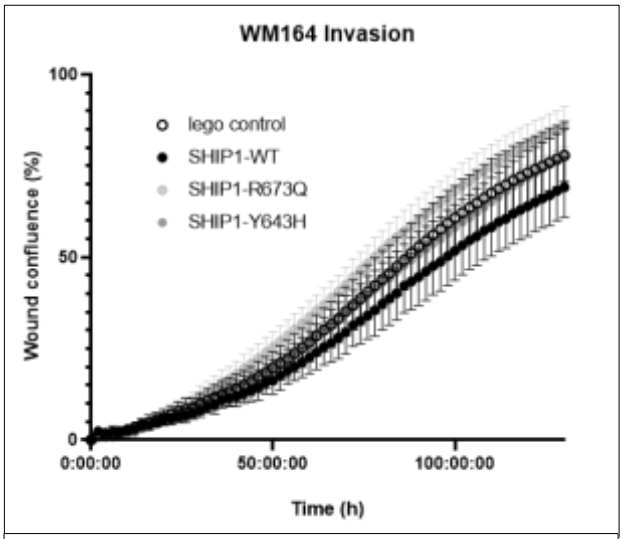

Figure 17.1: WM164 invasion in Matrigel

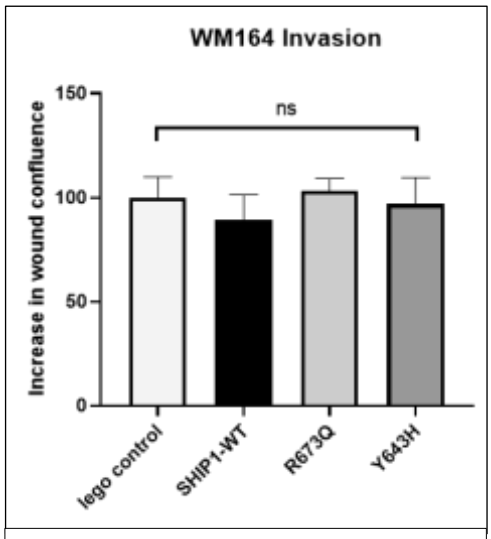

Figure 17.2: WM164 invasion in Matrigel, lego control normalized to 100%

WM164 cells were not quite as fast-invading as WM793 cells, reaching an average relative wound density of 65-80% after five days. Invasion started to slow down between 50% and 60% wound density, likely due to medium evaporation. To capture the linear phase, invasion rate was calculated from 20 to 50%. Wild type SHIP1 led to a decrease by 10,6%, R673Q and increase by 3,2% and Y643H a decrease by 3,2%, none of which was significant.

3.4.3.4 Rac1 and Rac1b transient knockdown

The Rac1-inhibitor NSC23766 curbed proliferation and migration of all three cell lines at relatively high, slightly varying concentrations and turned out to have a narrow “therapeutic range”. However, these effects might not result solely from Rac1-inhibition, as

NSC23766 has been shown to have off-target effects in the past (Dutting et al., 2015). For exemplary validation of the findings obtained with the inhibitor, a transient Rac1- and Rac1b knockdown was conducted with WM164 cells, and migration was measured. Cells were treated with siRNA on two consecutive days. Two different scrambled siRNAs were used as controls. The following day, they were plated for migration assays and scratched four hours later, so they would overgrow the scratches within about three days after the second transfection- while Rac1 and Rac1b levels would be lowered. Lysates for Western Blotting were made two days after the second transfection.

The informative value of this experiment is limited by the fact that only one cell line and one knockdown siRNA, for Rac1 and Rac1b each, were used. Also, transient transfection offers only a limited time span for experiments. For further validation, transfection with a second vector or ideally a stable transduction should be used and more cell lines included.

3.4.3.4.1 Rac1-knockdown

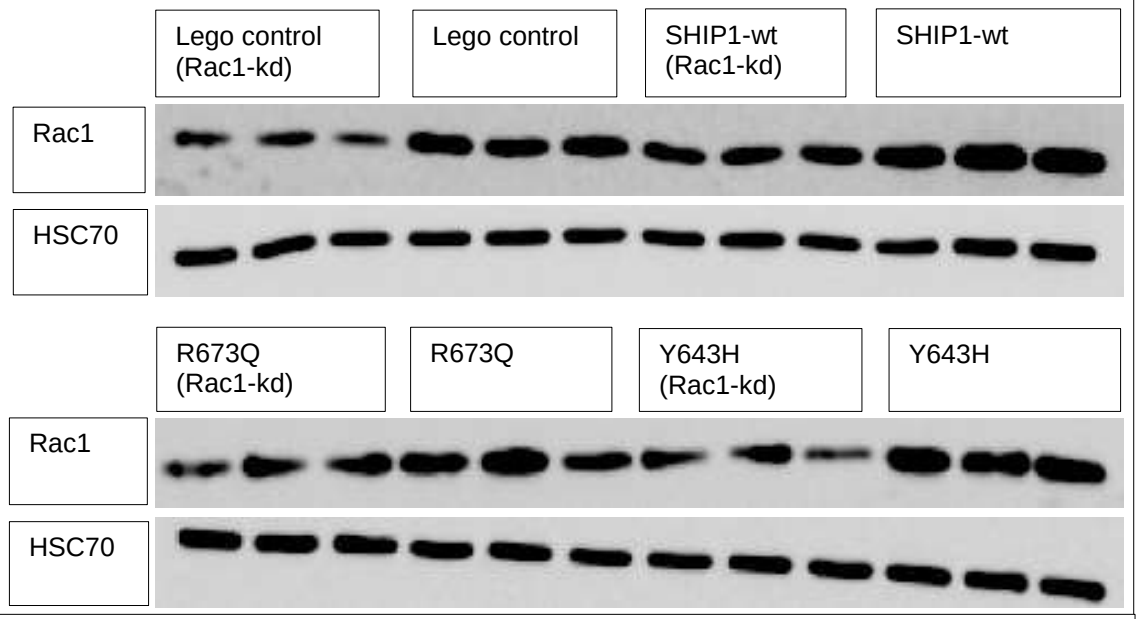

Figure 18.1: Western Blot of Rac1 in WM164 lego control, SHIP1-wt, R673Q and Y643H after Rac1-knockdown

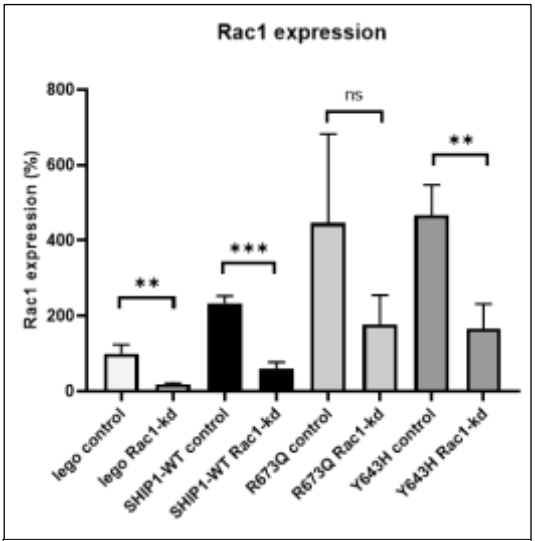

Figure 18.2: Rac1-expression before and after knockdown in WM164 lego control, SHIP1-wt, R673Q and A643H, lego control (before knockdown) normalized to 100%

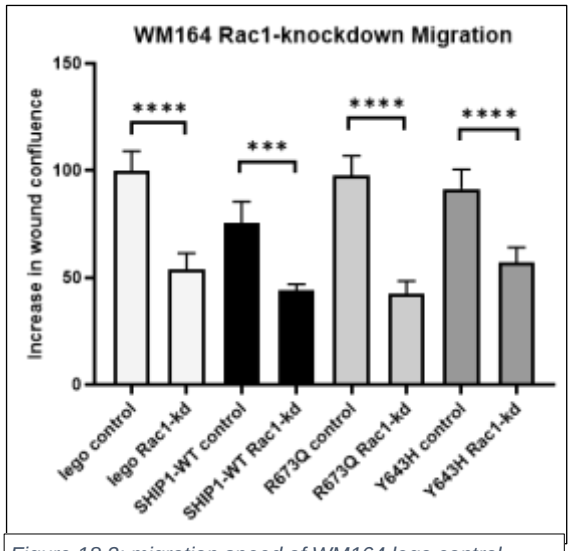

Figure 18.3: migration speed of WM164 lego control, SHIP1-wt, R673Q and A643H before and after Rac1-knockdown, lego control (before knockdown) normalized to 100%

Western blotting showed a significant reduction of Rac1-levels in control, SHIP1-wild type and Y643H-transduced cells by 81,5%, 74,7% and 64,7%, respectively. Due to a high standard deviation, the 60,5% decrease of Rac1-expression in R673Q-transduced cells was not significant. The scratch assay revealed a highly significant inhibition of migration in all cell lines with the Rac1-knockdown compared to the respective control, the greatest of them (56,7%) in R673Q cells before lego control cells (46,3%), wild type SHIP1 (42,8%) and Y643H (38,7%). Thus, it seems probable that Rac1 was knocked down in R673Q-transduced cells to a similar -or even greater- extent than in the other cell lines. Overall, transient Rac1-knockdown led to a decrease in migration rate similar to the effects of NSC23766, and there is no indication so far that the results obtained with moderate inhibitor concentrations are owed to off-target effects. As there was no inordinate extent of apoptosis observed in this trial, it remains unclear whether apoptosis caused by high inhibitor concentrations results solely from Rac1-inhibiton or a combination with other mechanisms.

3.4.3.4.2 Rac1b-knockdown

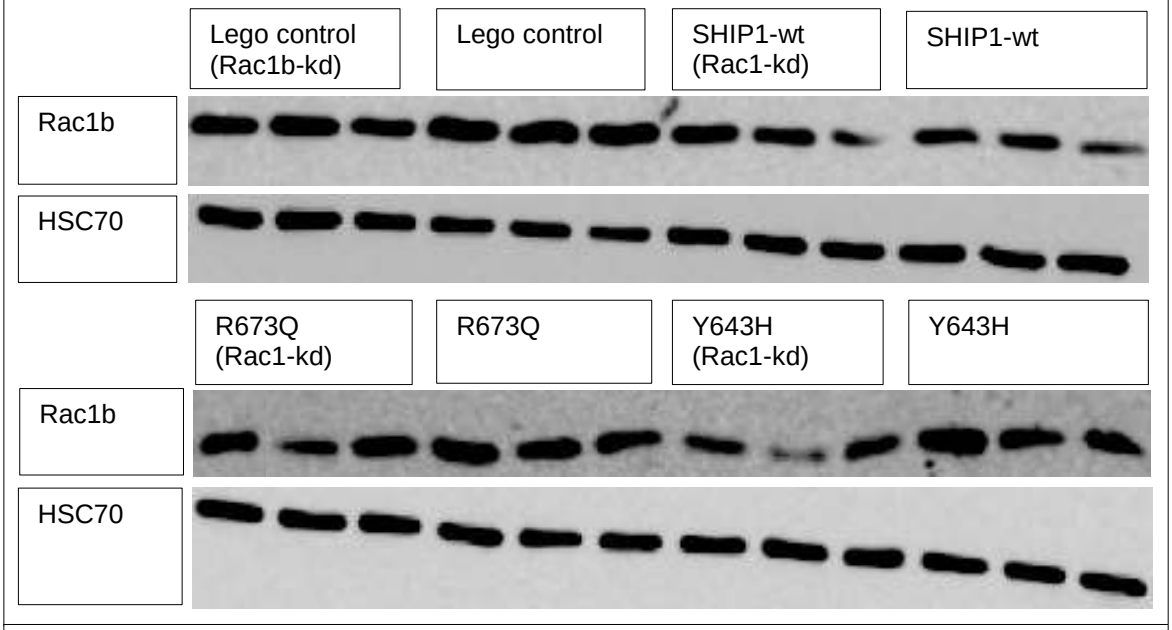

Figure 18.4: Western Blot of Rac1b in WM164 lego control, SHIP1-wt, R673Q and Y643H after Rac1b-knockdown

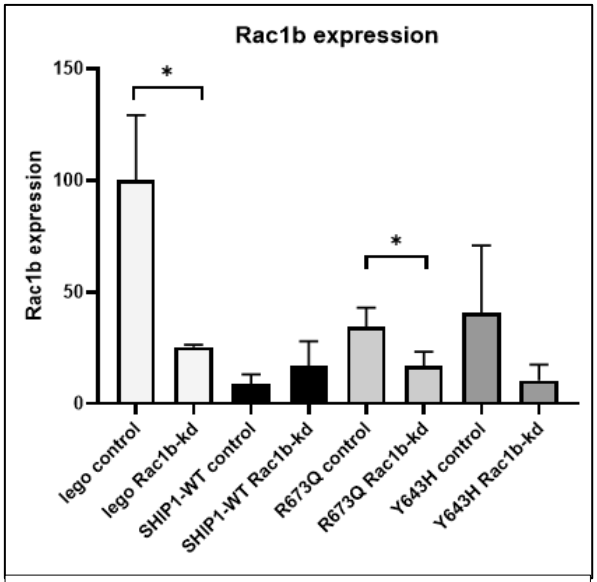

Figure 18.5: Rac1b-expression before and after knockdown in WM164 lego control, SHIP1-wt, R673Q and A643H, lego control (before knockdown) normalized to 100%

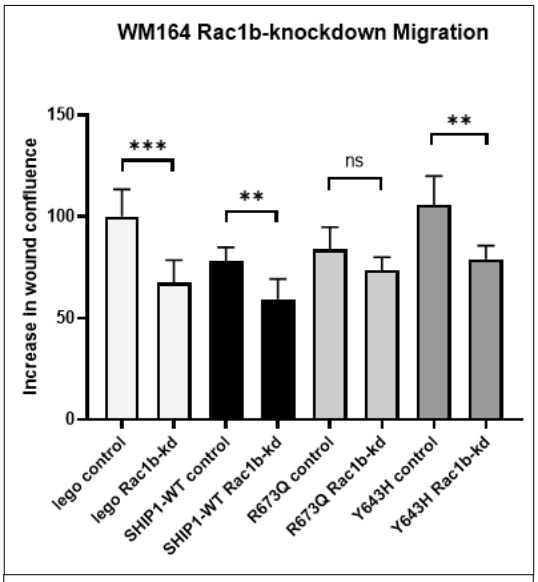

Figure 18.6: migration speed before and after Rac1b-knockdown in WM164 lego control, SHIP1-wt, R673Q and A643H, lego control (before knockdown) normalized to 100%

According to the Western Blot, transient knockdown led to a significant decrease of Rac1b levels in control and R673Q cells by 74,7% and 51,1%. In Y643H cells, there was a non-significant reduction by 74,5% and in wild type SHIP1 cells, a non-significant 47,1% increase. However, knockdown of Rac1b also inhibited migration significantly in all WM164 cell lines but R673Q. Thus, it seems probable that Rac1b was knocked in wild type SHIP1-cells as well and the corresponding western blot not too accurate. Reduction of migration rates is less pronounced than with Rac1-knockdown, ranging from 12,2% (R673Q) to 32,6%

(lego control). This may result either from a less effective depletion of Rac1b compared to Rac1 or distinct functions of the two Rac1s for migration in the examined cell line.

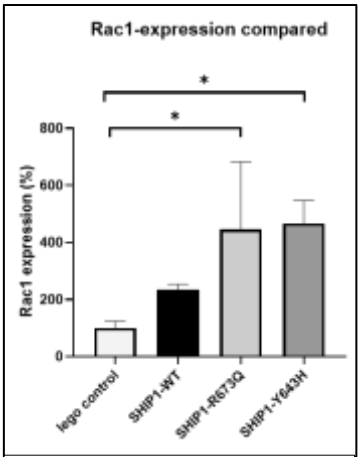

Figure 18.7: comparison of Rac1-expression in WM164 lego control, SHIP1-wt, R673Q and A643H, lego control normalized to 100%

The four cell lines showed distinct Rac1-expression patterns. Expression of Rac1 was enhanced in the three SHIP1-transduced cell lines by 133,5%, 346% and 366,5%, the latter two being significant by ANOVA as displayed in the graph. By t-test, there were significant differences between the control and SHIP1-WT, control and Y643H, as well as SHIP1-WT and Y643H with p-values <0,01 (**).

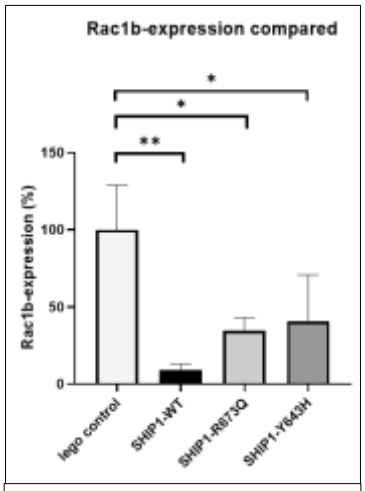

Figure 18.8: comparison of Rac1b-expression in WM164 lego control, SHIP1-wt, R673Q and A643H, lego control normalized to 100%

Rac1b-expression followed a different trend, with protein levels significantly reduced in all three SHIP1-overexpressing cell lines, by 91,1%, 56,6% and 59,3% respectively. However, this comparison is questionable in view of the flawed Rac1b western blot.

4 Discussion

4.1 pAKT levels

In HCT116 and WM793 cells, overexpression of wild type SHIP1 and R673Q led to alterations in pAKT (S473) levels. In HCT116 cells, wild type SHIP1 led to a significant increase by around 30% and R673Q to a significant decrease by more than 50%, despite low protein levels. These results indicate that in this cell line, AKT phosphorylation may correlate with $PI(3,4)P_2$ rather than $PI(3,4,5)P_3$ levels, if R673Q is assumed to trap its substrate to some degree, protecting it from phosphoinositide phosphatases. However, the affinity of other phosphoinositide binding proteins to $PI(3,4,5)P_3$ and $PI(3,4)P_2$ must be taken into consideration when suspecting substrate trapping by R673Q. AKT1 as well as the phosphatases PTEN and INPP4B have been described to have a higher affinity to $PI(3,4,5)P_3$ than R673Q, so in their presence, substrate trapping would be unlikely, except possibly in lipid rafts of the membrane (Nelson et al, 2021). To further elucidate the possibility of substrate trapping, expression levels of other phosphoinositide binding

proteins with higher affinity to PI(3,4,5)P_3 and PI(3,4)P_2 could be quantified in the respective cell lines in the future.

In WM793 cells, both wild type SHIP1 and R673Q caused declines of pAKT (S473) by over 80%, which were significant compared to Y643H and the control. Similar effects of wild type SHIP1 and Y643H had been observed before. Y643H's residual catalytic activity appears to make a crucial difference here. Possibly, both wild type SHIP1 and R673Q disrupt the PI(3,4,5)P_3/ PI(3,4)P_2 balance in a way that is unfavorable for AKT-phosphorylation, while Y643H doesn't. In WM164, there were no quantifiable amounts of pAKT detected, unlike previously described in our group (Drechsel, 2019). This cell line doesn't appear to rely primarily on constitutive PI3K-AKT pathway activation for growth. This substantiates the assumption that the presence of SHIP1 wild type can alter AKT phosphorylation to either direction, likely depending on the specific signaling context in the cells and resulting balance of PI(3,4,5)P_3 and PI(3,4)P_2, as described by the "Two-PIP hypothesis" (Kerr, 2011).

4.2 SHIP1 localization

The results of differential centrifugation, indicating that wild type SHIP1 is located predominantly at the membrane while R673Q has higher cytosolic levels, contradict earlier findings in our group. These had pointed towards a predominantly cytosolic localization of SHIP1 (Drechsel, 2019) (Cremer, 2018) and higher levels of membrane association for R673Q compared to wild type (Drechsel, 2019). My results, on the other hand, might indicate that R673Q has a lower affinity to PI(3,4,5)P_3 than wild type SHIP1- especially in WM793 cells. This interpretation is in line with later results from our group showing that R673Q is indeed less affine to PI(3,4,5)P_3 than a number of active phosphoinositide phosphatases, including widtype SHIP1 (Nelson et al, 2021). It may also be owed to the fact that SHIP1 is an allosteric enzyme, which binds to and is induced by its membrane-bound product PI(3,4)P_2 (Conde et al., 2011) (Nelson, 2017). The divergence may reflect higher levels of PI(3,4)P_2 in the membranes of cells overexpressing catalytically active SHIP1. Under this aspect, it is difficult to determine whether substrate or product trapping is responsible for SHIP1's membrane association.

However, considering the discrepancy to earlier results with differential centrifugation, the informative value of this method is somewhat questionable. A potential error source is the lack of a control for the cytosolic fraction's purity- if some pieces of membrane escaped into the other fraction, the p200/s200 ratio would be lowered. Yet, it is difficult to conceive how this could have happened for R673Q, but not wild type SHIP1-containing cell lysates, or vice versa. It should also be considered that with differential centrifugation, membrane association is measured under artificial conditions, which may

have little in common with the situation in living cells. Cells are shredded by sonification and kept on ice after that. However, despite cooling, differences in ambient temperature may interfere. As R673Q has a mutation in the catalytic domain, wild type SHIP1 and R673Q might differ in their temperature-dependent affinity to their substrate $PI(3,4,5)P_3$ and product $PI(3,4)P_2$, causing divergent results.

To verify differential centrifugation results, SHIP1 was dyed and examined by confocal microscopy in individual cells and fluorescence intensity quantified. Though this was an exemplary trial not suited for statistical analysis, it gave a rough impression of SHIP1 distribution. While visual diagnosis and fluorescence intensity graphs did show a few spikes of color intensity at the membrane- more pronouncedly in HCT116 than WM cells- most SHIP1 appeared to be located in the cytosol, challenging the validity of membrane fractionation results.

For further examination, confocal microscopy could be done with a larger number of cells and integrals of fluorescence intensity plots calculated to quantify membrane-associated and cytosolic SHIP1. Unlike differential centrifugation, it depicts SHIP1 distribution in largely intact cells. However, it's not always clear whether lateral spikes actually depict the membrane, and still doesn't allow discrimination between substrate and product trapping. Therefore, such experiments should be complemented with the use of $PI(3,4,5)P_3$ and $PI(3,4)P_2$ -specific probes to examine their co-localization with SHIP1 and mutants.

4.3 SHIP1 in HCT116 cells

In HCT116 cells, SHIP1-wild type led to a small but highly significant reduction in proliferation rate in two trials, while R673Q slightly increased proliferation in one of them. A decrease of proliferation in SHIP1-wild type transduced HCT116 as well as HT29 cells, measured by EdU flow cytometry proliferation assay, has previously been reported in our group, though with 0,5% FCS instead of 10% FCS cultivation medium (Allgöwer-Martin, 2015). A possible explanation would be reduced levels of $PI(3,4,5)P_3$ and subsequent AKT-phosphorylation in the presence of wild type SHIP1, and increased $PI(3,4,5)P_3$ and pAKT in the presence of catalytically inactive, substrate-trapping R673Q. However, quantification of pAKT levels by Western Blot doesn't support this assumption. With wild type SHIP1, pAKT levels were insignificantly heightened, and with R673Q significantly lowered, indicating that they correlate with $PI(3,4)P_2$ rather than $PI(3,4,5)P_3$ levels if R673Q is supposed to trap its substrate. But as previously mentioned, the absence of other phosphoinositide binding proteins with higher affinity to $PI(3,4,5)P_3$ than R673Q would be a prerequisite for the assumption of substrate trapping (Nelson et al, 2021).

Possibly, SHIP1's impact on proliferation is mediated by $PI(3,4,5)P_3$, but not pAKT levels in this cell line. Various paths of AKT-independent PI3K-signalling have been described in the past, among them the PDK1/ mTORC axis as well as Rac and TEC-family kinase pathways. PDK1 and mTORC2 not only activate AKT, but also some serum and glucocorticoid induced kinases (SGK) and members of the protein kinase C (PKC) family in response to $PI(3,4,5)P_3$ -generation by PI3K. SGKs resemble AKT with regard to substrates and functions for proliferation, migration and survival.

Rac is converted into its active, GTP-bound state by GEFs, i.e. PREX, Sos1 and Vav1, which are in turn activated by PIP3 (Lien et al., 2017). Besides regulating cell motility by promoting actin cytoskeleton reorganization, Rac1 also promotes glycolysis via a release of aldolase A from actin. Moreover, it is involved in stimulating PAKs (p21-activated kinases), which control cell cycle progression and survival (Kotelevets and Chastre, 2020). The splice variant Rac1b, expressed e.g. in colorectal cancer cells, has also been shown to promote cell cycle progression, survival and EMT (De et al., 2019). As AKT can inhibit Rac1-activity by phosphorylation, reducing its capacity to bind GTP (Kwon et al., 2000), lower AKT levels can actually be favorable for Rac1-signaling.

Lastly, TEC-family kinases like BTK are $PI(3,4,5)P_3$ -recruited, bringing forth the transcription repertoires of NFkB and NFAT via Ras activation. Some members of this kinase family also cross-talk with Rac signaling via activation of Rac-GEFs (Lien et al., 2017). If HCT116 cells rely heavily on one or more of these AKT-independent pathways for proliferation, reduced $PI(3,4,5)P_3$ levels may curb their growth despite increased levels of pAKT, and vice versa.

Unlike proliferation, migration was not significantly affected by wild type SHIP1-overexpression. A previous study in our group, conducted with a different kind of scratch assay, had hinted at a migration-enhancing effect. Several explanations for this were considered, one of them being the recruitment of lamellipodin to the membrane-bound SHIP1-product $PI(3,4)P_2$ (Allgöwer-Martin, 2015). Lamellipodin had been identified as an activator of the ENA/VASP actin-elongating protein complex and probably also other positive regulators of the actin cytoskeleton, promoting the formation of lamellipodia. These protrusions allow cells to adhere and drag themselves forward, enabling migration (Krause et al, 2014) (Ben-Chetrit et al., 2015). Furthermore, a stabilization of EGF-receptors was discussed, caused by SHIP1-mediated inhibition of the ubiquitin ligase c-Cbl, which induces EGFR-degradation. Increased EGFR-expression would subsequently raise PI3K-signalling. This hypothesis was substantiated by an increased susceptibility of SHIP1-overexpressing HCT116 cells to Erlotinib compared to control cells with regard to migration (Allgöwer-

Martin, 2015) (etc.). The latter hypothesis, however, is at odds with the suspected decrease in PI3K/ PIP3- signaling as a cause for reduced proliferation.

Although SHIP1's migration-promoting impact wasn't reproduced with IncuCyte live cell imaging, these mechanisms may be relevant, counteracting the above-mentioned paths that would mediate inhibitory effects not only on proliferation but also migration upon lowered $PI(3,4,5)P_3$ -levels. Especially $PI(3,4,5)P_3$ -dependent Rac1-signaling would be expected to decline in the presence of SHIP1. GTP-bound Rac1 in combination with $PI(3,4,5)P_3$ activates the WAVE-complex, which in turn enables actin polymerization by the Arp2/3-complex of actin nucleators and ENA/ VASP. Also, the (insignificantly) heightened levels of pAKT (S473) may come into play here, enhancing migration through various AKT-dependent paths. Active AKT phosphorylates the transcription factor Twist, which is linked to infiltration and metastasis- clinically- and the expression of EMT-associated proteins like N-cadherin- on a cellular level. It also modulates expression levels of the EMT-inducing transcription factors Snail and Slug, among many others (Xu et al., 2015). Therefore, it is conceivable that two or more of these opposing mechanisms are affected and balance each other out overall.

The catalytically inactive SHIP1-mutant R673Q, coming along with reduced pAKT-levels, led to a slightly significant increase in migration in one of two trials, similar to proliferation assay results. This may be conveyed by $PI(3,4,5)P_3$ -mediated signaling, especially via Rac1- disinhibited by reduced AKT-activation- but again possibly also SGKs and TEC-family kinases. The effect may be dampened by decreased AKT-phosphorylation and Lamellipodin recruitment as a result of lower $PI(3,4)P_2$ levels.

Though quickly proliferating and migrating, HCT116 cells were not very invasive. In the matrigel invasion assay, they only reached a wound confluence of around 25% in five days. There was a significant difference of 23,1% between SHIP1-wt and R673Q-transduced cells. When invading, cells may go through epithelial-mesenchymal transition and employ proteinases for extracellular matrix (ECM) decomposition, or take on an amoeboid shape to squeeze through ECM gaps. Expression of ECM-degrading proteinases, i.e. matrix metalloproteinases, has been described to be increased at the invasive front of some carcinomas (Gerashchenko et al., 2019). Rac1 and other Rho-GTPases- upregulated in many metastasized tumors- play a role not only for migration but also for amoeboid and EMT-related invasion, as both are associated with actin cytoskeleton remodeling and adhesion (Gkretsi and Stylianopoulos, 2018). The slightly reduced invasion rate in wild type SHIP1-overexpressing cells may also have to do with decreased $PI(3,4,5)P_3$ -dependent Rac1-activation.

4.3.1 Rac1-inhibition in HCT116 cells

The Rac1-inhibitor NSC23766 was applied to further investigate how proliferation and especially migration are mediated in wild type SHIP1- and R673Q-transduced cells compared to the control. The inhibitor proved rather difficult to work with for IncuCyte live cell imaging, having effective dosages in the double-digit micromolar range and a narrow therapeutic margin. Especially higher concentrations increased standard deviations considerably and yielded varying results. This was likely associated with medium evaporation from the wells during live cell imaging, causing deviations in concentration between the wells, especially with high dosages. Therefore, IC50-values were not calculated, and comparisons between cell lines at specific concentrations are discussed with reservation.

Beyond methodical limitations, genomic heterogeneity of HCT116 cells may have caused differential sensitivity to the inhibitor between cell subpopulations, both at the same time and over the course of cultivation. Genomic heterogeneity is a well-established cause for therapy resistance in malignant tumors (Dagogo-Jack and Shaw, 2018) and has also been observed in cultivated HeLa-cells (Hu et al., 2019). This assumption was supported by the observation that after a few days of treatment with high inhibitor concentrations, making most cells look senescent or apoptotic, some would recover and rapidly overgrow the wells. Moreover, possible off-target effects of NSC23766 should be taken into consideration. In mouse platelets, it has been described to reduce PAK1 and PAK2 phosphorylation without involvement of Rac1, especially at higher concentrations (Dutting et al., 2015). Dose-dependent off-target effects might have occurred in HCT116 cells (and the examined melanoma cell lines) as well.

Proliferation of HCT116 cells was strongly inhibited at 40µM NSC23766 and the three cell lines showed similar growth rates in relation to each other as without the inhibitor, wild type SHIP1-overexpressing cells proliferating significantly slower than control cells. This indicates that the three HCT116 cell lines depend on Rac1-signaling for proliferation to similar degrees, R673Q-transduced cells possibly a bit more. This may be explained with reduced pAKT (S473) levels in R673Q-transduced HCT116 cells. They might compensate for this with increased $PI(3,4,5)P_3$ -mediated, AKT-independent Rac1-signaling.

Migration was inhibited more strongly than proliferation at the same NSC23766 concentration in the final trial, though not in a pre-trial. This discrepancy may be owed to the general difficulties with the inhibitor, or reflect the greater importance of Rac1-signaling for migration over proliferation in this cell line. Interestingly, both SHIP1- and to a slightly lesser extent also R673Q-transduced cells were much more sensitive to the inhibitor than control cells with regard to migration. This challenges the above mentioned hypothesis that SHIP1-overexpressing cells can compensate for decreased $PI(3,4,5)P_3$-mediated (and

AKT-independent) signaling by direct Lamellipodin recruitment via PI(3,4)P_2. In that case, they should be less instead of more vulnerable to Rac1-inhibition. As wild type SHIP1 and R673Q confer similar reactions to NSC23766 in HCT116 cells, the adapter function of SHIP1 might play a role rather than the catalytic activity. It may downregulate pro-migrative signaling via other pathways, making the cells more dependent on Rac1-activity. In hematopoietic cells, SHIP1 can inhibit MAP-kinase activation in various ways, i.e. by interacting with Shc, thereby preventing its association with Grb2 and Sos. As a result, Ras- and subsequently MAPK-activation are reduced. Also, binding to Dok1 recruits Ras-GAP, which deactivates Ras (Conde et al., 2011). However, the question arises in how far these mechanisms apply to colorectal carcinoma cells, and if they do, why they don't impact migration under inhibitor-free conditions.

4.4 SHIP1 in WM793 cells

WM793 cells reacted quite differently to SHIP1 than HCT116 cells. Proliferation assays showed that Y643H-transduced cells grew significantly faster than those with SHIP1-wild type and R673Q. The difference between Y643H and R673Q had priorly been detected by cell counting and Alamar Blue Assay (Drechsel, 2019). Beyond that, they didn't give a clear picture of how proliferation was affected. This may have been due to methodic problems with the relatively low growth rate of this cell line, making it more difficult to hit the ideal starting confluence, as well as a lack of contrast, making them harder to distinguish from the background.

Either way, the obtained results are partly in agreement with pAKT levels. AKT phosphorylation levels were significantly lowered in response to both wild type SHIP1 as well as R673Q in comparison to the control and Y643H. Both of them may have shifted the PI(3,4,5)P_3 / PI(3,4)P_2 balance unfavorably for AKT phosphorylation, to opposite directions. Y643H, with residual catalytic activity, led to a slight, insignificant increase in pAKT levels. It seems this mutant didn't have an adverse effect on the PI(3,4,5)P_3 / PI(3,4)P_2 balance. The discrepancies in pAKT levels were more pronounced than those in proliferation rates, but showed a similar tendency. It seems proliferation of WM793 cells is at least in part mediated by AKT-phosphorylation, which depends on the balance of PI(3,4,5)P_3 and PI(3,4)P_2. Probably, further pathways are involved, mitigating the effect of lowered pAKT levels in wild type SHIP1- and R673Q-overexpressing cells. Knowing that WM793 possess a BRAF-mutation (Smalley et al., 2006), this could well be the Ras/Raf/MAPK pathway.

Scratch assays showed a clearer tendency- wild type SHIP1 inhibited migration of WM793 cells considerably in both, while the SHIP1-mutants accelerated it up in one of two trials. Boyden Chamber Assays previously conducted in our group hadn't shown the

inhibitory effect of SHIP1-wild type (Drechsel, 2019), perhaps because this type of assay measures chemotactic migration, unlike the IncuCyte scratch assay. For scratch assays, pAKT levels correlate with migration rate in wild type SHIP1- and Y643H- but not R673Q-transduced cells. Similar to HCT116 cells, WM793 cells may compensate for reduced AKT-activation with increased PI(3,4,5)P_3-dependent signaling via alternate pathways as described above, in the presence of R673Q- especially under the assumption of a substrate trapping effect. Again, the Rac1-pathway is a likely candidate.

Interestingly, results of the matrigel invasion assay showed a closer correlation with pAKT levels. Both SHIP1-wild type and R673Q caused a significant reduction in invasion rates compared to the control and Y643H, though for wild type SHIP1, this effect was less pronounced than in migration assays. For invasion, AKT-signaling may be more relevant than other PI(3,4,5)P_3 -dependent pathways, compared to migration. However, other pathways like Ras/Raf/MAPK are probably involved here as well.

4.4.1 Rac1-Inhibition

For WM793 cells, the same reservations for trials with NSC23766 should be considered as for HCT116 cells. Rac1-inhibition led to an inhibition of proliferation from around 2µM upwards, and brought it to a standstill at 50µM. Low concentrations seemed to have a stronger impact on cells transduced with the SHIP1-mutants, and at 10µM, there were no significant differences detectable between the four cell lines. So especially with Y643H, cells seemed to be slightly more susceptible to inhibition, indicating that they might be a little more dependent on Rac1-sigaling for proliferation. This is in line with the assumption that like R673Q, Y643H leads to some degree of PI(3,4,5)P_3 substrate trapping. So increased PI(3,4,5)P_3 -dependent Rac1-activation, together with slightly increased AKT-phosphorylation, may explain why Rac1-inhibition reverses the growth advantage of Y643H-transduced cells. Besides, it should also be considered that proliferation of WM793 cells was more difficult to measure by IncuCyte live cell imaging than that of HCT116, making small differences difficult to interpret.

In migration assays, Rac1-inhibition revealed a similar trend. Unlike HCT116, WM793 cells were a bit less sensitive to the inhibitor when seeded at higher confluences, compared to proliferation assays. Migration inhibition was dose-dependent between 2µM and 50µM in control, R673Q- and Y643H-, but not SHIP1-WT-transduced cells, which were impeded only at 50µM. At 10µM, there were no significant differences in migration rates, indicating that SHIP1-WT made WM793 cells less susceptible to moderate inhibitor concentrations with regard to migration. This effect may also be owed to already-reduced PIP3-dependent Rac1-signaling in WM793-cells. In the other three cell lines, Rac1-mediated migration signaling is probably reduced to a minimum, resembling the situation in

SHIP1-WT transduced cells. Again, at inhibitor concentrations as high as 50µM, off-target effects may come into play, which likely impact all four cell lines similarly.

4.5 SHIP1 in WM164 cells

WM164 cells differ strongly from the other two cell lines in that their pAKT (S473) levels are so low as to be unquantifiable. This suggests that they don't depend on the PI3K-AKT-pathway too much in the first place, and their highly aggressive phenotype relies primarily on one or more other over-activated pathways. Like WM793 cells, they are known to have a BRAF-mutation (Smalley et al., 2006), so the Ras/Raf/MAPK-pathway probably plays an important role. This can explain why overexpression of wild type SHIP1, R673Q and Y643H had no significant impact on their proliferation rate.

Migration, on the other hand, was indeed altered with SHIP1, though tendencies varied slightly between the two trials. R673Q and Y643H consistently led to increased migration rates compared to wild type SHIP1, while control cells ranged at disparate levels in the two trials. Hence, it is likely that their migration rate is in between those of wild type SHIP1 and the mutants. Here too, Boyden Chamber Assays previously performed in our group yielded different results for SHIP1-wild type, indicating an increase in migration compared to the control (Drechsel, 2019). As this divergence between Boyden Chamber and IncuCyte scratch assay results for wild type SHIP1 has been observed in both melanoma cell lines, wild type SHIP1 may have differential impacts on chemotactic and non-chemotactic migration.

Apparently, PI3K-signaling is more relevant for migration than proliferation, despite very low pAKT-levels in all four WM164 cell lines. Again, this may result from PI3K-dependent pathways other than AKT, like SGKs, TEC-family kinases and Rac1, which may be disinhibited in the absence of pAKT. Though mechanistically similar to migration, invasion is not significantly changed with SHIP1, perhaps because it is mediated predominantly by Ras/Raf/MAPK or yet another pathway.

4.5.1 Rac1-Inhibition

Rac1-inhibition teased out differences in proliferation rates- at 16µM NSC23766, control cells grew highly significantly faster than those transduced with either of the three SHIP1- versions. A similar trend had been observed with HCT116 cells, though in a migration and not proliferation assay. So here, too, adapter functions of SHIP1 might be more relevant than catalytic activity, being able to downregulate Ras-activity. However, it is questionable in how far this mechanism could actually reduce MAPK-activation when mutated BRAF is interposed.

In migration assays, WM164 cells were slightly more tolerant to NSC23766, and comparison between the four lines showed similar tendencies as the inhibitor-free trials. Cells with SHIP1-wild type were slower while those with mutants, especially Y643H, were faster migrating than the control. Assuming these two lines benefit from increased PI(3,4,5)P_3 -mediated Rac1-activation, one would expect inhibitor-treatment to align migration rates, especially in higher dosages. Possibly, approximation only takes place at higher concentrations. Otherwise, Rac1 may not be the main driver of their raised migration rates, or its protein levels may be altered.

4.5.2 Transient Rac1 and Rac1b-knockdown

A transient Rac1- and Rac1b-knockdown and subsequent scratch assay was performed exemplarily with WM164 cells to rule out the possibility that the observed alterations in proliferation and migration were caused by off-target effects. Western Blotting showed that a Rac1-knockdown of around 60%-80% was achieved, which yielded a reduction in migration rates of roughly 40%-55%. Due to the differences in knockdown rates, sensitivity of the four cell lines with regard to migration rates was not further compared. The findings with transient transfection resembled those with intermediate inhibitor concentrations. Migration was inhibited significantly, but cells showed no signs of an increased apoptosis rate. While it is possible that a more complete knockdown of Rac1 also causes apoptosis, it seems likely that the inhibitor has off-target effects that only become relevant at high dosages- especially when considering previous findings with NSC23766 (Dutting et al., 2015).

For Rac1b, knockdown rates of around 50%-75% were achieved- though not significant in one case- and one increase in protein level. The corresponding scratch assay showed reductions in migration rates between 12% and 33%, indicating that either knockdown efficacy was reduced or Rac1b less relevant for migration. Considering that the Western Blot lacked accuracy, either might be the case, but a combination of both aspects seems most likely. The splice variant Rac1b has been observed to differ from Rac1 in function, and even have opposing effects in some cases (Melzer et al., 2019). That, however, wasn't the case here- Rac1b seems to promote migration in WM164 cells, but probably doesn't play as dominant a role as Rac1. This may be due to an overall lower of expression compared to Rac1.

Interestingly, expression of both Rac1 and Rac1b varied between the four WM164 cell lines. Rac1-expression was considerably heightened in all SHIP1-transduced lines, especially with Y643H. Similar results with WM164 cells had previously been obtained in our group (Cremer, 2018). This can contribute to their higher migration rates, and explain why they retain their migration advantage at moderate inhibitor concentrations. For Rac1b,

it is more ventured to draw conclusions based on the Western Blot. Here, the opposite trend stands out, indicating that Rac1b-expression is reduced in those cell lines. It is conceivable that SHIP1-transduction is somehow associated with a shift of expression from Rac1b to Rac1.

5 Conclusion and Outlook

Taken together, the findings of this thesis point towards a tumor suppressive rather than oncogenic role for wild type SHIP1 in colorectal carcinoma and melanoma cells. SHIP1-mutants with reduced or nonexistent catalytic activity can have tumorigenic potential depending on the signaling context. Some degree of residual activity appeared to have a more favorable impact in the presented trials, possibly due to a more advantageous $PI(3,4,5)P_3$/ $PI(3,4)P_2$ -balance, and in WM164 cells apparently also raised Rac1 protein levels. Wild type SHIP1's effect is likely explained by PIP3-degradation and decreased activation of PI3K/ $PI(3,4,5)P_3$ -dependent pathways. This is not always mediated by AKT-phosphorylation, but possibly in many cases also by alternate pathways via Rac1, TEC-family kinases and SGKs. The impact of SHIP1-mutants with reduced catalytic activity, on the other hand, may be owed to substrate trapping. However, this would require the absence of other phosphoinositide binding proteins with higher affinity to $PI(3,4,5)P_3$, like AKT1, PTEN and INPP4B, and could not be proven here with the utilized methods.

These results pose the question why ectopic SHIP1-expression is so frequently found in some carcinomas, especially colorectal carcinoma. As SHIP1-expression is not linked to a more aggressive phenotype (Schaks et al., 2020), it may be a mere byproduct of genomic instability. Still, cancer cells with a growth disadvantage would be expected to fall victim to Darwinian selection in a malignant tumor. Therefore, it is possible that cancer cells intrinsically expressing high or moderate levels of SHIP1 have different patterns of pathway activation than those who do not, like the colorectal carcinoma and melanoma cells examined here. In another signaling context, ectopic expression of SHIP1 may protect colorectal carcinoma cells from cell death induced by hyperactivation of PI3K-AKT signaling and subsequent accumulation of reactive oxygen species (Ehm et al, 2023). Hence, more attention should be paid to cancer cells with intrinsic SHIP1 expression in the future. Also, it should be analyzed whether it is always wild type SHIP1 that is expressed, or mutated versions, which might have divergent effects.

Based on the findings with the three utilized cell lines, SHIP1-induction might be a future therapeutic option for patients with tumors expressing low levels of SHIP1. However, it is unclear how such a treatment would affect tumor cells with moderate or high levels of endogenous SHIP1, as well as the hematopoietic system. Considering the genetic heterogeneity of tumors, such a treatment could select for cancer cells with a signaling

context that benefits from higher $PI(3,4)P_2$ levels due to increased SHIP1 activity. In colorectal carcinoma with moderate or high ectopic SHIP1-expression, on the other hand, SHIP1-inhibition can lead to cell death (Ehm et al, 2023).

Rac1 plays a crucial role for migration, but also proliferation, in all three examined cell lines- and probably many tumors. High dosages of NSC23766 not only inhibited both functions, but induced apoptosis in a large share of cells. This is likely caused by off-target effects to some extent. While the narrow therapeutic range of NSC23766 is problematic for cancer treatment in vivo, other Rac1-inhibitors are being examined in *in vivo* trials and may be suitable as future therapeutic options (Kaneto et al., 2014).

6 Abstract

The PI3K/AKT-signaling pathway, mediating survival, proliferation, migration, adhesion, and differentiation, is frequently deregulated in cancer (Porta et al., 2014). Research on this pathway has largely focused on the oncogenic potential of activating messengers like PI3K and AKT. Meanwhile, the role of 5' phosphatases like SHIP1, dephosphorylating the second messenger PIP3 into PI(3,4)P2, is still ambiguous. Both their substrate PIP3 and product PI(3,4)P2 have the potential to activate AKT and other downstream effectors. SHIP1, whose expression is normally limited to hematopoietic cells, bone cells and mesenchymal stem cells, is ectopically expressed in some carcinoma, e.g. more than 50% of examined colorectal carcinoma samples. SHIP1-mutants with impaired catalytic activity have been described in leukemia and been suggested to 'trap' their product PIP3, thus causing increased pathway activation. This study aims at elucidating the role of wild type SHIP1, as well as mutants with impaired catalytic activity, in solid tumors. SHIP1 was localized with differential centrifugation and confocal microscopy to investigate substrate trapping, and live cell imaging was performed with colorectal cancer and melanoma cell lines to examine the effects of ectopically expressed SHIP1 on proliferation, migration and invasion. Rac1-inhibition was performed to further investigate signaling downstream of AKT.

Ectopic expression of wild type SHIP1 reduced proliferation but not migration rates significantly in the colorectal carcinoma cell line HCT116, while in melanoma cell lines, it significantly lowered migration rates – especially in WM793 cells- but not proliferation rates. Overall, wild type SHIP1 appeared to have a tumor suppressive rather than oncogenic impact when ectopically expressed, but this may not be the case in the signaling context of cancer cells with intrinsic SHIP1-expression. Meanwhile, SHIP1-mutants with reduced catalytic activity heightened migration rates in all cell lines to varying degrees, though not always significantly. This may be a consequence of substrate trapping.

However, differential centrifugation indicated that wild type SHIP1 may be localized mostly at the membrane, while the catalytically inactive mutant R673Q showed higher levels of cytosolic localization, possibly due to the trapping of SHIP1's membrane-bound product PI(3,4)P2. On the other hand, confocal microscopy pointed at a predominantly cytosolic localization of wild type SHIP1 as well as R673Q, in line with previous results from our group.

Inhibition of Rac1 with the inhibitor NSC23766 reduced migration as well as proliferation rates in all cell lines and caused apoptosis at higher concentrations, possibly resulting from off-target effects. In WM793 cells, overexpression of SHIP1 slightly reduced susceptibility with regard to migration, which may be explained by PI(3,4)P2-mediated, Rac1-independent signaling. While the consequences of SHIP1 induction as well as inhibition in vivo may be difficult to predict, Rac1 is a promising target for future therapies.

Zusammenfassung

Der PI3K/AKT-Signalweg vermittelt Zellüberleben, Differenzierung, Proliferation, Migration, Invasion und Adhäsion und ist in vielen Malignomen fehlreguliert. Die Rolle von 5'-Phosphatasen wie SHIP1 in diesem Signalweg ist bisher noch unklar, da sowohl ihr Substrat PIP3 als auch ihr Produkt PI(3,4)P2 AKT und andere Signalmoleküle stromabwärts aktivieren können. SHIP1 wird physiologischerweise nur in hämatopoetischen Zellen, Knochenzellen und mesenchymalen Stammzellen exprimiert, jedoch wurde auch in über 50% der untersuchten Kolonkarzinomproben SHIP1 nachgewiesen. In Leukämien wurden SHIP1-Mutanten mit reduzierter katalytischer Aktivität beschrieben, die vermutlich ihr Substrat PIP3 vor Abbau schützen und dadurch eine Überaktivierung des Signalwegs verursachen. In dieser Arbeit wurde die Rolle von Wildtyp-SHIP1 und Mutanten mit reduzierter katalytischer Aktivität in soliden Tumoren untersucht. Die Lokalisation von SHIP1 in der Zelle wurde mit differenzieller Zentrifugation und konfokaler Mikroskopie untersucht, sowie 'live cell imaging' mit zwei Melanomzelllinien sowie einer Kolonkarzinomzelllinie durchgeführt, um die Effekte von SHIP1-Überexpression auf Proliferation, Migration und Invasion zu ermitteln. Zusätzlich wurde ein Rac1-Inhibitor eingesetzt, um Rückschlüsse auf das signaling stromabwärts von AKT ziehen zu können.

Wildtyp-SHIP1 führte in der Kolonkarzinomzelllinie HCT116 zu einer geringen, aber signifikanten Reduktion der Proliferations-, jedoch nicht Migrationsrate, während es in den Melanomzelllinien, insbesondere WM793, die Migration aber nicht die Proliferation signifikant hemmte. Wildtyp-SHIP1 scheint bei ektoper Expression einen eher tumorsupressiven Effekt zu haben, doch dies könnte in Tumorzellen mit intrinsischer SHIP1-Expression anders sein. SHIP1-Mutanten mit eingeschränkter katalytischer Aktivität erhöhten die Migrationsraten in allen drei Zelllinien in unterschiedlichem Maß, jedoch nicht immer signifikant. Dies könnte eine Folge von 'substrate trapping' sein.

Die differenzielle Zentrifugation deutete darauf hin, dass Wildtyp-SHIP1 vor allem an der Membran lokalisiert ist, während die SHIP1-Mutanten eher im Zytosol vorkamen, was Folge von "Trapping" des Membran-gebundenen SHIP1-Produkts PI(3,4)P2 sein könnte. Die konfokale Mikroskopie wiederum zeigte eine überwiegend zytosolische Lokalisation von SHIP1 und Mutanten, was auch zu früheren Ergebnissen unserer Arbeitsgruppe passt.

Der Rac1-Inhibitor NSC23766 hemmte Proliferation und Migration in allen Zelllinien und führte in höheren Konzentrationen zu Apoptose, womöglich durch off-target Effekte. In WM793-Zellen verursachte Wildtyp-SHIP1-Überexpression eine leicht verringerte Sensitivität gegenüber NSC23766, möglicherweise durch PI(3,4)P2-vermitteltes, Rac1-unabhängiges signaling. Während die Folgen einer SHIP1-Induktion oder Hemmung *in vivo* schwer vorhersehbar sind, ist Rac1 ein vielversprechendes Ziel zukünftiger Therapien.

7 List of Abbreviations

adenomatous polyposis coli (APC); nonsteroidal anti-inflammatory drugs (NSAIDs); Bcl-2-Antagonist of Cell Death (BAD); cyclin dependent kinases (CDK); discoidin domain receptor 1/2; epidermal growth factor receptor (EGFR); epithelial to mesenchymal transition (EMT); forkhead box protein O1 (FOXO-1); glycogen synthase kinase 3β (GSK3β); half maximal inhibitory concentrations (IC50); mammalian target of rapamycin (mTOR); mammalian target of rapamycin complex 1 (mTORC1); mammalian target of rapamycin complex 2 (mTORC2); mitogen activated protein kinase (MAPK); phosphatase and tensin homolog (PTEN); phosphatidylinositol 3-kinase (PI3K); phosphatidylinositol-(3,4,5)-trisphosphate (PIP_3); phosphatidylinositol-(4,5)-bisphosphate (PIP_2); phosphoinositide dependent kinase 1 (PDK-1); phosphorylated extracellular-signal regulated kinase (pERK); pleckstrin homology domain (PH-domain); pleckstrin homology domain leucine rich repeat protein phosphatases (PHLPP); programmed death receptor 1 (PD1); protein phosphatase 2A (PP2A); receptor tyrosine kinases (RTK); retinoblastoma protein (Rb); vascular endothelial growth factor (VEGF), (somatic mutation theory), TOFT (tissue organization field theory), HNPCC (Lynch Syndrome), FAP (Familial adenomatous polyposis), APC (adenomatous polyposis coli), NSAIDs (Nonsteroid anti-inflammatory drugs), Wnt (wingless int-1),TGF-ß (transforming growth factor ß), FIT (fecal immune-chemical test), gFOBT (guaiac fecal occult blood test), FOLFOX (folinic acid+ flourouracil+ oxaliplatin),FOLFIRI (folinic acid+ flourouracil+irinotecan), KRAS (Kirsten rat sarcoma 2 viral oncogene homologue), NRAS (neuroblastoma rat sarcoma 2 viral oncogene homolog), α-MSH (α melanocyte stimulating hormone), UVR (Ultra-violet radiation), ROS (reactive oxygen species), RAC1 (RAS-related C3 botulinum toxin substrate 1), TP53 (tumor protein p53), CDKN2A (cyclin-dependent kinase inhibitor 2a), MET (mesenchymal epithelial transition factor), SSM (superficial spreading melanoma), NMM (nodular melanoma), LMM (lentigo maligna melanoma), IFN (Interferon), MEK1(dual specificity mitogen-activated protein kinase kinase 1), CTLA4 (cytotoxic t-lymphocyte associated antigen), GPCRs (G-protein coupled receptors), GDP (guanosine diphosphate), GTP (guanosine triphosphate), NFkB (nuclear factor kappa B), Arp2/3 (actin related protein 2/3), ENA/VASP (enabled vasodilator-stimulated phosphoprotein), INPP4B (inositol polyphosphate-4-phosphatase type II), IP(1,2,3,4,5)P5 (inositol-(1,2,3,4,5)-pentaphosphate), WAVE (WASP family Verprolin homolog), PREX1 (phosphatidyl-inositol(3,4,5)triphosphate-dependent ran exchange factor 1), TIAM1 (t-lymphoma invasion and metastasis inducing factor), Sos1 (son of sevenless homolog 1), VAV1 (vav guanine nucleotide exchange factor 1), JNK (Janus kinase), ERK (extracellular signal regulated kinase), Shc1 (src-homology 2 domain containing transforming protein), Dok1 (docking protein 1), Grb2 (growth factor receptor-bound protein 2), PTB

(polypyrimidine tract-binding protein), mRNA (messenger RNA), miR (microRNA), M-CSF (macrophage colony-stimulating factor), IL (interleukin), LPS (lipopolysaccharide), TLR (toll-like receptor), ko (knock-out), Ig (immunoglobulin), NK-cell (natural killer cell), BCR (b-cell receptor), ALL (acute lymphatic leukemia), CLL (chronic lymphatic leukemia), ALL (acute myeloid leukemia), CML (chronic myeloid leukemia), HTLV1 (human t-lymphotrophic virus type 1), siRNA (small interfering RNA), shRNA (short hairpin RNA), DLBCL (diffuse large b-cell lymphoma), PIB5PA (PI(4,5)P_2-5'-phosphatase), INPP5J (inositol 5'polyphosphate phosphatase), NSCLC (non-small-cell lung carcinoma), HSC70 (heat shock cognate 71kDa), GAPDH (glycerinaldehyde-3-phosphate dehydrogenase), DMSO (dimethyl sulfoxide), DMEM (Dulbecco's modified eagle medium), FCS (fetal calf serum), SGK (serum and glucocorticoid induced kinase), PKC (protein kinase C), PAK (p21-activated kinase), BTK (Bruton's tyrosine kinase), NFAT (nuclear factor of activated t-cells), c-Cbl (casitas b-lineage lymphoma), ECM (extracellular matrix), BRAF (v-raf murine sarcoma viral homologue B1), LB (Luria-Bertani medium), SDS-PAGE (sodium dodecylsulfate polyacrylamide gel), DTT (dithiothreitol), EDTA (ethylene diaminetetraaceitic acid), PBS (phosphate-buffered saline), APS (ammonium per sulfate), TEMED (tetramethylethylenediamine), SCR (scrambled), HEK293 (human embryonic kidney cell line 293), vsv-g (vesicular stomatitis virus g protein), BSA (bovine serum albumine), TCA (trichloroacetic acid)

8 References

ARAUJO, F., GOUVINHAS, C., FONTES, F., LA VECCHIA, C., AZEVEDO, A. & LUNET, N. 2014. Trends in cardiovascular diseases and cancer mortality in 45 countries from five continents (1980-2010). *Eur J Prev Cardiol,* 21**,** 1004-17.

BARAN, C. P., TRIDANDAPANI, S., HELGASON, C. D., HUMPHRIES, R. K., KRYSTAL, G. & MARSH, C. B. 2003. The inositol 5'-phosphatase SHIP-1 and the Src kinase Lyn negatively regulate macrophage colony-stimulating factor-induced Akt activity. *J Biol Chem,* 278**,** 38628-36.

BEN-CHETRIT, N., CHETRIT, D., RUSSELL, R., KORNER, C., MANCINI, M., ABDUL-HAI, A., ITKIN, T., CARVALHO, S., COHEN-DVASHI, H., KOESTLER, W. J., SHUKLA, K., LINDZEN, M., KEDMI, M., LAURIOLA, M., SHULMAN, Z., BARR, H., SEGER, D., FERRARO, D. A., PAREJA, F., GIL-HENN, H., LAPIDOT, T., ALON, R., MILANEZI, F., SYMONS, M., BEN-HAMO, R., EFRONI, S., SCHMITT, F., WIEMANN, S., CALDAS, C., EHRLICH, M. & YARDEN, Y. 2015. Synaptojanin 2 is a druggable mediator of metastasis and the gene is overexpressed and amplified in breast cancer. *Sci Signal,* 8**,** ra7.

BRATTAIN, M. G., BRATTAIN, D. E., FINE, W. D., KHALED, F. M., MARKS, M. E., KIMBALL, P. M., ARCOLANO, L. A. & DANBURY, B. H. 1981. Initiation and characterization of cultures of human colonic carcinoma with different biological characteristics utilizing feeder layers of confluent fibroblasts. *Oncodev Biol Med,* 2**,** 355-66.

BRAUER, H., STRAUSS, J., WEGNER, W., MULLER-TIDOW, C., HORSTMANN, M. & JUCKER, M. 2012. Leukemia-associated mutations in SHIP1 inhibit its enzymatic activity, interaction with the GM-CSF receptor and Grb2, and its ability to inactivate PI3K/AKT signaling. *Cell Signal,* 24**,** 2095-101.

CHENG, L., ENG, C., NIEMAN, L. Z., KAPADIA, A. S. & DU, X. L. 2011. Trends in colorectal cancer incidence by anatomic site and disease stage in the United States from 1976 to 2005. *Am J Clin Oncol,* 34**,** 573-80.

CHUANG, Y. Y., TRAN, N. L., RUSK, N., NAKADA, M., BERENS, M. E. & SYMONS, M. 2004. Role of synaptojanin 2 in glioma cell migration and invasion. *Cancer Res,* 64**,** 8271-5.

CONDE, C., GLOIRE, G. & PIETTE, J. 2011. Enzymatic and non-enzymatic activities of SHIP-1 in signal transduction and cancer. *Biochem Pharmacol,* 82**,** 1320-34.

DAGOGO-JACK, I. & SHAW, A. T. 2018. Tumour heterogeneity and resistance to cancer therapies. *Nat Rev Clin Oncol,* 15**,** 81-94.

DE, P., ASKE, J. C. & DEY, N. 2019. RAC1 Takes the Lead in Solid Tumors. *Cells,* 8.

DU, Z. & LOVLY, C. M. 2018. Mechanisms of receptor tyrosine kinase activation in cancer. *Mol Cancer,* 17**,** 58.

DUTTING, S., HEIDENREICH, J., CHERPOKOVA, D., AMIN, E., ZHANG, S. C., AHMADIAN, M. R., BRAKEBUSCH, C. & NIESWANDT, B. 2015. Critical off-target effects of the widely used Rac1 inhibitors NSC23766 and EHT1864 in mouse platelets. *J Thromb Haemost,* 13**,** 827-38.

EDIMO, W. E., JANSSENS, V., WAELKENS, E. & ERNEUX, C. 2012. Reversible Ser/Thr SHIP phosphorylation: a new paradigm in phosphoinositide signalling?: Targeting of SHIP1/2 phosphatases may be controlled by phosphorylation on Ser and Thr residues. *Bioessays,* 34**,** 634-42.

EHM, P., BETTIN, B., & JÜCKER, M. 2023. Activated Src kinases downstream of BCR-ABL and Flt3 induces proteasomal degradation of SHIP1 by phosphorylation of tyrosine 1021. *Biochimica et biophysica acta. Molecular cell research*, *1870*(5), 119467.

Ehm, P., GROTTKE, A., BETTIN, B., & JÜCKER, M. 2022. Investigation of the function of the PI3-Kinase / AKT signaling pathway for leukemogenesis and therapy of acute childhood lymphoblastic leukemia (ALL). *Cellular signalling*, *93*, 110301.

Ehm, P. A. H., LINNEBACHER, M., BLOCK, A., REHBACH, C., & JÜCKER, M. 2023. Targeted hyperactivation of AKT through inhibition of ectopic expressed SHIP1 induces cell death in colon carcinoma cells and derived metastases. *Cellular signalling*, *108*, 110720

EHM, P., NELSON, N., GIEHLER, S., SCHAKS, M., BETTIN, B., KIRCHMAIR, J., & JÜCKER, M. 2023. Reduced expression and activity of patient-derived SHIP1 phosphatase domain mutants. *Cellular signalling*, *101*, 110485.

EHM, P., RIETOW, R., WEGNER, W., BUßMANN, L., KRIEGS, M., DIERCK, K., HORN, S., STREICHERT, T., HORSTMANN, M., & JÜCKER, M. (2023). SHIP1 Is Present but Strongly Downregulated in T-ALL, and after Restoration Suppresses Leukemia Growth in a T-ALL Xenotransplantation Mouse Model. *Cells*, *12*(13), 1798.

FEARON, E. R. & VOGELSTEIN, B. 1990. A genetic model for colorectal tumorigenesis. *Cell,* 61**,** 759-67.

FERNANDES, S., IYER, S. & KERR, W. G. 2013. Role of SHIP1 in cancer and mucosal inflammation. *Ann N Y Acad Sci,* 1280**,** 6-10.

FU, Q., HUANG, Y., GE, C., LI, Z., TIAN, H., LI, Q., LI, H., LI, R., TAO, X., XUE, Y., WANG, Y., YANG, G., FANG, W. & SONG, X. 2019. SHIP1 inhibits cell growth, migration, and invasion in nonsmall cell lung cancer through the PI3K/AKT pathway. *Oncol Rep,* 41**,** 2337-2350.

FUHLER, G. M., BROOKS, R., TOMS, B., IYER, S., GENGO, E. A., PARK, M. Y., GUMBLETON, M., VIERNES, D. R., CHISHOLM, J. D. & KERR, W. G. 2012. Therapeutic potential of SH2 domain-containing inositol-5'-phosphatase 1 (SHIP1) and SHIP2 inhibition in cancer. *Mol Med,* 18**,** 65-75.

GERASHCHENKO, T. S., NOVIKOV, N. M., KRAKHMAL, N. V., ZOLOTARYOVA, S. Y., ZAVYALOVA, M. V., CHERDYNTSEVA, N. V., DENISOV, E. V. & PERELMUTER, V. M. 2019. Markers of Cancer Cell Invasion: Are They Good Enough? *J Clin Med,* 8.

GKRETSI, V. & STYLIANOPOULOS, T. 2018. Cell Adhesion and Matrix Stiffness: Coordinating Cancer Cell Invasion and Metastasis. *Front Oncol,* 8**,** 145.

GLÜCK, M., DALLY, L., JÜCKER, M., & EHM, P. (2022). JAK2-V617F is a negative regulation factor of SHIP1 protein and thus influences the AKT signaling pathway in patients with Myeloproliferative neoplasm (MPN). *The international journal of biochemistry & cell biology*, *149*, 106229.

GRAHAM, F. L., SMILEY, J., RUSSELL, W. C. & NAIRN, R. 1977. Characteristics of a human cell line transformed by DNA from human adenovirus type 5. *J Gen Virol,* 36**,** 59-74.

HAKIM, S., BERTUCCI, M. C., CONDUIT, S. E., VUONG, D. L. & MITCHELL, C. A. 2012. Inositol polyphosphate phosphatases in human disease. *Curr Top Microbiol Immunol,* 362**,** 247-314.

HANAHAN, D. & WEINBERG, R. A. 2011. Hallmarks of cancer: the next generation. *Cell,* 144**,** 646-74.

HASSAN, S. S., EL-KHAZRAGY, N., ELSHIMY, A. A., ABOELHUSSEIN, M. M., SALEH, S. A., FADEL, S., ATIA, H. A., MATBOULY, S. & TAMER, N. 2020. In vitro knock-out of miR-155 suppresses leukemic and HCV virus loads in pediatric HCV-4-associated acute lymphoid leukemia: A promising target therapy. *J Cell Biochem,* 121**,** 2811-2817.

HENDERSON, V., SMITH, B., BURTON, L. J., RANDLE, D., MORRIS, M. & ODERO-MARAH, V. A. 2015. Snail promotes cell migration through PI3K/AKT-dependent Rac1 activation as well as PI3K/AKT-independent pathways during prostate cancer progression. *Cell Adh Migr,* 9**,** 255-64.

HERLYN, M., BALABAN, G., BENNICELLI, J., GUERRY, D. T., HALABAN, R., HERLYN, D., ELDER, D. E., MAUL, G. G., STEPLEWSKI, Z., NOWELL, P. C. & ET AL. 1985. Primary melanoma cells of the vertical growth phase: similarities to metastatic cells. *J Natl Cancer Inst,* 74**,** 283-9.

HOXHAJ, G. & MANNING, B. D. 2020. The PI3K-AKT network at the interface of oncogenic signalling and cancer metabolism. *Nat Rev Cancer,* 20**,** 74-88.

HU, W. E., ZHANG, X., GUO, Q. F., YANG, J. W., YANG, Y., WEI, S. C. & SU, X. D. 2019. HeLa-CCL2 cell heterogeneity studied by single-cell DNA and RNA sequencing. *PLoS One,* 14**,** e0225466.

IYER, S., MARGULIES, B. S. & KERR, W. G. 2013. Role of SHIP1 in bone biology. *Ann N Y Acad Sci,* 1280**,** 11-4.

KANETO, N., YOKOYAMA, S., HAYAKAWA, Y., KATO, S., SAKURAI, H. & SAIKI, I. 2014. RAC1 inhibition as a therapeutic target for gefitinib-resistant non-small-cell lung cancer. *Cancer Sci,* 105**,** 788-94.

KENNAH, M., YAU, T. Y., NODWELL, M., KRYSTAL, G., ANDERSEN, R. J., ONG, C. J. & MUI, A. L. 2009. Activation of SHIP via a small molecule agonist kills multiple myeloma cells. *Exp Hematol,* 37**,** 1274-83.

KERR, W. G. 2011. Inhibitor and activator: dual functions for SHIP in immunity and cancer. *Ann N Y Acad Sci,* 1217**,** 1-17.

KOTELEVETS, L. & CHASTRE, E. 2020. Rac1 Signaling: From Intestinal Homeostasis to Colorectal Cancer Metastasis. *Cancers (Basel),* 12.

KOZOVSKA, Z., GABRISOVA, V. & KUCEROVA, L. 2016. Malignant melanoma: diagnosis, treatment and cancer stem cells. *Neoplasma,* 63**,** 510-7.

KRAUSE, M. & GAUTREAU, A. 2014. Steering cell migration: lamellipodium dynamics and the regulation of directional persistence. *Nat Rev Mol Cell Biol,* 15**,** 577-90.

KUIPERS, E. J., GRADY, W. M., LIEBERMAN, D., SEUFFERLEIN, T., SUNG, J. J., BOELENS, P. G., VAN DE VELDE, C. J. & WATANABE, T. 2015. Colorectal cancer. *Nat Rev Dis Primers,* 1**,** 15065.

KWON, T., KWON, D. Y., CHUN, J., KIM, J. H. & KANG, S. S. 2000. Akt protein kinase inhibits Rac1-GTP binding through phosphorylation at serine 71 of Rac1. *J Biol Chem,* 275**,** 423-8.

LATEK, D., MODZELEWSKA, A., TRZASKOWSKI, B., PALCZEWSKI, K. & FILIPEK, S. 2012. G protein-coupled receptors--recent advances. *Acta Biochim Pol,* 59**,** 515-29.

LEMM, E. A., VALLE-ARGOS, B., SMITH, L. D., RICHTER, J., GEBRESELASSIE, Y., CARTER, M. J., KAROLOVA, J., SVATON, M., HELMAN, K., WESTON-BELL, N. J., KARYDIS, L., WILLIAMSON, C. T., LENZ, G., PETTIGREW, J., HARWIG, C., STEVENSON, F. K., CRAGG, M., FORCONI, F., STEELE, A. J., CROSS, J., MACKENZIE, L., KLENER, P. & PACKHAM, G. 2020. Preclinical Evaluation of a Novel SHIP1 Phosphatase Activator for Inhibition of PI3K Signaling in Malignant B Cells. *Clin Cancer Res,* 26**,** 1700-1711.

LIEN, E. C., DIBBLE, C. C. & TOKER, A. 2017. PI3K signaling in cancer: beyond AKT. *Curr Opin Cell Biol,* 45**,** 62-71.

LO, T. C., BARNHILL, L. M., KIM, Y., NAKAE, E. A., YU, A. L. & DICCIANNI, M. B. 2009. Inactivation of SHIP1 in T-cell acute lymphoblastic leukemia due to mutation and extensive alternative splicing. *Leuk Res,* 33**,** 1562-6.

LUO, J. M., YOSHIDA, H., KOMURA, S., OHISHI, N., PAN, L., SHIGENO, K., HANAMURA, I., MIURA, K., IIDA, S., UEDA, R., NAOE, T., AKAO, Y., OHNO, R. & OHNISHI, K. 2003. Possible dominant-negative mutation of the SHIP gene in acute myeloid leukemia. *Leukemia,* 17**,** 1-8.

MANNING, B. D. & TOKER, A. 2017. AKT/PKB Signaling: Navigating the Network. *Cell,* 169**,** 381-405.

MARTINI, M., DE SANTIS, M. C., BRACCINI, L., GULLUNI, F. & HIRSCH, E. 2014. PI3K/AKT signaling pathway and cancer: an updated review. *Ann Med,* 46**,** 372-83.

MAXWELL, M. J., SRIVASTAVA, N., PARK, M. Y., TSANTIKOS, E., ENGELMAN, R. W., KERR, W. G. & HIBBS, M. L. 2014. SHIP-1 deficiency in the myeloid compartment is insufficient to induce myeloid expansion or chronic inflammation. *Genes Immun,* 15**,** 233-40.

MELZER, C., HASS, R., LEHNERT, H. & UNGEFROREN, H. 2019. RAC1B: A Rho GTPase with Versatile Functions in Malignant Transformation and Tumor Progression. *Cells,* 8.

METZNER, A., PRECHT, C., FEHSE, B., FIEDLER, W., STOCKING, C., GUNTHER, A., MAYR, G. W. & JUCKER, M. 2009. Reduced proliferation of CD34(+) cells from patients with acute myeloid leukemia after gene transfer of INPP5D. *Gene Ther,* 16**,** 570-3.

MORENO, C. C., MITTAL, P. K., SULLIVAN, P. S., RUTHERFORD, R., STALEY, C. A., CARDONA, K., HAWK, N. N., DIXON, W. T., KITAJIMA, H. D., KANG, J., SMALL, W. C., OSHINSKI, J. & VOTAW, J. R. 2016. Colorectal Cancer Initial Diagnosis: Screening Colonoscopy, Diagnostic Colonoscopy, or Emergent Surgery, and Tumor Stage and Size at Initial Presentation. *Clin Colorectal Cancer,* 15**,** 67-73.

MRAZ, M. & KIPPS, T. J. 2013. MicroRNAs and B cell receptor signaling in chronic lymphocytic leukemia. *Leuk Lymphoma,* 54**,** 1836-9.

MYERS, M. P., PASS, I., BATTY, I. H., VAN DER KAAY, J., STOLAROV, J. P., HEMMINGS, B. A., WIGLER, M. H., DOWNES, C. P. & TONKS, N. K. 1998. The lipid phosphatase activity of PTEN is critical for its tumor supressor function. *Proc Natl Acad Sci U S A,* 95**,** 13513-8.

NELSON, N., RAZETO, A., GILARDI, A., GRÄTTINGER, M., KIRCHMAIR, J., & JÜCKER, M. 2021. AKT1 and PTEN show the highest affinities among phosphoinositide binding proteins for the second messengers PtdIns(3,4,5)P_3 and

PtdIns(3,4)P_2. *Biochemical and biophysical research communications*, *568*, 110–115.

NELSON, N., WUNDENBERG, T., LIN, H., REHBACH, C., HORN, S., WINDHORST, S., & JÜCKER, M. 2020. Characterization of the substrate specificity of the inositol 5-phosphatase SHIP1. *Biochemical and biophysical research communications*, *524*(2), 366–370.

NOWELL, P. C. 1976. The clonal evolution of tumor cell populations. *Science,* 194**,** 23-8.

PARK, M. Y., SRIVASTAVA, N., SUDAN, R., VIERNES, D. R., CHISHOLM, J. D., ENGELMAN, R. W. & KERR, W. G. 2014. Impaired T-cell survival promotes mucosal inflammatory disease in SHIP1-deficient mice. *Mucosal Immunol,* 7**,** 1429-1439.

PAVRI, S. N., CLUNE, J., ARIYAN, S. & NARAYAN, D. 2016. Malignant Melanoma: Beyond the Basics. *Plast Reconstr Surg,* 138**,** 330e-340e.

PAYNE, S. R. & KEMP, C. J. 2005. Tumor suppressor genetics. *Carcinogenesis,* 26**,** 2031-45.

PEREZ-HERRERO, E. & FERNANDEZ-MEDARDE, A. 2015. Advanced targeted therapies in cancer: Drug nanocarriers, the future of chemotherapy. *Eur J Pharm Biopharm,* 93**,** 52-79.

PORTA, C., PAGLINO, C. & MOSCA, A. 2014. Targeting PI3K/Akt/mTOR Signaling in Cancer. *Front Oncol,* 4**,** 64.

PRASAD, N. K. 2009. SHIP2 phosphoinositol phosphatase positively regulates EGFR-Akt pathway, CXCR4 expression, and cell migration in MDA-MB-231 breast cancer cells. *Int J Oncol,* 34**,** 97-105.

RASTRELLI, M., TROPEA, S., ROSSI, C. R. & ALAIBAC, M. 2014. Melanoma: epidemiology, risk factors, pathogenesis, diagnosis and classification. *In Vivo,* 28**,** 1005-11.

RUSCHMANN, J., HO, V., ANTIGNANO, F., KURODA, E., LAM, V., IBARAKI, M., SNYDER, K., KIM, C., FLAVELL, R. A., KAWAKAMI, T., SLY, L., TURHAN, A. G. & KRYSTAL, G. 2010. Tyrosine phosphorylation of SHIP promotes its proteasomal degradation. *Exp Hematol,* 38**,** 392-402, 402 e1.

SCHAKS, M., ALLGOEWER, K., NELSON, N., EHM, P., HEUMANN, A., EWALD, F., SCHUMACHER, U., SIMON, R., SAUTER, G. & JUCKER, M. 2020. Ectopic Expression of Hematopoietic SHIP1 in Human Colorectal Cancer. *Biomedicines,* 8.

SLY, L. M., RAUH, M. J., KALESNIKOFF, J., BUCHSE, T. & KRYSTAL, G. 2003. SHIP, SHIP2, and PTEN activities are regulated in vivo by modulation of their protein levels: SHIP is up-regulated in macrophages and mast cells by lipopolysaccharide. *Exp Hematol,* 31**,** 1170-81.

SMALLEY, K. S., HAASS, N. K., BRAFFORD, P. A., LIONI, M., FLAHERTY, K. T. & HERLYN, M. 2006. Multiple signaling pathways must be targeted to overcome drug resistance in cell lines derived from melanoma metastases. *Mol Cancer Ther,* 5**,** 1136-44.

SO, E. Y., SUN, C., WU, K. Q., DRIESMAN, A., LEGGETT, S., ISAAC, M., SPANGLER, T., DUBIELECKA-SZCZERBA, P. M., REGINATO, A. M. & LIANG, O. D. 2020. Lipid phosphatase SHIP-1 regulates chondrocyte hypertrophy and skeletal development. *J Cell Physiol,* 235**,** 1425-1437.

STRATE, L. L. & SYNGAL, S. 2005. Hereditary colorectal cancer syndromes. *Cancer Causes Control,* 16**,** 201-13.

TAGER, M., HORN, S., LATUSKE, E., EHM, P., SCHAKS, M., NALASKOWSKI, M., FEHSE, B., FIEDLER, W., STOCKING, C., WELLBROCK, J. & JUCKER, M. 2017. SHIP1, but not an AML-derived SHIP1 mutant, suppresses myeloid leukemia growth in a xenotransplantation mouse model. *Gene Ther,* 24**,** 749-753.

THANIKACHALAM, K. & KHAN, G. 2019. Colorectal Cancer and Nutrition. *Nutrients,* 11.

TORRE, L. A., SIEGEL, R. L., WARD, E. M. & JEMAL, A. 2016. Global Cancer Incidence and Mortality Rates and Trends--An Update. *Cancer Epidemiol Biomarkers Prev,* 25**,** 16-27.

VIERNES, D. R., CHOI, L. B., KERR, W. G. & CHISHOLM, J. D. 2014. Discovery and development of small molecule SHIP phosphatase modulators. *Med Res Rev,* 34**,** 795-824.

WEINBERG, R. A. 1994. Oncogenes and tumor suppressor genes. *CA Cancer J Clin,* 44**,** 160-70.

XU, W., YANG, Z. & LU, N. 2015. A new role for the PI3K/Akt signaling pathway in the epithelial-mesenchymal transition. *Cell Adh Migr,* 9**,** 317-24.

XUE, H., HUA, L. M., GUO, M. & LUO, J. M. 2014. SHIP1 is targeted by miR-155 in acute myeloid leukemia. *Oncol Rep,* 32**,** 2253-9.

YE, Y., JIN, L., WILMOTT, J. S., HU, W. L., YOSUFI, B., THORNE, R. F., LIU, T., RIZOS, H., YAN, X. G., DONG, L., TAY, K. H., TSENG, H. Y., GUO, S. T., DE BOCK, C. E., JIANG, C. C., WANG, C. Y., WU, M., ZHANG, L. J., HERSEY, P., SCOLYER, R. A. & ZHANG, X. D. 2013. PI(4,5)P2 5-phosphatase A regulates PI3K/Akt signalling and has a tumour suppressive role in human melanoma. *Nat Commun,* 4**,** 1508.

ALLGÖWER-MARTIN, C. (2015). Functional Analysis of Inositol 5-Phosphatase SHIP1 in the Regulation of Migration, Proliferation, and Invasion of Colon Carcinoma Cells *(Bachelor Thesis Molecular Life Sciences M.Sc.; Institute for Biochemistry and Signal transduction, University Medical Center Hamburg-Eppendorf)*

CREMER, P. (2018). Functional Role of SHIP1 in Tumorigenesis and Substrate-trapping in Malignant Melanoma Cell Lines *(Master Thesis Molecular Life Sciences M.Sc.; Institute for Biochemistry and Signal transduction, University Medical Center Hamburg-Eppendorf; in cooperation with Radboud University Nijmegen)*

DRECHSEL, O. (2019). Untersuchungen zur Funktion der Inositol-5-Phosphatase SHIP1 für die Pathogenese von Hauttumoren *(Doctoral Thesis Dentistry; Institute for Biochemistry and Signal transduction, University Medical Center Hamburg-Eppendorf)*

NELSON, N. (2017). Functional analysis of SH2 domain containing Inositol poly-phosphate-5- Phosphatase 1 (SHIP1) in human non- hematopoietic cancers *(Master Thesis Molecular Life Sciences M.Sc.; Institute for Biochemistry and Signal transduction, University Medical Center Hamburg-Eppendorf)*

WEINBERG, R. In Retrospect: The chromosome trail. *Nature* **453,** 725 (2008). *(https://doi.org/10.1038/453725a)*

CANCER TODAY, Data from GLOBOCAN 2018 *(https://gco.iarc.fr/today/online-analysis-multibars?v=2018&mode=cancer&mode_population=countries&population=900&populations=900&key=asr&sex=0&cancer=39&type=0&statistic=5&prevalence=0&population_group=0&ages_group%5B%5D=0&ages_group%5B%5D=17&nb_items=10&group_cancer=1&include_nmsc=1&include_nmsc_other=1&type_multiple=%257B%2522inc%2522%253Atrue%252C%2522mort%2522%253Afalse%252C%2522prev%2522%253Afalse%257D&orientation=horizontal&type_sort=0&type_nb_items=%257B%2522top%2522%253Atrue%252C%2522bottom%2522%253Afalse%257D&population_group_globocan_id=)*

https://www.merckmillipore.com/DE/de/product/Rac1-Inhibitor-CAS-1177865-17-6-Calbiochem,EMD_BIO-553502

9 List of Illustrations

10 Erklärung des Eigenanteils

Ich versichere ausdrücklich, dass ich die beschriebenen Experimente selbst geplant und durchgeführt habe, z.T. unter Anleitung. Die Zelllinien wurden, wie beschrieben, teilweise selbst kloniert, teilweise nach Klonierung von anderen AG-Mitgliedern übernommen. Das konfokale Mikroskop wurde freundlicherweise von Dr. rer. nat. Antonio Virgilio Failla (UKE Microscopy Imaging Facility) bedient. Die gezeigten Ergebnisse habe ich selbst ausgewertet und graphisch dargestellt. Das Projekt wurde von meinem Doktorvater Prof. Dr. Manfred Jücker entwickelt.

11 Affidavit

Ich versichere ausdrücklich, dass ich die Arbeit selbständig und ohne fremde Hilfe, insbesondere ohne entgeltliche Hilfe von Vermittlungs- und Beratungsdiensten, verfasst, andere als die von mir angegebenen Quellen und Hilfsmittel nicht benutzt und die aus den benutzten Werken wörtlich oder inhaltlich entnommenen Stellen einzeln nach Ausgabe (Auflage und Jahr des Erscheinens), Band und Seite des benutzten Werkes kenntlich gemacht habe. Das gilt insbesondere auch für alle Informationen aus Internetquellen.
Soweit beim Verfassen der Dissertation KI-basierte Tools („Chatbots“) verwendet wurden, versichere ich ausdrücklich, den daraus generierten Anteil deutlich kenntlich gemacht zu haben. Die „Stellungnahme des Präsidiums der Deutschen Forschungsgemeinschaft (DFG) zum Einfluss generativer Modelle für die Text- und Bilderstellung auf die Wissenschaften und das Förderhandeln der DFG“ aus September 2023 wurde dabei beachtet.
Ferner versichere ich, dass ich die Dissertation bisher nicht einem Fachvertreter an einer anderen Hochschule zur Überprüfung vorgelegt oder mich anderweitig um Zulassung zur Promotion beworben habe.
Ich erkläre mich damit einverstanden, dass meine Dissertation vom Dekanat der Medizinischen Fakultät mit einer gängigen Software zur Erkennung von Plagiaten überprüft werden kann.

Datum Unterschrift

12 Acknowledgements

An dieser Stelle möchte ich mich von ganzem Herzen bei allen Menschen bedanken, die mich auf meinem Weg zur Promotion begleitet und unterstützt haben.

Besonders danke ich meiner guten Freundin und Promotionskollegin Franzi. Deine fachliche Expertise und emotionale Unterstützung waren für mich während der gesamten Arbeit von unschätzbarem Wert. Du hast viele Sonntage mit mir beim Schreiben unserer Doktorarbeiten verbracht, und mir immer wieder aufs Neue geholfen, schwierige Phasen zu überwinden und den Fokus zu behalten. Auch meinen guten Freunden Freya, Nico und Aziz danke ich ganz herzlich für ihren fachlichen Input und ihre aufbauenden Worte.

Ein herzliches Dankeschön geht auch an meine Eltern, die mich immer bedingungslos unterstützt haben. Meine Mama hatte stets ein offenes Ohr für mich, und mein Papa hatte stets Ratschläge parat, nach denen ich nicht fragen musste.

Nicht zuletzt danke ich meinem Doktorvater, der mir mit seiner fachlichen Expertise und seinem Rat zur Seite stand. Sein Vertrauen in meine Arbeit und seine konstruktiven Rückmeldungen waren eine wichtige Grundlage für den erfolgreichen Abschluss dieser Dissertation.

Schließlich danke ich auch allen anderen Freund*innen und Wegbegleiter*innen, die mich während dieser intensiven Zeit motiviert, unterstützt und an mich geglaubt haben.

Vielen Dank für alles!